C.P. No. 930

C.P. No. 930

MINISTRY OF TECHNOLOGY

AERONAUTICAL RESEARCH COUNCIL

CURRENT PAPERS

The Lift and Drag Characteristics of Caret Wings at Mach Numbers between 5 and 10

by

J. R. Collingbourne and D. H. Peckham

LONDON: HER MAJESTY'S STATIONERY OFFICE

1967

PRICE 18*s* 6*d* NET

U.D.C. No. 533.693.3 : 533.6.013.13 : 533.6.013.12 : 533.6.011.55

C.P. No. 930*
February 1966

THE LIFT AND DRAG CHARACTERISTICS OF CARET WINGS AT MACH NUMBERS BETWEEN 5 AND 10

by

J. R. Collingbourne

D. H. Peckham

SUMMARY

The broad effects of certain variables on the aerodynamic efficiency of caret wings are investigated. The variables considered are slenderness ratio, volume coefficient and upper surface incidence; skin friction, including the effects of wing loading, altitude and transition Reynolds number; and parasite drag. This study highlights the important areas for future investigation, and suggestions are made for experimental and theoretical work. Detailed conclusions are given at the end of the Report.

---

* Replaces R.A.E. Technical Report No. 66036 - A.R.C. 28,172.

CONTENTS

1 INTRODUCTION

In recent years a number of methods[1-4] have been suggested for designing wing shapes to support known inviscid supersonic and hypersonic flow fields. The advantage of using this approach is that, apart from viscosity effects, the pressure distribution over at least part of the overall surface is specified exactly, thus avoiding the difficulties and inaccuracies associated with the use of approximate theories to calculate pressures on wings of arbitrary shape. The term waverider has been coined[5] to denote a wing of this kind, the shock system of which is contained below the wing between the leading edges.

The simplest wing in this class is the caret wing proposed by Nonweiler[1], and this forms the subject of the present study. This type of wing at its 'design' condition generates below it a plane oblique shock wave attached to its leading edges, and hence has a uniform pressure over its lower surface. Although the caret waverider is not necessarily the most efficient aerodynamically it has the advantage for the purpose of the present study compared with other types (e.g. the 'Jones' wing[2], based on a conical flow field) that its volume and the overall aerodynamic forces acting on it are comparatively easy to calculate, and it offers a wider degree of freedom in the choice of planform for a given Mach number and volume.

Since the flows on the upper and lower surfaces of waveriders at their 'design' condition are independent (apart from the minor effect of leading edge blunting), a variety of upper-surface shapes can in principle be chosen (e.g. Ref.6), although to be classed as a waverider the upper-surface of the wing should strictly be shock-free, i.e. the pressures on this surface should be at or below the ambient value. Theoretical studies of caret wings to date have usually assumed the upper-surface to be generated by lines parallel with the free stream direction. In this case, and in the absence of viscous or extraneous drag items, the ratio of lift to drag is given simply by the cotangent of the lower-surface incidence.

The purpose of this Report is to investigate systematically the broad effects of certain variables on the aerodynamic efficiency of caret wings. The caret wing is assumed to have a delta planform and plane surfaces on each side of the centre line, (see Fig.1). This approach is a convenient way of relating the aerodynamics and geometry of families of vehicle shapes to their operating conditions. The variables investigated in this study are:-

(i) Slenderness ratio (i.e. semispan/length) and volume coefficient (i.e. volume/plan area$^{3/2}$) at zero upper-surface incidence.

(ii) Upper-surface incidence, at given values of slenderness ratio and volume coefficient.

(iii) Mach number, in the range 5-10.

(iv) Skin friction, including both the effect of typical arbitrary values of skin friction coefficient, and also of calculated skin friction assuming various wing loadings, attitudes and transition Reynolds numbers.

(v) Parasite drag, present in various arbitrary amounts. This item would include base, fin and leading-edge bluntness drag; (although the basic wing of Fig.1 has sharp leading edges, the effects of blunting the leading edge are considered).

In Appendix A it is shown that aerodynamic efficiency is measured more correctly by the weight to drag ratio rather than by the more familiar lift to drag ratio. Aerodynamic lift is less than the weight due to the effect of the Earth's curvature causing a centrifugal lift to be developed which of course varies as (flight speed)^2. Hence in this Report aerodynamic efficiency is presented as weight to drag ratio where comparisons are being made or implied between one speed and another, but as the more familiar lift to drag ratio where speed effects are essentially irrelevant. Since aerodynamic efficiency is only one factor affecting overall range it is obviously most important that investigations of the present kind should be linked with others which consider propulsion, flight trajectory, stability and control, and structural aspects, (see Section 4).

Section 2 of this Report and also the five Appendices give details of the theoretical background to the estimates of lift to drag and weight to drag ratios described later. In Section 3 the effects of the variables (i)-(v) listed above are as far as possible considered separately. Finally in Section 4 suggestions are made for further work, both experimental and theoretical.

2 THEORY

2.1 Geometry

Fig.1 shows a caret wing* of delta planform of span $2s$ and length ℓ, whose upper and lower surfaces are at incidences of α_U and α_L to the free-stream direction, respectively, measured in the XZ-plane. The base of the

* The basic wing considered here has sharp leading edges. Changes in geometry caused by leading-edge blunting are discussed in Appendix D.

wing is chosen to be at right angles to the free-stream direction in all cases. Thus the plan and base area, and volume, of the wing are:-

$$\text{Plan area} = s\ell = S \tag{1}$$

$$\text{Base area} = s\ell\,(\tan\alpha_L - \tan\alpha_U) \tag{2}$$

$$\text{Volume} = \frac{1}{3}\,s\ell\,(\tan\alpha_L - \tan\alpha_U)\ . \tag{3}$$

It is convenient at this stage to introduce the volume coefficient*, τ = volume/(plan area)$^{3/2}$.

Thus,

$$\tau = \frac{1}{3}\left(\frac{\ell}{s}\right)^{\frac{1}{2}}(\tan\alpha_L - \tan\alpha_U)\ . \tag{4}$$

In order to calculate the contribution to drag from skin friction, it is necessary to know the wetted areas of the upper and lower surfaces, S_U and S_L respectively. These are given by:-

$$\frac{S_U}{S} = \sec\alpha_U\left\{1 + \frac{\ell^2}{s^2}\cos^2\alpha_U\,(\tan\zeta - \tan\alpha_U)^2\right\}^{\frac{1}{2}} \tag{5a}$$

$$\frac{S_L}{S} = \sec\alpha_L\left\{1 + \frac{\ell^2}{s^2}\cos^2\alpha_L\,(\tan\zeta - \tan\alpha_L)^2\right\}^{\frac{1}{2}} \tag{5b}$$

where ζ is the incidence of the plane of the leading edges to the free-stream direction, i.e. the angle between the free-stream and the attached oblique shock wave, which is a function of M_o and α_L.

It is sometimes convenient to express these wetted areas in terms of α_U, α_L and the anhedral angles of the upper and lower surfaces in the plane of the base ψ_U and ψ_L respectively, in which case equations (5a) and (5b) become:-

$$\frac{S_U}{S} = \sec\alpha_U \sec\psi_U\,(1 - \sin^2\psi_U \sin^2\alpha_U)^{\frac{1}{2}} \tag{6a}$$

---

* Volume coefficient is a parameter particularly appropriate to project studies, and those concerned with the aerodynamic forces on particular shapes may prefer to express the geometry in terms of the included angle between upper and lower surfaces in the plane of symmetry = 2ϑ say. From equation (4),

$$\tan\alpha_L - \tan\alpha_U = 3\tau\,(s/\ell)^{\frac{1}{2}} \simeq \tan 2\vartheta \quad \text{for small } \alpha_U\ .$$

$$\frac{S_L}{S} = \sec \alpha_L \sec \psi_L \left(1 - \sin^2 \psi_L \sin^2 \alpha_L\right)^{\frac{1}{2}} \qquad (6b)$$

where

$$\tan \psi_U = \frac{\ell}{s} \left(\tan \zeta - \tan \alpha_U\right) \qquad (6c)$$

$$\tan \psi_L = \frac{\ell}{s} \left(\tan \zeta - \tan \alpha_L\right) \qquad (6d)$$

In equations (6a) and (6b) above it is normally sufficiently accurate to equate the terms in brackets to unity.

Using equations (5) in conjunction with the equations given below in Section 2.3, the area ratios S_U/S and S_L/S have been calculated as functions of $\beta_o s/\ell$, $M_o^2 C_{p_L}$ and M_o, for $\alpha_U = 0$ and $0.2/\beta_o$, and these have been plotted on Fig.2. It will be noted that the ratio S_L/S depends almost entirely on $\beta_o s/\ell$ whereas the upper-surface ratio is affected by $M_o^2 C_{p_L}$ and $\beta_o \alpha_U$ as well as by $\beta_o s/\ell$. The effect of upper-surface incidence on S_U can be estimated to a close approximateion by dividing the value at $\alpha_U = 0$, and the same $\beta_o s/\ell$ and $M_o^2 C_{p_L}$, by $\left(1 + \frac{\alpha_U}{2s/\ell}\right)$.

From the foregoing, it can be seen that three independent geometrical variables must be specified to define the shape of the caret wing and its attitude relative to the free-stream direction. The three which will usually be specified in this Report are

(i) Volume coefficient, τ = volume/(plan area)$^{3/2}$,

(ii) Slenderness ratio, s/ℓ,

(iii) Upper-surface incidence, α_U.

If these are fixed, along with the Mach number, then the shock angle ζ and the normal pressure distribution - and hence to a very close approximation the lift coefficient - are determined. Conversely, lift coefficient can be varied by varying any one of these parameters and hence can replace any one of them as an independent variable; this is done in this study, e.g. C_L replaces α_U unless the latter is fixed. The lift to drag ratio at a given Mach number, with arbitrary values for the skin friction force coefficients on each surface is of course also a function only of these three variables. But if the friction drag is to be calculated, the wing loading and size

(or weight) of the aircraft must be specified also, along with some criterion for estimating the transition position.

It may be required to know the flow conditions in a plane normal to the leading edge, for example in calculating effects of leading-edge blunting, (see Section 2.4.1 and Appendix D) or the conditions for shock detachment, (see Section 2.3 below). Denoting the velocity component of the free-stream normal to the leading edge by V_{N_o} and the corresponding Mach number by M_{N_o}, the ratios V_{N_o}/V_o, and M_{N_o}/M_o are given simply by the sine of the angle between the leading edge and the free-stream vector through the wing apex:-

$$\frac{V_{N_o}}{V_o} = \frac{M_{N_o}}{M_o} = \left\{\frac{\tan^2 \zeta + s^2/\ell^2}{\sec^2 \zeta + s^2/\ell^2}\right\}^{\frac{1}{2}} \tag{7}$$

Since both the X-Z plane and the plane normal to the leading edge are normal to the shock plane, the velocity components **normal** to the shock evaluated in these two planes must be identical. Thus, if ζ_N is the shock angle measured in the plane normal to the leading edge and α_N the lower-surface incidence in this plane,

$$\frac{M_{N_o}}{M_o} = \frac{\sin \zeta}{\sin \zeta_N} \tag{8}$$

Similarly, the ratio of the heights above the shock, of the surface and of the free-stream vector through the leading edge must be the same in the two planes, i.e.

$$\frac{\tan (\zeta_N - \alpha_N)}{\tan \zeta_N} = \frac{\tan (\zeta - \alpha)}{\tan \zeta} \tag{9}$$

Here, α and α_N of course refer to the same surface, which may be either the upper **or** lower surface. Equations (7), (8), (9) may be combined to give α_N in terms of α, τ and s/ℓ

$$\tan \alpha_N = \frac{s}{\ell} \frac{(\sec^2 \zeta + s^2/\ell^2)^{\frac{1}{2}} \tan \alpha}{\tan^2 \zeta + s^2/\ell^2 - \tan \zeta \tan \alpha} \tag{10}$$

Some observations can be made about the likely limits of variation of τ and s/ℓ. A typical value of τ for large supersonic aircraft is about 0.04 (see Ref.8), though for small aircraft somewhat larger values are obtained since the dimensions of certain items remain constant, e.g. crew dimensions. However, for a hypersonic aircraft based on the caret wing higher values of τ will probably be needed. This is because with increase of Mach number the size of the propulsion system will most likely increase, and if it is integrated with the airframe this would take up part of the volume of the caret wing as defined in Fig.1, i.e. the propulsion nozzle would partly or wholly fill the base area. Also, at high Mach numbers the use of hydrogen as a fuel has certain attractions[10,11], but its low density would require a large storage volume. For these reasons, values of τ for the basic caret wing significantly higher than 0.04 would seem to be needed. In this investigation therefore, values centred round 0.08 will be considered.

The slenderness ratio s/ℓ must have a practical lower limit determined by considerations of low-speed handling, airfield performance etc., which is likely to be between 0.2 and 0.3. Following Ref.8, the minimum slenderness ratio which is considered in this study is 0.2.

2.2 Overall lift and drag

The overall lift and drag coefficients based on plan area are:-

$$C_L = C_{p_L} - C_{p_U} - C_{FU}\frac{S_U}{S}\sin\alpha_U - C_{FL}\frac{S_L}{S}\sin\alpha_L \qquad (11)$$

$$C_D = C_{p_L}\tan\alpha_L - C_{p_U}\tan\alpha_U + C_{FU}\frac{S_U}{S}\cos\alpha_U + C_{FL}\frac{S_L}{S}\cos\alpha_L + C_{DP} \qquad (12a)$$

where C_{FU} and C_{FL} are the mean tangential force coefficients due to skin friction, each based on the appropriate surface area for the upper and lower surfaces respectively, and C_{DP} is a parasite-drag coefficient based on plan area S. For convenience, we may write

$$C_{DF} = C_{FU}\frac{S_U}{S}\cos\alpha_U + C_{FL}\frac{S_L}{S}\cos\alpha_L \qquad (12b)$$

i.e. C_{DF} is the total skin-friction drag coefficient based on S. Then

$$C_D = C_{p_L}\tan\alpha_L - C_{p_U}\tan\alpha_U + C_{DF} + C_{DP} \qquad (12c)$$

2.3 Pressure coefficients

The pressure coefficient C_{p_L} on the lower-surface of a caret wing can be expressed in terms of the shock wave angle ζ and the free-stream Mach number M_o by means of the well-known equation from two-dimensional oblique-shock theory[12]

$$C_{p_L} = \frac{4}{\gamma + 1} (\sin^2 \zeta - 1/M_o^2) \tag{13}$$

The relationship between the lower-surface incidence α_L, the shock-wave angle and the free-stream Mach number can also be obtained from classical theory[12]

$$\tan \alpha_L = \frac{2 \cot \zeta (\sin^2 \zeta - 1/M_o^2)}{\gamma + 1 - 2 (\sin^2 \zeta - 1/M_o^2)} \tag{14}$$

For $\gamma = 1.4$, these equations become

$$C_{p_L} = \frac{5}{3} (\sin^2 \zeta - 1/M_o^2) \tag{15}$$

and

$$\tan \alpha_L = \frac{5 \cot \zeta (\sin^2 \zeta - 1/M_o^2)}{6 - 5 (\sin^2 \zeta - 1/M_o^2)} \tag{16}$$

The shock-wave angle ζ can be eliminated from (15) and (16) giving $\tan \alpha_L$ in terms of C_{p_L} and M_o

$$\tan \alpha_L = \frac{C_{p_L}}{2 - C_{p_L}} \left\{ \frac{1 - 0.6\, C_{p_L} - 1/M_o^2}{0.6\, C_{p_L} + 1/M_o^2} \right\}^{\frac{1}{2}} \tag{17}$$

There is no explicit relation for C_{p_L} in terms of M_o and α_L. If α_L is given, equation (17), which is virtually a cubic in C_{p_L}, must be solved. For desk computation, it is sometimes more convenient to use an approximation for C_{p_L} in terms of α_L and M_o. A number of such approximations are discussed in Appendix B.

The foregoing equations apply at angles of incidence of the lower-surface below the maximum at which a shock can be attached to the leading edges. To calculate this maximum incidence and the associated maximum pressure coefficient, it is necessary to consider flow conditions normal to the attachment line, i.e. in a plane normal to the leading edge. Shock detachment occurs if a maximum turning angle in this plane, $(\alpha_N)_{max}$ is exceeded. This critical angle increases as the Mach number in this plane M_{N_o} increases, but the shock angle at $(\alpha_N)_{max}$, which is also a maximum for that particular Mach number, exhibits only a small variation[12] - between 64^o and 68^o - for all Mach numbers M_{N_o} greater than 1.40. Now, from equations (8) and (15),

$$M_{N_o} = \frac{(1 + 0.6\ M_o^2\ C_{PL})^{\frac{1}{2}}}{\sin \zeta_N}$$

and since the relevant values of $M_o^2\ C_{p_L}$ in this study exceed unity, $M_{N_o} > 1.40$ and so we can use $\zeta_N \leqslant 64^o$ as a convenient condition for ensuring that the shock is attached to the leading edges. From equations (7), (8) and (15),

$$\cos^2 \zeta_N = \frac{(s/\ell)^2\ (\beta_o^2 - 0.6\ M_o^2\ C_{p_L})^2}{M_\infty^2 \left\{1 + 0.6\ M_o^2\ C_{p_L} + \frac{s^2}{\ell^2}\ (\beta_o^2 - 0.6\ M_o^2\ C_{p_L})\right\}}$$

Making the approximations $\beta_o \simeq M_o$ and that $0.36\ C_{p_L}^2$ is small cf. unity, C_{p_L} can be expressed in terms of ζ_N, M_o and s/ℓ:-

$$C_{p_L} \simeq \frac{5}{3}\ \frac{(s/\ell)^2\ \tan^2 \zeta_N - 1/M_o^2}{1 + (s/\ell)^2\ (1 + 2\ \tan \zeta_N)}$$

Assuming a minimum s/ℓ of 0.2 and a minimum Mach number of 5, the pressure coefficient corresponding to a shock detachment angle of 64^o is $\geqslant 0.177$. This is likely to be well above the values appropriate to cruising flight.

At the present time no exact solution exists for the pressure distribution on the upper-surface of a caret wing with $\alpha_U \neq 0$. However, since at hypersonic Mach numbers the contribution to overall lift and drag from the

pressure distribution on the upper-surface is likely to be much less than the contribution from the lower-surface, an approximate value of the mean pressure coefficient on the upper-surface should be adequate for the purposes of calculating overall lift and drag. It has therefore been assumed that the mean pressure coefficient on the upper-surface, C_{p_U}, is that corresponding to a two-dimensional expansion or compression, as the case may be, through the "surface incidence", α'_U, where surface incidence is defined as the complement of the angle between the free-stream vector and the normal to the surface. Since the upper-surfaces of the caret wings considered in this Report are composed of two flat facets, the surface incidence and the pressure coefficient over each facet will be constant. The surface incidence, α'_U, is given by:-

$$\sin \alpha'_U = \sin \alpha_U \cos \psi_U \qquad (18)$$

where ψ_U is the anhedral angle of the upper-surface in the plane of the base (equation (6c)).

Measurements of upper-surface pressures have been made[13] at $M_o = 4.3$ on a caret wing of slenderness ratio 0.25, for which the design condition was $\alpha_U = 0$. The following table gives the measured increments in negative pressure coefficient on the upper-surface, at various spanwise stations, due to increasing upper-surface incidence from zero to 4° and also to 10°.

Distance from wing C_L						
Local semispan	0	0.2	0.4	0.6	0.8	0.9
$-\Delta C_{p_U}$, $\alpha_U = 4^\circ$	0.010	0.0145	0.0185	0.0185	0.021	0.020
$-\Delta C_{p_U}$, $\alpha_U = 10^\circ$	0.029	0.033	0.0345	0.0375	0.042	0.0395

Values of the mean pressure coefficient on the upper-surface estimated by the method described above are -0.017 for $\alpha_U = 4^\circ$ and -0.0365 for $\alpha_U = 10^\circ$, the anhedral angle ψ_U being 55° in this case. Thus, although the pressure on the upper-surface varies somewhat across the span, - as might be expected - from a low value near the ridge line to a high value near the leading edge, the method used in this study to calculate C_{p_U} gives a reasonable mean value.

Convenient approximations for calculating C_{p_U} in terms of α'_U are given in Appendix B.

The above equations for the pressures on the wing surfaces, which are used for the estimates of lift and drag described later in this Report, apply strictly to the basic caret wing of Fig.1 which has sharp leading edges. It is assumed that any rounding of the leading edges which may be necessary for structural reasons will be small - a radius of the order of 0.1% of overall length, say. A simple analysis of the lift and drag penalties due to leading edge blunting is given in Appendix D based on the assumption that the pressures on the flat after-surfaces behind the tangent lines to the leading edge radius are the same as those given above for a sharp-edged wing.

2.4 Skin friction

2.4.1 Transition location

Before estimates can be made of overall skin-friction drag it is of course necessary to know the extent of laminar and turbulent flow on each surface of the wing. Unfortunately, information on this topic is very limited at hypersonic speeds. A useful summary of the present state of knowledge on transition at supersonic speeds, with a limited indication of hypersonic trends, has been made by Michel[14].

For smooth, flat plates with zero heat transfer from the surface, it is known that Re_t, the Reynolds number based on conditions at the edge of the boundary layer and distance from the leading edge to the midpoint of the transition zone, increases as Mach number increases above about 3. Heat loss from the surface by radiation and conduction has the effect - within certain limits - of increasing Re_t still further, the combined effect of Mach number and heat loss increasing Re_t typically by an order of magnitude between subsonic speeds and a Mach number of about 10. Yet another effect of Mach number on the laminar boundary layer is to decrease its sensitivity to roughness[15], - again, typically, for a flat plate the size of roughness necessary to have a significant affect on Re_t increases by an order of magnitude between subsonic speeds and $M_o = 5$.

For these reasons, hypersonic flight speeds offer the prospect of higher values of Re_t than those normally obtained at lower speeds, without special attention to surface finish.

On the basis of the very slender available evidence, a 'datum' value for Re_t of 10^7 will be assumed for the calculations in this study of skin friction drag at Mach numbers in the range 5-10, but in view of the many unknowns, and to illustrate the effect of variation of Re_t, two other values will be considered also in some cases. These are, an 'optimistic' Re_t of 2.5×10^7 and a very 'pessimistic' value of zero, - i.e. an all-turbulent boundary layer. For the cases considered in this Report, the ratio of wall temperature T_ω to boundary-layer recovery temperature T_r, calculated at a point just ahead of the transition zone, varies from about 0.5 at $M_o = 5$ and a relatively low attitude to about 0.2 at $M_o = 10$ at a relatively high altitude.

The datum Re_t of 10^7 is based on the results of experiments with flat plates having sharp, unswept leading edges in two-dimensional flow. Now although the flow over the surfaces of a caret wing having sharp leading edges is a close approximation to that on a two-dimensional flat plate, some rounding of the leading edge might be necessary to keep local temperatures in this region within practical limits, - and it is known that the combination of leading-edge rounding with sweepback can cause boundary-layer transition at or near the leading edge, this being attributed at low speeds[16] to so-called cross-flow instability. Criteria for estimating the critical leading-edge radius which just causes transition near the leading edge have been developed for low speeds, but although it is known that a similar phenomenon exists at supersonic and hypersonic speeds, the conditions under which it occurs at these speeds are not well understood. Topham[17] has correlated available experimental data from wind tunnels on heat transfer rates to yawed cylinders at hypersonic speeds up to $M_o = 10$. He suggests a method for calculating the critical cylinder radius below which heat transfer rates correspond to theoretical values for a laminar boundary-layer and above which the heating rates exceed the laminar values and hence, it is inferred, transition to turbulent flow has begun at the stagnation line. Topham's criterion, (which is nominally a critical Reynolds number of 130 based on stagnation-line conditions and the boundary-layer momentum thickness derived from velocity components parallel with the stagnation line), involves a knowledge of the velocity distribution near the stagnation line, in a plane normal to it. To make an estimate of critical leading-edge radius for the caret wing, a pressure distribution round the leading edge in this plane of the Newtonian type has been assumed

(as in Appendix D), since a correlation[18] of experimental results for yawed cylinders shows that this is a good approximation where the Mach number component normal to the stagnation line lies between 1.5 and 3.0 - the typical range for caret wings. Hence, the following values of the critical leading-edge radius, r_{crit}, have been calculated for caret wings of delta planform with $\alpha_U = 0$.

M_o	5	5	5	5	10	10	10	10
s/ℓ	0.2	0.2	0.3	0.3	0.2	0.2	0.3	0.3
C_{p_L}	0.06	0.10	0.06	0.10	0.05	0.08	0.05	0.08
r_{crit} (in) W/S = 25 lb/ft^2	0.6	1.2	0.6	1.2	0.8	1.5	1.0	1.8
r_{crit} (in) W/S = 50 lb/ft^2	0.3	0.5	0.3	0.5	0.4	0.7	0.5	0.8

Present indications are, then, that to achieve a significant proportion of laminar flow over the wing surfaces the leading-edge radius must be below - perhaps well below - these values. Recent studies[19] in Structures Department, R.A.E. suggest that in fact this is quite practical. Therefore the datum Re_t of 10^7 can be regarded as feasible, although a real degree of uncertainty must attach to any particular value, in view of the dearth of information on hypersonic transition.

Apart from its effect on skin-friction drag and hence on the ratio of lift to drag, the proportion of wing area on which the boundary layer is laminar has a direct effect on the kinetic-heating problem, since equilibrium temperatures in the laminar region are likely to be several hundred degrees lower than those in the turbulent region at the higher hypersonic speeds. For a given transition Reynolds number the proportion of laminar flow on one wing surface will depend on the length of the wing, Mach number, wing loading, lift coefficient and the division of lift between the two surfaces. Fig.3 shows an example for $\tau = 0.08$ and a wing loading of 25 lb/ft^2. Curves of S_{LAM}/S_S at $M_o = 5$, 7 and 10 are given for the upper and lower surfaces as a function of overall lift coefficient. Results are shown for three ways of varying C_L:-

(a) by varying upper-surface incidence with s/ℓ constant at 0.2

(b) by varying upper-surface incidence with s/ℓ constant at 0.3, and

(c) by varying s/ℓ with the upper-surface streamwise.

The ratio S_{LAM}/S_S is readily presented for an arbitrary transition Reynolds number Re_t, so while the curves shown apply to $Re_t = \sqrt{10^9 W}$ (i.e. $= 10^7$ for W = 100 000 lb), a correction chart is given for other values of Re_t. For the particular volume and wing loading chosen, the upper surface has roughly 50% more laminar flow than the lower. An important feature is that the area of laminar flow on both surfaces increases both with C_L and M_o. For flight at the higher Mach numbers where the kinetic heating problem is severe, it may be advantageous therefore to fly at a relatively high lift coefficient and slenderness ratio even if this implies an increase in drag above the minimum. This point is discussed further in Section 3.4.2.

2.4.2 Estimation of skin friction

The method used to estimate skin friction for each surface of the caret wing, in order to obtain the results discussed later in this Report, is fully described in Appendix C. Zero conduction into the wing surface has been assumed, heat loss being by radiation only, with emissivity = 0.8. Figs.C1 to C5 of Appendix C enable a rapid estimate to be made of skin friction for any constant pressure wing surface of delta planform, given the values of stream Mach number, surface pressure coefficient, altitude, overall length and transition Reynolds number.

Figs.4(a) and 4(b) present examples of the tangential-force coefficients due to skin friction, C_{FU} and C_{FL} for the upper and lower surfaces respectively, each based on the appropriate wetted area. Values are shown as functions of overall lift coefficient for M_o = 5, 7, and 10, and wing loadings of 25 and 50 lb/ft^2, assuming the 'datum' transition Reynolds number (10^7). It will be noted that there is typically a very large difference between the upper and lower surface values of friction-force coefficient which becomes more marked as Mach number increases. Changes in overall length and upper-surface incidence do not have a large effect, although the latter is favourable and would tend to reduce the variation in overall friction drag with C_L at constant τ and s/ℓ. A typical mean friction-force coefficient biased towards upper-surface values to take account of its greater wetted area would be 0.0012.

Some examples of the overall friction-drag coefficient (equation (12b)) have been calculated for the datum transition Reynolds number, and are

presented in Fig.5 as functions of C_L. The effect on C_{DF} is compared of varying C_L by varying, individually, α_U, s/ℓ and τ. It will be noted that C_{DF} is far from being independent of C_L and it is difficult to draw general conclusions regarding the trend of this variation. The increase of C_{DF} with increase of C_L is greatest if the latter is obtained by increasing τ. Changing C_L by changing s/ℓ at constant τ and α_U tends to produce the smallest variation in C_{DF}.

2.5 Parasite drag

In this study, arbitrary values have been postulated for C_{DP}, the parasite-drag coefficient based on plan area. The term parasite drag is here intended to cover the drag of fins, control surfaces, any base area not filled by the engine efflux, engine installation items not debited to net thrust, the drag penalty of rounding the wing leading edge to achieve an acceptable leading-edge heating rate, and the drag of miscellaneous excresences not included in this list. Clearly it is not possible to assign specific values to these quantities at this stage. Appendix D presents an approximate method for estimating the drag of a given amount of leading-edge rounding.

2.6 Maximum lift to drag ratio with $(C_{DF} + C_{DP})$ constant and $\alpha_U = 0$

Relatively simple expressions can be derived for the maximum lift to drag ratio developed by a caret wing at a given Mach number, and for the lift coefficient and incidence at which this occurs, if two conditions or constraints are specified. These are

(i) $(C_{DF} + C_{DP})$ is sensibly invariant with incidence (i.e. C_L) ,

(ii) the upper-surface incidence is always zero.

These conditions, particularly the second, impose restrictions on the generality of the results obtained and these will be discussed at the end of the analysis. It should be noted from the outset however that zero upper-surface incidence - which may be a desirable constraint because it ensures an orderly and predictable flow - has the result that variation of lift coefficient (i.e. lower-surface incidence) at a given Mach number implies variation of the volume coefficient τ and/or of the span/length ratio, in accordance with the relationship of equation (4) with $\alpha_U = 0$.

Denoting overall lift and drag with α_U zero by L_Z, D_Z, and neglecting the very small contribution to lift from the friction force on the lower-surface

equation (11) gives

$$C_{L_Z} = C_{p_L}$$

and therefore from equation (12c)

$$\frac{D_Z}{L_Z} = \frac{C_{DF} + C_{DP}}{C_{L_Z}} + \tan \alpha_L \qquad (19)$$

Substituting for $\tan \alpha_L$ from (17), we have for $\gamma = 1.4$

$$\frac{D_Z}{L_Z} = \frac{C_{DF} + C_{DP}}{C_{L_Z}} + \frac{C_{L_Z}}{2 - C_{L_Z}} \left[\frac{1 - 0.6\, C_{L_Z} - 1/M_o^2}{0.6\, C_{L_Z} + 1/M_o^2} \right]^{\frac{1}{2}} \qquad (20)$$

Hence, by differentiation with respect to C_{L_Z}, and with the first assumption listed above, viz that $(C_{DF} + C_{DP})$ is invariant with C_{L_Z}, it can be shown that $C^*_{L_Z}$, the lift coefficient for maximum ratio of lift to drag with $\alpha_U = 0$, is given by solutions of the equation

$$\frac{C^*_{L_Z}}{(C_{DF} + C_{DP})^{2/3}} = \frac{9.6^{1/3} \{1 + 5/(3 M_o^2 C^*_{L_Z})\}}{\{1 + 10/(3 M_o^2 C^*_{L_Z})\}^{2/3}} (1 + \delta) \qquad (21a)$$

where

$$(1 + \delta)^{3/2} = \frac{(1 + 0.3 M_o^2 C^*_{L_Z})(1 - 0.6 C^*_{L_Z} - 1/M_o^2)^{\frac{1}{2}} (1 - 0.5 C^*_{L_Z})^2}{(1 - 0.7 C^*_{L_Z} - 1/M_o^2)(1 + 0.3 M_o^2 C^*_{L_Z}) - 0.2 C^*_{L_Z}} . \qquad (21b)$$

Now for values of $C^*_{L_Z}$ less than 0.1 - and this will be found to be normally the case - and for Mach numbers in excess of 3, then $-0.04 < \delta < 0.04$. Therefore it is valid to regard the dependent variable on the L.H. side of equation (21a) as a function mainly of $M_o^2 C^*_{L_Z}$, Mach number itself being a second, much less important variable. Therefore we can write

$$\frac{C^*_{L_Z}}{(C_{DF} + C_{DP})^{2/3}} = \frac{M_o^2\, C^*_{L_Z}}{[M_o\,(C_{DF} + C_{DP})^{1/3}]^2} \simeq f\,(M_o^2\, C^*_{L_Z}) \simeq f[M_o\,(C_{DF} + C_{DP})^{1/3}]. \quad \ldots \quad (22)$$

In Fig.6, values of $C^*_{L_Z}/(C_{DF} + C_{DP})^{2/3}$ calculated from equation (21) have been plotted against $M_o\,(C_{DF} + C_{DP})^{1/3}$ for M_o = 3, 7 and 15. It can be seen that for all likely values of $(C_{DF} + C_{DP})$, - 0.0005 to 0.01 say - variation of M_o between 3 and 15 has only a very small effect on the relationship between $C^*_{L_Z}/(C_{DF} + C_{DP})^{2/3}$ and $M_o\,(C_{DF} + C_{DP})^{1/3}$. Further, for $M_o\,(C_{DF} + C_{DP})^{1/3} \geqslant 0.9$, the approximation

$$C^*_{L_Z} \simeq 2\,(C_{DF} + C_{DP})^{2/3}$$

gives $C^*_{L_Z}$ to an accuracy better than ±2%.

Maximum lift to drag ratio is readily obtained from equation (20) with $C_{L_Z} = C^*_{L_Z}$. In this case the appropriate approximation is

$$\left(\frac{L_Z}{D_Z}\right)_{max} (C_{DF} + C_{DP})^{1/3} \simeq f[M_o\,(C_{DF} + C_{DP})^{1/3}]$$

The exact relationship is plotted in Fig.7 and again Mach number itself has only a very minor effect. A good approximation to the results shown, for $0.5 < M_o\,(C_{DF} + C_{DP})^{1/3} < 2.5$ is

$$\left(\frac{L_Z}{D_Z}\right)_{max} \simeq \frac{0.62}{(C_{DF} + C_{DP})^{1/3}} + \frac{0.24}{M_o\,(C_{DF} + C_{DP})^{2/3}} \quad (23)$$

Finally, $(\alpha_L)^*_Z$, the lower-surface incidence for maximum lift to drag ratio with zero upper-surface incidence, is obtained from equation (19) in the form

$$\frac{(\tan \alpha_L)^*_Z}{(C_{DF} + C_{DP})^{1/3}} = \frac{1}{(L_Z/D_Z)_{max}\,(C_{DF} + C_{DP})^{1/3}} - \frac{(C_{DF} + C_{DP})^{2/3}}{C^*_{L_Z}} \simeq f[M_o\,(C_{DF} + C_{DP})^{1/3}]$$

Fig.8 shows the variation of $(\tan \alpha_L)^*_Z/(C_{DF} + C_{DP})^{1/3}$ with $M_o\,(C_{DF} + C_{DP})^{1/3}$

A useful result from the foregoing is that the product of the ordinates of Figs.7 and 8, viz $(\tan \alpha_L)^*_Z \times (L_Z/D_Z)_{max}$, does not vary rapidly with the

primary independent variable, $M_o\,(C_{DF} + C_{DP})^{1/3}$. The following table gives values of this product, along with $(L_Z/D_Z)_{max}/M_o$ obtained by dividing the ordinates of Fig.7 by $M_o\,(C_{DF} + C_{DP})^{1/3}$.

$M_o(C_{DF} + C_{DP})^{1/3}$	0.5	1.0	1.5	2.0
$(L_Z/D_Z)_{max}/M_o$	2.2	0.86	0.52	0.37
$(\tan \alpha_L)^*_Z\,(L_Z/D_Z)_{max}$	0.53	0.58	0.61	0.62

It is adequate to regard the interesting range of $(L_Z/D_Z)_{max}/M_o$ as 0.4-2.0 in the present context, from which we can conclude

$$(\tan \alpha_L)^*_Z\,(L_Z/D_Z)_{max} = 0.58 \pm 0.04 \qquad (24)$$

All the foregoing results apply strictly within the constraints imposed on the analysis, i.e. $(C_{DF} + C_{DP})$ invariant with C_L and upper-surface streamwise. Considering the first of these conditions. C_{DP} is an arbitrary allowance for extra-to-wing drag items and it is normal practice to regard these as essentially invariant at a given Mach number. C_{DF} on the other hand will in general vary with C_L, and although in principle this variation can be calculated from the data given in Appendix C - examples have already been given in Figs.5(a) and 5(b) - in practice this would complicate this analysis enormously. Hence constant values of C_{DF} have perforce to be assumed. Now, from the curves of C_{DF} presented in Figs.5(a) and 5(b) for streamwise upper-surface it can be seen that it is more nearly correct to assume a constant C_{DF} if C_L is changed by variation of s/ℓ at a given τ than by variation of τ at a given s/ℓ. Hence the analytical results derived above are best interpreted as applying to the case of a caret wing with streamwise upper-surface for which the value of τ is given, and α_L and C_L are changed by varying s/ℓ. It is in any case natural to regard τ as an independent variable, the value of which is determined essentially from considerations of stowage. So, with given values of M_o and τ and with an estimate of $(C_{DF} + C_{DP})$, $(\tan \alpha_L)^*_Z$ can be obtained from Fig.8 and this corresponds to a particular 'optimum' value of s/ℓ for the upper-surface streamwise case, given from equation (4) by

$$(s/\ell)^*_Z = \left\{\frac{(\tan \alpha_L)^*_Z}{3\tau}\right\}^2 \qquad (25)$$

The interpretation of this and indeed all the foregoing results in this section requires special care in view of the second constraint imposed on the analysis, i.e. that the upper-surface incidence shall be zero. The significance of this constraint can be understood best by reference to Fig.E2 of Appendix E which shows, for M_o = 5 and 10, both $(L/D)_{max}$ and L_Z/D_Z for a two-dimensional wedge as functions of wedge semi-angle ϑ and $(C_{DF} + C_{DP})$. Values of L_Z/D_Z for the caret wing correspond exactly to those of the wedge of semi-angle $\frac{1}{2}(\alpha_L)_Z$ having the same $(C_{DF} + C_{DP})$, and the maxima in the wedge L_Z/D_Z curves on Fig.E2 are precisely the values of $(L_Z/D_Z)_{max}$ for the caret given on Fig.7, and occur at $\vartheta = \frac{1}{2}(\alpha_i)^*_Z$ as given by Fig.8. The curves of $(L/D)_{max}$ on Fig.E2 refer to the maximum with respect to variation of incidence at a given semi-angle and $(C_{DF} + C_{DP})$, and these only coincide with the L_Z/D_Z curves where this optimum incidence happens to correspond to $\alpha_U \doteq 0$, (see Fig.E1). The $(L/D)_{max}$ values for wedges are not exactly the same as those for caret wings with the same $(C_{DF} + C_{DP})$ and $(\alpha_L - \alpha_U) = 2\vartheta$, because the anhedral on the caret reduces upper-surface lift at a given α_U. However, the general trend of $(L/D)_{max}$ will clearly be similar. In particular, for the highest $(L/D)_{max}$, $(\alpha_L - \alpha_U)$ should be reduced to a very low value, - less than 2° - so long as C_{DF} is not thereby increased. For given values of τ thought to be relevant to this study, this corresponds to extremely low values of slenderness ratio as given by equation (4), much lower than the minimum practical value as determined by low-speed considerations, i.e. about 0.2. Since Fig.5 shows that at Mach numbers of 7 and 10 there is not much variation in C_{DF} with s/ℓ down to 0.2, at these speeds the optimum slenderness ratio from the standpoint of lift to drag ratio when α_U is free to vary will be the minimum practicable value. At Mach 5 on the other hand, Fig.5 shows an appreciable increase in C_{DF} due to decreasing s/ℓ from 0.3 to 0.2; therefore the best slenderness ratio at this speed is likely to be in this range depending on the value of τ.

To sum up, the analytical results obtained in this section may be broadly interpreted as follows

(1) If $(s/\ell)^*_Z$ is less than the minimum practical value of 0.2 or thereabouts, then the best ratio of lift to drag is obtained with

this minimum slenderness ratio and with approximately zero upper-surface incidence, although this lift to drag ratio will be less than $(L_Z/D_Z)_{max}$ as given by Fig.7.

(2) If $(s/\ell)_Z^*$ is equal to or greater than the minimum practical value of around 0.2, the results of course apply to the case $\alpha_U = 0$ but $(L_Z/D_Z)_{max}$ will be significantly less than the best lift to drag ratio using upper-surface lift, with $s/\ell \simeq 0.2$ at $M_o = 7$-10 and $s/\ell \simeq 0.2$-0.3 at $M_o = 5$.

The following are some typical values of $(\tan \alpha_L)_Z^*$ derived from Fig.8 using typical skin-friction drag coefficients from Fig.5:-

M_o	5	7	10
C_{DF}	0.0038	0.0031	0.0026
$(\tan \alpha_L)_Z^*$ $C_{DP} = 0$	0.095	0.099	0.104
$(\tan \alpha_L)_Z^*$ $C_{DP} = 0.001$	0.105	0.113	0.120

Taking $(\tan \alpha_L)_Z^* = 0.105$ as typical, from equation (25) $(s/\ell)_Z^* > 0.2$ if $\tau < 0.08$ or thereabouts. Hence if $\tau < 0.08$, restriction to $\alpha_U = 0$ would cause a loss in lift to drag ratio. If $\tau \geq 0.08$, optimum α_U is near to zero but a minimum practical slenderness ratio of 0.2 involves some sacrifice in lift to drag ratio. These points are illustrated further in Section 3.2.

3 REVIEW OF FACTORS AFFECTING DRAG

3.1 Slenderness ratio and volume coefficient

In this and the next section the effects of variation of the geometrical variables τ, s/ℓ and α_U on the lift to drag ratio at particular Mach numbers are considered; this section deals with variation of τ and s/ℓ with the upper-surface streamwise, the next with variation of α_U at particular values of τ and s/ℓ. In both cases, the effect of variation of the surface friction coefficients is excluded - to reduce the number of variables affecting the results - by assuming an arbitrary constant value of 0.001 for both C_{FU} and C_{FL}.

Lift to drag ratio with $\alpha_U = 0$ has been plotted against s/ℓ in Figs.9(a) to (c) and against C_L in Figs 10(a)-(c), for Mach numbers 5, 7 and 10 in each case. These results show the rapid fall-off in L_Z/D_Z as s/ℓ is reduced

below the value for $(L_Z/D_Z)_{max}$ at a given τ, which has already been discussed in Section 2.6; this is in effect the penalty for not making use of upper-surface lift. Also evident is the decrease in optimum slenderness ratio below a practical lower limit of 0.2 when τ exceeds 0.08.

Due to variation in wetted area these results do not correspond exactly to the constant C_{DF} case treated analytically in Section 2.6. However, if we take for $C_F = 0.001$ an approximate mean C_{DF} of 0.0025, Fig.8 and equation (25) give for $\tau(s/\ell)^*_Z$, 0.026, 0.030 and 0.034 at Mach numbers 5, 7 and 10 respectively. These values agree closely with those shown on Figs.9(a)-(c) on the envelope curves of lift to drag ratio vs slenderness ratio. This is to be expected since for a given slenderness ratio, C_{FU} and C_{FL}, the variation of C_{DF} with τ is small.

Fig.11 shows maximum ratio of lift to drag plotted against volume coefficient, the maximum being with respect to variation of slenderness ratio at constant volume coefficient unless this occurs at $s/\ell < 0.2$, in which case the value at $s/\ell = 0.2$ is plotted. The appropriate values of s/ℓ are shown on the curves. This picture underlines the importance of τ as the main geometrical variable, the decreasing importance of Mach number as τ increases, and the need for low values of slenderness ratio if $\tau \geq 0.06$.

3.2 Upper-surface incidence

In the preceding section and in 2.6, the constraint is imposed of assuming the upper-surface to be aligned in the free stream direction, so that variation of C_L implies variation of either τ or s/ℓ. If we now allow α_U to vary, C_L can be regarded as an additional, independent variable and for given values of M_o, τ, s/ℓ, C_{FU}, C_{FL} and C_{DP}, maximum lift to drag ratio does not necessarily occur when α_U is zero.

In Figs.12(a)-12(c), lift to drag ratio for caret wings at Mach numbers of 5, 7 and 10 has been plotted against C_L, assuming $C_{FU} = C_{FL} = 0.001$ as in Figs.9 and 10, $C_{DP} = 0$ and (in some cases) 0.002, and various values of τ and s/ℓ, incidence now being free to vary independently. These results confirm the expectation from the wedge calculations of Appendix E, already discussed in Section 2.6, that restriction of α_U to zero involves a significant loss in lift to drag ratio only if $(\alpha_L - \alpha_U) < 6^\circ$-$7^\circ$ depending on C_{DP}, i.e. from equation (4), and assuming $s/\ell = 0.2$, if $\tau < 0.08$-0.09. It will also be noted that making α_U a variable enhances the favourable effect of a low

slenderness ratio at a given τ. The best slenderness ratio for maximising L/D at constant C_{FU} amd C_{FL} is the minimum practical value of 0.2 in all cases considered except $M_o = 5$ and $\tau = 0.06$, for which $s/\ell = 0.25$ is marginally better.

Fig.13 shows maximum lift to drag ratio vs τ where the maximum is with respect to variation of both α_U and s/ℓ, but again with the proviso that $s/\ell \geq 0.2$. The corresponding curves from Fig.11 for $\alpha_U = 0$ are also shown for comparison. With α_U varying, the effect of τ is even greater than if $\alpha_U = 0$. Oddly enough, the favourable effect of upper-surface lift at low τ is greater at the higher Mach numbers.

A point which emerges from Fig.12 is that at lift coefficients considerably greater than those for maximum lift to drag ratio, as it varies with α_U, variation of slenderness ratio at constant τ and C_L has little effect on L/D. This raises the question, if it is required to use a lift coefficient appreciably in excess of that corresponding, say, to $\alpha_U = 0$ (for example, in order to reduce surface temperatures), what are the relative merits of achieving this by (a) increasing α_U, (b) increasing s/ℓ or (c) by increasing τ? Figs.14(a) and 14(b) answer the question for $\tau = 0.08$, $s/\ell = 0.2$ and 0.3. In all cases, variation of upper-surface incidence is significantly superior to the other ways of increasing C_L for given values of C_{FU} and C_{FL}, and since upper-surface incidence tends to reduce C_{FU} (see Fig.4) this result is likely to be valid also for actual, as distinct from arbitrary values of skin friction force coefficients. However, Fig.14 considers the case of variation of the three geometric parameters separately; it is clear from Fig.12 that increasing s/ℓ has little or no adverse effect, provided α_U is increased as well. A higher value of slenderness ratio may be advantageous, if high lift coefficients can be developed, in increasing the proportion of laminar flow by reducing overall length.

3.3 Mach number

Considering next the effect of free-stream Mach number on drag, this can be approached in several ways according to the constraints imposed on the relevant variables.

The simplest case is that treated theoretically in Section 2.6 in which the upper-surface is maintained streamwise and it is postulated that $(C_{DF} + C_{DP})$ is independent of C_L at a given Mach number. Fig.15 shows maximum lift to drag ratio calculated with these assumptions, plotted

against Mach number for a range of values of $(C_{DF} + C_{DP})$. It will be noted that maximum L_Z/D_Z at constant $(C_{DF} + C_{DP})$ falls markedly as Mach number increases, a typical example being $(C_{DF} + C_{DP}) = 0.0030$, for which $(L_Z/D_Z)_{max}$ decreases by over 17% between $M_o = 5$ and $M_o = 10$.

For the purpose of showing the effect of Mach number on drag, the above results are misleading inasmuch as they take no account of the fact that for given values of τ, s/ℓ and plan area, wetted area falls as Mach number increases, and hence for this reason alone, C_{DF} will decrease also. Further, for some values of τ, the slenderness ratios implied by the results on Fig.15 are below the minimum practical value. Fig.16 which shows maximum lift to drag ratio vs Mach number for given values of τ assuming surface-friction coefficients C_{FU} and C_{FL} constant and equal to 0.001 takes account of these points. These curves have been obtained by cross-plotting from the results already discussed in Sections 3.1 and 3.2. The upper figure is for a streamwise upper surface, the lower shows values at the optimum upper-surface incidence; in both cases the lift to drag ratio shown is the maximum as it varies with slenderness ratio, subject to the restriction that this is never less than a lower practical limit of 0.2. A noticeable feature of these results is that the decrease of maximum lift to drag ratio with Mach number is much less than that shown on the previous figure, for the reasons already given. With $\alpha_U = 0$, maximum L_Z/D_Z decreases between Mach numbers of 5 and 10 by about 10% if $\tau = 0.06$, by 6% if $\tau = 0.08$, and by only 3% if $\tau = 0.10$. Allowing the upper surface to take up the best incidence reduces slightly the variation with Mach number for those cases affected.

The above results apply if C_{FU} and C_{FL} are constant. However, Fig.4 shows that there are considerable variations of these coefficients with both Mach number and lift coefficient. The effect of this on lift to drag ratio is presented on Fig.17 for a particular example, $\tau = 0.08$, $C_{DP} = 0$, and a wing loading of 25 lb/ft^2, friction being calculated for the 'datum' transition Reynolds number of 10^7, (see Section 2.4.1). The upper graph of Fig.17 shows the variation with Mach number of (a) the friction-drag coefficient as given by Fig.5(a) for the case τ constant and slenderness ratio varying and (b) the variation with Mach number of the wave-drag coefficient $C^*_{L_Z}$ $(\tan \alpha_L)^*_Z$. The lift coefficient for maximum lift to drag ratio $C^*_{L_Z}$ has been obtained in

this case by starting with the theoretical value given by Fig.6 (which applies strictly to constant C_{DF}), then increasing this by small steps to find the optimum. Having determined $C^*_{L_Z}$ - shown on the upper graph for M_o = 5, 7, 10 - the corresponding slenderness ratio was calculated, and was found to be approximately 0.2 at all Mach numbers, i.e. about the minimum practical value. Both friction and wave drag fall as Mach number increases, as does $C^*_{L_Z}$, the net result being that maximum lift/drag, shown on the lower graph, falls by only 3% between M_o = 5 and M_o = 10. This can also be inferred from Fig.15 by taking appropriate values of C_{DF} from Fig.5(a). It happens that the results shown on Fig.17 also apply to the case of an all-turbulent boundary layer with a wing loading of 50 lb/ft^2; in fact the general conclusion may be drawn that variations in maximum L/D with Mach number in the range 5-10 are, typically, small.

Finally, it is argued in Appendix A that in considering the effect of speed on airframe cruise efficiency, the weight to drag ratio is a more relevant criterion than the lift to drag ratio, where

$$\frac{W}{D} = \frac{L/D}{L/W} \doteq \frac{L/D}{1 - (M_o/26)^2} \qquad (26)$$

the factor L/W being the effect of the Earth's curvature in reducing the aerodynamic lift required to support the vehicle at a given speed. Maximum W/D, also shown on the lower graph of Fig.17, increases continuously with Mach number from M_o = 5 upwards.

To sum up, increasing Mach number tends to improve the aerodynamic efficiency criterion W/D, and slenderness ratios in the range 0.2-0.25 seem to be the optimum for volume coefficients of 0.08 or thereabouts.

3.4 Skin friction

3.4.1 Arbitrary skin friction

To gain some idea of the importance of skin friction, weight to drag ratios with zero upper-surface incidence are presented in the following table for three arbitrary values of friction-force coefficient, -0, 0.001 and 0.002, assumed to be the same on both upper and lower-surfaces. Two cases are considered; a caret wing with τ = 0.08, and s/ℓ = 0.02, and the two-dimensional wedge which has the same lower-surface incidence as the caret wing. The

latter can be regarded as an equivalent 'ideal' wing with the same planform, section and volume as the caret, but with zero anhedral and yet pressures on the lower-surface corresponding to two-dimensional flow, as on the caret.

$$\tau = 0.08,\ s/\ell = 0.2,\ \alpha_U = 0,\ C_{DP} = 0$$

C_{FU} and C_{FL}		0	0.001	0.002
W/D_Z caret	$M_o = 5$	9.7	6.55	4.9
W/D_Z wedge	$M_o = 5$	9.7	7.35	5.9
W/D_Z caret	$M_o = 10$	11.0	6.85	5.0
W/D_Z wedge	$M_o = 10$	11.0	7.4	5.6

Since the upper-surface incidence is here presumed to be zero, the only difference between the ideal wedge and the caret wing from the point of view of lift and drag for given values of C_{FU} and C_{FL} is the greater surface area of the caret. For friction coefficients in the range 0.001-0.002, this surface area penalty reduces the weight to drag ratio of the particular caret considered by 0.8-1.0 at Mach 5, and by 0.55-0.6 at Mach 10. The effect of a friction coefficient of 0.001 is to reduce the weight to drag ratio by about a third compared with the wing in inviscid flow. This large effect underlines the necessity for including calculated rather than arbitrary values of skin friction drag in weight to drag ratio estimates. This is done in Section 3.4.2 below.

An effect of increasing the friction-force coefficient from 0.001 to 0.002 is to increase slightly the optimum slenderness ratio for best weight to drag ratio at given values of τ. Thus, if $\tau = 0.08$ and $M_o = 7$, $s/\ell = 0.25$ is better than 0.2 if the friction coefficient is 0.002, but not if it is 0.001.

3.4.2 Calculated skin friction

The skin-friction drag coefficient for a caret wing with fixed τ, s/ℓ, length and Mach number depends on the lift coefficient (i.e. α_U) wing loading W/S and transition Reynolds number Re_t. Figs 18(a), (b), (c) show W/D vs C_L

at Mach numbers 5, 7, 10 respectively, for a caret wing having $\tau = 0.08$, $s/\ell = 0.2$ and zero parasitic drag, where friction drag has been calculated by the method described in Appendix C. On each figure, curves are shown for the three assumptions concerning transition mentioned in Section 2.4.1, the middle curve in each case representing an average 'datum' value, the upper one an optimistic and the lower a pessimistic value. The two groups of curves on each figure are for two wing loadings, 25 lb/ft^2 on the left, 50 lb/ft^2 on the right. Also shown on the figures, as numbers above and below the line for upper and lower-surfaces respectively, are the percentage areas of each surface covered by a laminar boundary layer. Surface temperatures at a point 10 ft behind the leading edge in the laminar flow region and 10 ft behind the nominal transition line in the turbulent flow region are shown in the boxes at each end of the C_I/EAS scale, the first number referring to the laminar, the second to the turbulent region, upper and lower numbers applying to upper and lower wing surfaces.

The following points emerge from a study of these results:-

(a) Weight to drag ratio at a given wing loading increases with Mach number, not only the maximum values as anticipated in Section 3.3 , but also values at a given EAS below that for maximum W/D.

(b) Increasing Mach number and lift coefficient at a given wing loading both increase the percentage area of laminar flow on each surface. With $Re_t = 10^7$, a wing loading of 25 lb/ft^2, $M_o = 10$, $C_L \geq 0.08$ and $\ell = 100$ ft, the whole of the upper-surface and more than 2/3 of the lower-surface is covered by a laminar boundary layer, the associated surface temperatures in the laminar region being 600°C or less, and the weight to drag ratio about 6. At this relatively high C_L, it would probably be advantageous to increase s/ℓ and thus decrease overall length.

(c) Increasing wing loading from 25 lb/ft^2 to 50 lb/ft^2 increases W/D if $Re_t < 12 \times 10^6$, reduces it if $Re_t > 12 \times 10^6$.

(d) The area of laminar flow on the upper-surface is roughly 50% greater than that on the lower for the 'datum' transition case.

(e) At the particular volume coefficient and slenderness ratio considered, the weight to drag ratio with upper-surface streamwise is less than 3% below the maximum for a given wing loading, Mach number and Re_t. Increasing α_U does however reduce EAS and the mean surface temperatures, and could be important on this account.

3.5 Parasite drag

It is probably true to say that the sum of the parasite drag items listed in Section 2.5 constitute the biggest area of uncertainty in the estimation of lift to drag ratio for a hypersonic aircraft. Considering the main items in turn, if a fin area of roughly 10% of wing plan area is required - which is typical of conventional aircraft - this would account for about 0.0005 in C_{DP} at $M_o = 5$ decreasing to about half that value at $M_o = 10$. It could well be less than this however, and until the lateral characteristics of caret wing configurations over the whole speed range have been studied no better estimate can be made. The penalties in lift and drag of blunting the leading edges have been evaluated in Appendix D and it is shown there that if radii as large as the critical for leading-edge transition have to be used these are equivalent to parasite drag coefficients varying between 0.0003 and 0.001. However, much smaller leading-edge radii may be structurally feasible. Even more difficult to estimate is the base drag contribution since this depends on the effective nozzle area, which will vary between climb, cruise and glide phases of the flight. The ratio of base to reference area is $3\tau\ (s/\ell)^{\frac{1}{2}}$, so for a typical wing having $\tau = 0.08$ and $s/\ell = 0.2$, and assuming the base pressure coefficient suggested in Ref.7, then if fraction b of the total base area is not filled by the efflux, the base parasite drag coefficient is $0.15b\ (1/M_o^2 - 1/M_o^3)$. The maximum value of this (i.e. b = 1, appropriate to gliding flight) would therefore be as high as 0.0048 at $M_o = 5$ falling to 0.0014 at $M_o = 10$. For cruising flight $b \ll 1$, and much smaller values would be appropriate. Until specific studies of propulsion and flight trajectories are made it will clearly not be possible to assign realistic values to base drag coefficient. Sundry excrescences, controls etc are another unknown. Thus the aggregate C_{DP} for cruising flight might be as low as 0.001 or even less, or as great as 0.002 or more, with a tendency to fall as M_o increases.

Figs.12(a) to (c) show the effect of a parasite drag coefficient C_{DP} of 0.002, which is typically to reduce $(L/D)_{max}$ by about unity, and to increase the lift coefficient at which this is obtained by about 0.015. Variation of C_{DP} does not affect optimum slenderness ratio significantly.

It can easily be shown that the decrease in lift to drag ratio due to parasite drag, at a given C_L is approximately equal to $C_{DP} \times (L/D)_o^2/C_L$, where $(L/D)_o$ is the lift to drag ratio at $C_{DP} = 0$.

4 POSSIBLE FURTHER WORK

The foregoing study constitutes only a small preliminary part of the work which would be necessary to establish the potentialities of hypersonic air-breathing vehicles. Items of work which are essentially continuations of that described herein, and which would be required for an overall assessment, are as follows:-

(a) A wider range of speeds, weights and basic configurations would be considered; the latter might include double carets, non-delta planforms, curved upper surfaces and non-planar shocks.

(b) The effects of adding propulsion systems to the wing should of course be investigated. These could be limited in the first instance to cruise propulsion and later extended to systems for acceleration and cruise. A range of flow cycles with heat addition from various fuels could be studied, together with their effect on airframe volume requirements.

(c) In association with (a) and (b) above, the effects of flight profile on overall range performance would have to be established, particular attention being paid to airfield performance and transonic acceleration capability.

(d) Finally, these preliminary assessments would lead into more detailed considerations of layout, weights, balance and stowage and also of the problems of stability and control over the whole speed range. At this stage also, a review of the formidable propulsion, structural and mechanical design problems would be necessary.

Besides suggesting lines of further study as outlined above, the present Report has highlighted certain aspects of basic hypersonic aerodynamics where new data and a better understanding would benefit future assessment work. These include the following:-

(a) Criteria for boundary layer transition are required at Mach numbers up to at least 10, taking into account effects of blunted and swept leading edges, surface roughness, heat transfer and pressure gradients. Free flight experiments in addition to wind tunnel tests are desirable - if not essential - for this.

(b) The characteristics of upper-surface flow fields requires further investigation, including effects of vortices, shocks and viscous interaction.

(c) Methods would be required for the reliable prediction of the lift and drag of simple hypersonic aircraft configurations at off-design conditions, and also for calculating other forces and moments relevant to problems of flight dynamics.

5 CONCLUSIONS

(1) In order to demonstrate one aspect of the relationship between the geometry and aerodynamic characteristics of a hypersonic aircraft, a simple case has been chosen which exhibits the essential features, i.e. the caret wing at its design condition. The lift and drag of families of such wings have been calculated for the Mach number range 5-10 in terms of three independent geometrical variables, volume coefficient = volume/(plan area)$^{3/2}$, slenderness ratio = semispan/length, and upper-surface incidence. In order to calculate skin friction drag, particular values of wing loading have been chosen, and certain criteria have been assumed for boundary layer transition. It is important to note that valid comparisons between different hypersonic aircraft configurations must take account of any differences between these, or related, parameters.

(2) The volume coefficient τ is the most significant geometric parameter affecting maximum lift to drag ratio, L/D. At low values of τ (less than about 0.09), maximum L/D is obtained with lift developed on the upper as well as the lower surface, and constraining the upper surface to be streamwise causes appreciable loss in L/D at all Mach numbers. With increase of τ, the upper-surface incidence for maximum L/D falls, and is about zero for $\tau \geq 0.09$. The slenderness ratio s/ℓ for maximum L/D is about 0.3 at $\tau = 0.06$ and $M_o = 5$, decreasing as M_o and τ increase, so that in general for maximum lift to drag ratio, the best slenderness ratio is close to the minimum likely to be dictated by considerations of low speed handling.

(3) The lift coefficient for maximum L/D increases slightly with increase of τ, and decreases slightly with increase of M_o, its value being typically within the range 0.05-0.07 for most practical configurations.

(4) If it is required to use a lift coefficient in excess of that for maximum L/D (e.g. to increase the area of laminar flow on the wing surfaces), then an increase in upper-surface incidence α_U, either alone or in combination with some increase in s/ℓ, is superior to increasing either τ or s/ℓ with α_U constant.

(5) Wide variations in skin friction and heating can result from different operating conditions, and assumptions regarding transition location. In particular:-

(i) Increasing Mach number and increasing lift coefficient (at a given wing loading) both increase the percentage area of laminar flow on each surface. The area of laminar flow on the upper-surface is typically 50% greater than on the lower surface (for the assumption of $Re_t = 10^7$). All-laminar boundary layers on both surfaces is a feasible prospect for a small (W = 50000 lb) aircraft with a low wing loading for cruise ($W/S = 25$ lb/ft^2) at a Mach number of about 10; the associated surface temperatures would be 600°C or less.

(ii) The skin-friction force coefficient on the upper surface is appreciably less than that on the lower surface, the difference becoming more marked as Mach number and lift coefficient increase.

(iii) With increase of Mach number, a favourable variation of wetted area and skin friction drag coefficient opposes the unfavourable variation of wave drag, with the result that L/D is approximately invariant with Mach number for the range considered, i.e. M_o of 5-10. Thus the aerodynamic efficiency factor W/D increases continuously from Mach 5 upwards.

(iv) The use of an arbitrary value for skin friction force coefficient (0.001 is commonly used) may be misleading, since it has been shown that there are large variations in skin-friction force coefficient with Mach number, incidence and wing loading, as well as large differences between values for the upper and lower surfaces of the wing.

(6) Reducing wing loading from 50 to 25 lb/ft^2 reduces the equilibrium skin temperatures in both the laminar and turbulent region on the wing surfaces, and increases the area of laminar flow. The effect of wing loading on W/D depends on the size of the aircraft and the value of transition Reynolds number; for example, it has been calculated that for a wing of 100 ft root chord, reduction of wing loading from 50 to 25 lb/ft^2 reduces W/D for $Re_t < 12 \times 10^6$, and increases it for $Re_t > 12 \times 10^6$.

(7) Only in the case of zero upper-surface incidence, and skin-friction drag coefficient invariant with lower-surface incidence, is it possible to derive simple theoretical expressions for maximum L/D and the lift coefficient at which it is obtained. For all other conditions, numerical

calculations are required to obtain a clear picture of the effects of variation in Mach number and geometry.

(8) The precise value to assign to the parasite drag items (viz:- drag due to fins, leading edge blunting, base area and miscellaneous excrescences) constitutes a large area of uncertainty in the estimation of L/D. The range of possible values of C_{DP} might well be equivalent to a 15% variation in maximum L/D, with the likelihood of higher values at the lower Mach numbers.

Appendix A

AERODYNAMIC EFFICIENCY CRITERIA FOR HYPERSONIC LONG RANGE AIRCRAFT
(See Section 1)

For long range hypersonic aircraft, consideration must be given to the contribution to range from the acceleration, cruise and deceleration phases of the flight trajectory. To obtain estimates of range, assumptions must be made regarding the type of fuel and the amount that can be carried, the performance of the propulsion unit, the aerodynamic efficiency of the vehicle, and the form of the flight trajectory.

In this Appendix, the discussion is limited to that of aerodynamic efficiency. Conventionally, this efficiency is expressed by the ratio of lift to drag, but as will be shown below this criterion is insufficient for high flight speeds when the curvature of the vehicle's flight path (due to the curvature of the Earth) is taken into account.

(a) Acceleration phase

Equating forces along the flight path,

$$F = D + \frac{W}{g}\frac{dV_o}{dt} + W \sin \gamma \qquad (A1)$$

While normal to the flight path,

$$L = W \cos \gamma - \frac{WV_o^2}{\mathcal{R} g} \simeq W\left(1 - \frac{V_o^2}{\mathcal{R}_o g}\right) = W\left(1 - \frac{V_o^2}{V_S^2}\right) \qquad (A2)$$

where F = net thrust
L = lift
D = drag
W = weight
V_o = speed
$\mathcal{R}$ = radius of flight path
$\mathcal{R}_o$ = earth radius
V_S = satellite speed
γ = angle of climb.

Combining equations (A1) and (A2), putting $T = -\frac{1}{\sigma}\frac{dW}{dt}$, and neglecting the small effect of the angle of climb, we get

$$\frac{1}{W}\frac{dW}{dt} = -\sigma\left[\frac{1}{g}\frac{dV_o}{dt} + \frac{(1 - V_o^2/V_S^2)}{(L/D)}\right] \qquad (A3)$$

where σ = specific fuel consumption.

Thus the instantaneous value of the aerodynamic efficiency is given by $(L/D)(1/1 - V_o^2/V_S^2)$, which from equation (A2) we find is equal to the ratio weight/drag. The <u>mean</u> value of the aerodynamic efficiency during the acceleration phase will clearly depend on the variation of L/D and dV_o/dt over this part of the flight trajectory, but a simple solution to equation (A3) can be obtained for the case of constant (L/D) and constant acceleration $dV_o/dt = ng$. Thus

$$\log_e\left(\frac{W_1}{W_2}\right) = \frac{\bar{\sigma}_A V_C}{n g}\left[n + \frac{(1 - V_C^2/3V_S^2)}{(L/D)}\right] \qquad (A4)$$

where V_C = cruise speed

$\bar{\sigma}_A$ = average s.f.c. for the acceleration phase

suffix 1 = initial conditions $(V_1 = 0)$

2 = final conditions $(V_2$ = cruise speed $V_C)$

The range covered during the acceleration phase, if the acceleration is constant, is given by

$$R_A = \frac{V_C^2}{2ng} \qquad (A5)$$

or

$$R_A = \frac{V_C}{2\bar{\sigma}_A}\left[\frac{(L/D)}{n(L/D) + (1 - V_C^2/3V_S^2)}\right]\log_e\left(\frac{W_1}{W_2}\right) \qquad (A6)$$

Thus the mean value of the aerodynamic efficiency during the acceleration phase, for the case of constant L/D and acceleration, is $(L/D)/(1 - V_C^2/3V_S^2)$

(b) Cruise phase

Now the familiar Breguet range equation for an aircraft cruising at constant speed is

$$\text{Cruise range } R_C = \frac{V_C}{\sigma_C} \frac{L}{D} \log_e \frac{W_2}{W_3}$$

where suffices 2 and 3 refer to initial and final conditions for the cruise phase, respectively ($V_2 = V_3 = V_C$).

This equation is obtained from

$$R_C = \int_2^3 V_2 \, dt = -\int_2^3 \frac{V_C}{\sigma_C} \frac{dW}{T} = -\int_2^3 \frac{V_C}{\sigma_C} \frac{L}{D} \frac{dW}{L} \qquad (A6)$$

with the following assumptions

(i) That $\frac{V_C}{\sigma_C} \frac{L}{D}$ is a constant.

(ii) That the speed is low enough for the difference between lift and weight to be ignored (i.e. $L \simeq W$).

It can be shown that assumption (i) remains substantially valid for hypersonic speeds. But the second assumption is obviously invalid (see equation (A2)), since it leads to errors in excess of 5% at Mach numbers above about 6.

Substituting the value for lift from equation (A2) in equation (A6) we get, after integration

$$R_C = \frac{V_C}{\sigma_C} \frac{(L/D)}{(1 - V_C^2/V_S^2)} \log_e \frac{W_2}{W_3} \qquad (A7)$$

or

$$R_C = \frac{V_C}{\sigma_C} \frac{W}{D} \log_e \frac{W_2}{W_3} \qquad (A8)$$

Thus the weight/drag ratio is the important airframe efficiency criterion for cruising flight.

(c) Glide phase

Equating forces along the flight path, assuming zero thrust, we get

$$0 = D + \frac{W}{g} V_o \frac{dV_o}{dR} - W \sin \gamma \qquad (A9)$$

Combining equation (A9) with (A2), and neglecting the small effect of the angle of descent*, we get

$$dR = -\frac{1}{g}\left(\frac{L}{D}\right) \frac{V_o \, dV}{1 - V_o^2/V_S^2} \qquad (A10)$$

Integration of equation (A10) for a glide from the cruise speed V_C to zero speed, at a constant L/D, gives the glide range, R_G as

$$R_G = \frac{V_S^2}{2g}\left(\frac{L}{D}\right) \log_e \left(\frac{1}{1 - V_C^2/V_S^2}\right) \qquad (A11)$$

i.e.

$$R_G = \frac{V_C^2}{2g}\left(\frac{L}{D}\right)\left[1 + \tfrac{1}{2}\left(\frac{V_C^2}{V_S^2}\right) + \tfrac{1}{3}\left(\frac{V_C^2}{V_S^2}\right)^2 + \ldots\right] \qquad (A12)$$

The deceleration during a glide at constant L/D will vary, thus from equation (A9)

$$V \frac{dV}{dR} = -g \frac{(1 - V_o^2/V_S^2)}{(L/D)} \qquad (A13)$$

Thus the mean value of the aerodynamic efficiency during the glide phase, for the case of constant L/D, is

$$\left(\frac{L}{D}\right)\left[1 + \tfrac{1}{2}\left(\frac{V_C^2}{V_S^2}\right) + \tfrac{1}{3}\left(\frac{V_C^2}{V_S^2}\right)^2 + \ldots\right]$$

---

* Neglecting the term W sin γ in both the acceleration and glide phases virtually eliminates the error.

Appendix B

APPROXIMATIONS FOR THE PRESSURE BEHIND A PLANE SHOCK OR A PRANDTL-MEYER EXPANSION

(See Section 2.3)

No explicit relations exist which give the pressure behind a single, plane shock or following a Prandtl-Meyer expansion in terms of upstream Mach number and flow turning angle. In many cases, e.g. the present study, incidence is virtually specified as an independent variable, and the lack of an adequate direct method for calculating the surface pressure is inconvenient. Accordingly, to simplify the computation required for the results presented in this Report, the following approximate relations were developed and used, and their accuracy and ranges of applicability assessed by comparison with exact values.

Pressure behind a plane, oblique shock

From the oblique shock equations[12], the following relation can readily be obtained between the shock angle ζ, the turning angle (i.e. incidence) α and the upstream Mach number M_o

$$M_o^2 \sin^2 \zeta - \frac{\gamma + 1}{2} \frac{M_o \sin \zeta \, M_o \sin \alpha}{\cos (\zeta - \alpha)} - 1 = 0$$

Hence for $\alpha \to 0$

$$\sin \zeta = \frac{1}{M_o}$$

and

$$\cos \zeta = \frac{\beta_o}{M_o}$$

where

$$\beta_o = \sqrt{M_o^2 - 1} \ .$$

Now if the approximation is made that

$$\cos (\zeta - \alpha) \simeq \cos (\zeta - \alpha)_{\alpha \to 0} = \frac{\beta_o}{M_o} \qquad \text{(B1)}$$

i.e. that the cosine of the angle between the shock and the surface behind the shock is invariable with α then

$$M_o^2 \sin^2 \zeta - \frac{\gamma + 1}{2} \frac{M_o^2}{\beta_o} \sin \alpha \, M_o \sin \zeta - 1 \simeq 0$$

Hence,

$$M_o \sin \zeta \simeq \frac{\gamma + 1}{4} \frac{M_o^2}{\beta_o} \sin \alpha + \sqrt{1 + \left(\frac{\gamma + 1}{4} \frac{M_o^2}{\beta_o} \sin \alpha \right)^2}$$

or, writing $$\eta = \frac{\gamma + 1}{4} \frac{M_o^2}{\beta_o} \sin \alpha$$

$$M_o \sin \zeta \simeq \eta + \sqrt{1 + \eta^2} \qquad \text{(B2)}$$

Now from the oblique shock relations

$$M_o^2 C_p = \frac{4}{\gamma + 1} (M_o^2 \sin^2 \zeta - 1)$$

Hence,

$$M_o^2 C_p \simeq \frac{8}{\gamma + 1} \left\{ \eta^2 + \eta \sqrt{1 + \eta^2} \right\} \qquad \text{(B3)}$$

or

$$\frac{\beta_o C_p}{2 \sin \alpha} \simeq \eta + \sqrt{1 + \eta^2} \qquad \text{(B3)}$$

Equation (B3) with M_o instead of β_o and α instead of $\sin \alpha$ is sometimes known as the hypersonic approximation (e.g. Ref.20), in which form it is commonly regarded as being valid only for large M_o and small α. The range of useful accuracy of the approximation in the form given by equation (B3) is rather wider than this would imply however. Fig.B1 shows the ratio of the exact pressure coefficient to that given by equation (B3) for a range of Mach numbers and turning angles, with $\gamma = 1.4$. For Mach numbers below 3 the approximation gives pressure to within 2% for angles up to about 7° below that for shock detachment, and for Mach numbers of 3 or above this accuracy is maintained for angles up to at least 29°.

For $M_o = \infty$ the exact solution for pressure coefficient is

$$C_p\ (M_o=\infty) = \frac{2}{\gamma+1}\left\{1 + \gamma \sin^2\alpha - \sqrt{1 - (\gamma^2+1)\sin^2\alpha + \gamma^2 \sin^4\alpha}\right\} \quad (B4)$$

whereas the value given by equation (B3) is

$$C_p\ (M_o=\infty) \doteq (\gamma+1)\sin^2\alpha \quad (B5)$$

Equation (B4) reduces to (B5) for small $\sin^2\alpha$, and gives values within 1% of equation (B5) for angles up to 25°.

The accuracy of equation (B3) for moderate angles can be improved considerably by a relatively simple modification. In the so-called Busemann expansion (Ref.12, equation (152)) for pressure coefficient as a series in powers of α, the coefficient of α^2 is

$$B = \frac{(\gamma+1)M_o^4 - 4\beta_o^2}{2\beta_o^4}$$

Equation (B3) may be modified so that the coefficient of $\sin^2\alpha$ in the expansion of C_p as a series in $\sin\alpha$ is the same as the Busemann coefficient of α^2, (the coefficients of $\sin\alpha$ and α are of course already the same), by writing

$$M_o^2 C_p \doteq \frac{8}{\gamma+1}\left\{\eta^2(1-\varepsilon) + \eta\sqrt{1+\eta^2}\right\} \quad (B6)$$

or

$$\frac{\beta_o C_p}{2\sin\alpha} \doteq \eta(1-\varepsilon) + \sqrt{1+\eta^2} \quad (B6)$$

where

$$\varepsilon = \frac{4}{(\gamma+1)M_o^2} - \frac{1}{\beta_o^2}$$

The addition of the 'correction' factor $(1-\varepsilon)$ to equation (B3), (the maximum value of ε for $\gamma = 1.4$ is 0.085 at $M_o = 2.1$) gives a useful improvement in accuracy at the lower angles. For Mach numbers of 3 or more Fig.B1 shows that equation (B6) predicts C_p to within $\frac{1}{2}\%$ for turning angles up to about 20°, an

accuracy likely to be adequate for almost all practical purposes. Since $\varepsilon \to 0$ when $M_o \to \infty$, equation (B6) reduces like equation (B3) to equation (B5) in this limit.

Equation (19) in Ref.21 gives an alternative expression for the pressure coefficient behind an oblique shock. Although expressed in a somewhat different form, this in fact differs from equation (B6) above only by the addition of a small term Δ inside the square root of the latter equation, where

$$\Delta = \tan^2 \alpha - \left(\frac{\gamma + 1}{4}\right)^2 \left(1 + \frac{M_o^2}{\beta_o^2}\right) \sin^2 \alpha$$

The effect of this is to increase the incidence range over which accuracy is better than 1% by about 5° for Mach numbers between 3 and 7, at the cost of a very slight loss in mean accuracy within this incidence range. At other Mach numbers the differences between the two expressions are very small.

Finally, for many purposes adequate accuracy over a smaller range of turning angles at the higher Mach numbers is given by a simple cubic equation in η. Fig.B1 shows the accuracy of the following polynomial for $\gamma = 1.4$.

$$M_o^2 C_p \simeq 2 \frac{M_o^2}{\beta_o} \sin \alpha + 1.2 \left(\frac{M_o^2}{\beta_o} \sin \alpha\right)^2 + 0.28 \left(\frac{M_o^2}{\beta_o} \sin \alpha\right)^3 \qquad (B7)$$

For Mach numbers of 4 or above, this expression predicts C_p to within 1½% accuracy up to an incidence of about $130/M_o$ degrees, which corresponds to $M_o^2 C_p \leq 13.5$. With the additional restriction $\alpha \leq 15^\circ$, the same expression with $\sin \alpha$ replaced by α in radians gives a similar accuracy for Mach numbers above 2.2.

Once the surface pressure coefficient behind an oblique shock is known, the other characteristics of the flow can readily be calculated from the following well known relations,

$$M_o^2 \sin^2 \zeta = 1 + \frac{\gamma + 1}{4} M_o^2 C_p$$

$$\frac{p}{p_o} = \frac{\rho T}{\rho_o T_o} = 1 + \frac{\gamma}{2} M_o^2 C_p$$

$$\frac{\rho}{\rho_o} = \frac{(\gamma + 1) M_o^2 \sin^2 \zeta}{(\gamma - 1) M_o^2 \sin^2 \zeta + 2}$$

$$\frac{M}{M_o} = \frac{T_o}{T} \left\{ 1 - \frac{4 (M_o^2 \sin^2 \zeta - 1)(\gamma M_o^2 \sin^2 \zeta + 1)}{M_o^4 (\gamma + 1)^2 \sin^2 \zeta} \right\}$$

and if viscosity $\sim \frac{T^{3/2}}{T + 117}$

$$\frac{Re}{Re_o} = \frac{\rho}{\rho_o} \frac{M}{M_o} \frac{T_o}{T} \frac{T/T_o + 117/T_o}{1 + 117/T_o}$$

Pressure following a Prandtl-Meyer expansion

It is well known that the expression which can be derived for the pressure coefficient behind a plane, oblique shock with turning angle α, in the form of a series in ascending powers of α (the latter being assumed small) has the same coefficients of α and α^2 as the analogous series which can be derived for the pressure coefficient after a Prandtl-Meyer expansion through an angle $(-\alpha)$. Hence it might be expected that the foregoing approximations would apply with reasonable accuracy to expansions through angle α if the sign of α is changed throughout.

In fact, fortuitously, equation (B3) above is remarkably accurate in this respect. With the sign of α changed, this equation gives the pressure coefficient following a Prandtl-Meyer expansion to within 2% of the exact inviscid values for $\gamma = 1.4$ at all Mach numbers, provided the turning angle does not exceed $90\beta_o/M_o^2$ degrees, (i.e. $-M_o^2 C_p < 1.33$).

A simpler equation which gives the Prandtl-Meyer pressures for $\gamma = 1.4$ to a similar accuracy up to a lower limiting turning angle α of $50\beta_o/M_o^2$ degrees $(-M_o^2 C_p < 1.05)$ is

$$- M_o^2 C_p = 2 \frac{M_o^2}{\beta_o} \alpha - 1.2 \left(\frac{M_o^2}{\beta_o} \alpha \right)^2 + 0.36 \left(\frac{M_o^2}{\beta_o} \alpha \right)^3 \qquad (B8)$$

where α is measured in radians.

Appendix C

MEAN SKIN FRICTION IN SUPERSONIC FLOW ON A DELTA WING SURFACE ASSUMING ZERO CONDUCTION AND CONSTANT SURFACE PRESSURE

(See Section 2.4 etc)

The mean skin friction drag on each surface of a delta caret wing has been estimated by the following method and used to derive some of the results (e.g. Section 3.4.2) discussed in the main text of this Report. The numerical results obtained are presented in full in a convenient graphical form in this Appendix. 'Datum' values of mean friction for all-laminar or all-turbulent boundary layers, which include the effects of Mach number, surface pressure, altitude and surface length are first derived, then the skin friction drag for one wing surface obtained from these. The calculation method assumes a constant surface pressure coefficient C_p, and therefore applies strictly only to the lower-surface of a delta caret wing. However, the results can reasonably be applied generally to sensibly plane delta wing surfaces with fully supersonic leading edges, provided C_p is interpreted as the mean value for the surface.

C.1 Datum skin friction

'Datum' values of mean skin friction coefficient on flat plates at incidence have been calculated for all-laminar and all-turbulent boundary layers, assuming for the former a constant chord surface and for the latter a surface of delta planform. In all cases, the flow is taken to be two-dimensional, with a specified constant pressure coefficient over the surface, local stream conditions being those following a single oblique shock in the case of pressures above free stream and those following an isentropic expansion in the case of pressures below free stream.

The effect of compressibility on skin friction has been allowed for by the intermediate enthalpy method[22], whereby the incompressible equations for skin friction are applied to an 'equivalent' incompressible stream having the same pressure and velocity just outside the boundary layer but an effective intermediate enthalpy i_{int}, where

$$i_{int} = 0.22\, i_r + 0.28\, i + 0.5\, i_\omega$$

i_r = recovery enthalpy

i = enthalpy just outside the boundary layer

i_ω = enthalpy corresponding to surface temperature.

Datum values of mean skin friction coefficient have been calculated for a range of values of the four variables:- free stream Mach number M_o, surface pressure coefficient C_p, altitude z and chord length x_{LAM} or x_{TURB}, (x_{TURB} is the root chord of the delta planform assumed for the turbulent boundary layer). To avoid excessive numerical computation, the following two simplifying assumptions were made:-

(a) For given values of the four variables listed above, a single, representative value of i_ω has been taken for the whole datum surface. By ignoring temperature variation over the surface in this way, local skin friction can be expressed in the incompressible form for each case and integrated over the surface to give the datum mean value. The enthalpy corresponding to surface equilibrium temperature at the mid chord point of the laminar or turbulent surface, as the case may be, has been taken as this mean value of i_ω. Surface temperature has been obtained from the charts given in Ref.23 for zero conduction. These cover the same range of variables and assumptions, and have been computed for an emissivity of 0.8. They show that the variation of surface temperature with distance from the leading edge is in fact not large over most of the surface.

(b) For the turbulent boundary layer, local skin friction in incompressible flow at a point distant x behind the leading edge has been taken as

$$(C_f)_{TURB} = \frac{0.0592}{Re^{1/5}}$$

where Re is Reynolds number based on conditions at the edge of the boundary layer and distance x. This has the advantage over the more accurate Wieghardt and other commonly used formulae that it can readily be integrated to give a mean value over the delta planform assumed for the datum turbulent friction. For a constant chord surface, the above formula gives the same mean skin friction as the Prandtl-Schlichting formula, which is widely used, at a Reynolds number based on chord of 10^7, but is 10% lower at Re = 10^8. Now from Fig.31 which shows Reynolds number per foot in terms of free stream Mach number, C_L and wing loading, and from Fig.12 which shows L/D vs C_L,

it can be inferred that flight Reynolds numbers are likely to be in the range $0.25 - 1.0 \times 10^6$ per foot, i.e. the Reynolds number based on mean turbulent boundary layer length is likely to be in the range 10^7-10^8. On average then, the estimate of datum mean friction for the turbulent boundary layer may be a few per cent low; however, this will be partially offset by a pessimistic assumption in the method used to obtain overall friction from the datum values, which is described in the second part of this Appendix.

It is found that datum values of mean skin friction C_{Fd} computed in this way can be expressed, to an accuracy better than 2% for the ranges of the variables considered, as a constant multiplied by the product of four functions, each one of which depends on only one of the variables M_o, $M_o^2 C_p$, altitude and chord length x. Accordingly, it has been possible to present the results in the convenient graphical form shown on Figs.C2 and C3. Fig.C2 shows C_{Fd} vs $M_o^2 C_p$ for three Mach numbers and an arbitrary fixed altitude of 150 000 ft and a chord length of 10 ft. Fig.C3 presents the altitude and chord length functions by which the values derived from the previous figure must be multiplied to obtain datum mean skin friction coefficient at other altitudes and for other chord lengths.

C.2 Skin friction for a delta surface

To obtain the skin friction for one delta wing surface (i.e. either upper or lower) with given values of stream Mach number, surface pressure coefficient, altitude and overall surface length, it is necessary first to determine the distance to transition on the wing centre-line, x_{LAM}. For this, the transition Reynolds number Re_t must first be decided, (values assumed for the caret wing are given in the main body of this Report, Section 2.4.1). Then

$$x_{LAM} = \frac{Re_t}{(Re_o/x)(Re/Re_o)}$$

where Re_o/x = stream Reynolds number/ft, given on Fig.C1,

Re/Re_o = local/stream Reynolds number, given on Fig.C4.

On the delta surface for which the overall skin friction is required the areas of laminar and turbulent flow will in general look like those shown in the sketch on Fig.C5. The ratios of laminar and turbulent areas on the surface to the total area of the surface S_S are respectively,

$$\frac{S_{LAM}}{S_S} = 2\frac{x_{LAM}}{\ell} - \left(\frac{x_{LAM}}{\ell}\right)^2$$

$$\frac{S_{TURB}}{S_S} = \left(1 - \frac{x_{LAM}}{\ell}\right)^2$$

The laminar area S_{LAM} comprises a constant chord region, of area

$$2\left[\frac{x_{LAM}}{\ell} - \left(\frac{x_{LAM}}{\ell}\right)^2\right] S_S$$

and a delta planform region, comprising two halves, outboard of the constant chord region, having an aggregate area

$$\left(\frac{x_{LAM}}{\ell}\right)^2 S_S$$

Now in order to calculate the friction force acting on the whole surface comprising these areas of laminar and turbulent flow, two simplifying assumptions have been made as follows:-

(i) The mean laminar skin friction over a narrow strip of local chord C in the 'delta' region of laminar flow has been taken as equal to the datum mean value which applies over the constant chord region further inboard, multiplied by $(x_{LAM}/C)^{\frac{1}{2}}$. For calculating incompressible mean laminar friction the usual Blasius formula has been used, i.e. $C_F \sim Re^{-\frac{1}{2}}$, so what this assumption implies is that the effective mean wall temperature for the delta region of laminar flow is taken to be the same as that used to calculate the datum values of mean laminar skin friction, which is the temperature at distance $\frac{1}{2} x_{LAM}$ behind the leading edge. It follows that the mean skin friction over the delta region of laminar flow is

$$(C_{F\Delta})_{LAM} = \frac{4}{3}(C_{Fd})_{LAM}$$

(ii) The second assumption is that the mean turbulent skin friction drag acting over the appropriate region of the surface is the datum value, with $x_{TURB} = \ell - x_{LAM}$. Thus, the mean turbulent skin friction is calculated as if the transition line were a leading edge and the laminar boundary layer did not exist. This means that the turbulent boundary layer is assumed to begin from zero thickness at transition whereas in fact its thickness here will be approximately that of the laminar layer. This assumption is somewhat pessimistic (i.e. leads to higher drag) but is tacitly taken to be offset by the slightly optimistic formula used to calculate the datum values of mean turbulent skin friction.

From the foregoing, it follows that the mean skin friction drag coefficient for the upper or lower surface of a delta wing is given by

$$C_{FS} = \left[2\frac{x_{LAM}}{\ell} - \frac{2}{3}\left(\frac{x_{LAM}}{\ell}\right)^2\right](C_{Fd})_{LAM} + \left[1 - \frac{x_{LAM}}{\ell}\right]^2 (C_{Fd})_{TURB}$$

where $(C_{Fd})_{LAM}$ and $(C_{Fd})_{TURB}$ are obtained from Figs.C2 and C3 for x_{LAM} and $x_{TURB} = \ell - x_{LAM}$ respectively. Fig.C5 expresses the above equation graphically. Thus, for given values of stream Mach number, surface pressure coefficient, altitude, overall length and transition Reynolds number, Figs.C2-C5 inclusive contain all the information required to make a rapid estimate of the mean skin friction on a delta wing with supersonic leading edges, assuming zero conduction and sensibly constant pressure over each surface.

C.3 Acknowledgement

The authors would like to thank Mr. A. Naysmith, who supervised all the numerical skin friction calculations on which Figs.2 and 3 are based.

Appendix D

EFFECT OF LEADING EDGE BLUNTNESS ON LIFT/DRAG

(See Sections 2.3, 2.5, 3.5)

Some blunting of the wing leading edges may be required in order to avoid excessive local temperatures, but it is desirable to keep such blunting as small as possible so as to keep the flow around the leading edges laminar (as discussed in Section 2.4.1) and also to minimise the effect on the wing flow field.

To obtain an estimate of the change in lift/drag arising from such bluntness let us consider a section normal to the leading edge of a caret wing, as shown in Fig.D1. To simplify the problem the wing upper-surface is taken to be in the streamwise direction (i.e. $\alpha_U = 0$, $C_{p_U} = 0$), such that the anhedral angle of the wing upper-surface in the YZ-plane is

$$\psi_U = \sec^{-1}\left[1 + \left(\frac{\ell}{s}\right)^2 \tan^2 \zeta\right]^{\frac{1}{2}},$$

where ζ is the shock-wave angle. This angle ζ determines the lower-surface pressure coefficient, the lower-surface incidence, and the volume of the wing since (see Sections 2.1 and 2.3):-

$$C_{p_L} = \frac{5}{3}\left(\sin^2 \zeta - \frac{1}{M_o^2}\right) \tag{D1}$$

and

$$\tan \alpha_L = \frac{C_{p_L} \cot \zeta}{2 - C_{p_L}} = 3\tau \left(\frac{s}{\ell}\right)^{\frac{1}{2}} \tag{D2}$$

The length of each leading edge is

$$\ell' = (s^2 + \ell^2 \sec^2 \zeta)^{\frac{1}{2}} \tag{D3}$$

The effective leading edge sweep is

$$\Lambda = \cos^{-1} \frac{(s^2 + \ell^2 \tan^2 \zeta)^{\frac{1}{2}}}{(s^2 + \ell^2 \sec^2 \zeta)^{\frac{1}{2}}} \tag{D4}$$

and the Mach number component normal to the leading edge is

$$M_{N_o} = M_o \cos \Lambda \tag{D5}$$

To blunt the wing leading edge it is assumed that the triangular portion of the wing OAB shown in Fig.D1 is removed (OB = d), and that an approximately hemi-cylindrical leading edge (of diameter 2r = AB) is added in its place.

Now the change in force per unit length of leading edge due to blunting, acting normal to the leading edge, is from Fig.D1

$$P = 2r \int_o^{\pi/2} (p - p_o) \cos \theta \, d\theta - p_L \, 2r \tag{D6}$$

and the total drag from both leading edges is

$$D_{LE} = 2P s \sec \psi_U \tag{D7}$$

Thus

$$C_{D_{LE}} = \frac{D_{LE}}{\frac{1}{2} \rho_o V_o^2 \, s\ell} = 4 \frac{r}{\ell} \sec \psi_U \left[\int_o^{\pi/2} C_p \cos \theta \, d\theta - C_{p_L} \right] \tag{D8}$$

where $C_{D_{LE}}$ is based on the plan area $s\ell$ of the original sharp edged wing.

Now from the modified Newtonian approximation for blunt bodies (which experiments[18] have shown to be a close approximation to the pressure distribution on a yawed cylinder, for $1.5 < M_{N_o} < 3.5$) we know that $C_p = C_{p_{stag}} \cos^2 \theta$, where $C_{p_{stag}}$ is the pressure coefficient at the stagnation point, $\theta = 0$.

Thus from equation (D8) we get

$$C_{D_{LE}} = 4 \frac{r}{\ell} \sec \psi_U \left[\int_0^{\pi/2} C_{p_{stag}} \cos^3 \theta \, d\theta - C_{p_L} \right]$$

i.e.

$$C_{D_{LE}} = 4 \frac{r}{\ell} \sec \psi_U \left[\frac{2}{3} C_{p_{stag}} - C_{p_L} \right] \tag{D9}$$

Now

$$C_{p_{stag}} = \overline{C}_{p_{stag}} \cos^2 \Lambda$$

where $\overline{C}_{p_{stag}}$ = stagnation pressure coefficient appropriate to M_{N_o} (based on free stream dynamic pressure)

So equation (D9) becomes

$$C_{D_{LE}} = 4 \frac{r}{\ell} \sec \psi_U \left[\frac{2}{3} \overline{C}_{p_{stag}} \cos^2 \Lambda - C_{p_L} \right] \tag{D10}$$

It should be noted that equation (D10) applies only to a caret wing, where the variables ψ_U, $\overline{C}_{p_{stag}}$, Λ and C_{p_L} are related by the condition that a plane shock wave of incidence ζ is contained between the leading edges (as described earlier), and not to a wing with arbitrarily assigned values for these variables.

For a caret wing of given slenderness ratio s/ℓ, and lower-surface pressure coefficient, increase of Mach number increases $\overline{C}_{p_{stag}}$ but decreases the anhedral angle ψ_U, with the net result that $C_{D_{LE}}/(r/\ell)$ is reduced; increase of lower-surface pressure coefficient though increasing the required anhedral angle, decreases the term in square brackets in equation (D10) to give a net decrease in $C_{D_{LE}}/(r/\ell)$. These effects are illustrated by the

values of $C_{D_{LE}}/(r/\ell)$ tabulated at the end of this Appendix for a range of Mach number, lower-surface pressure coefficient and slenderness ratio.

Also tabulated at the end of this Appendix are values of the critical leading edge radius in feet for two values of wing loading (from Section 2.4.1), together with the resulting leading edge drag coefficients for a wing of 100 ft root chord. Since C_{p_L} in this table is approximately equal to the overall lift coefficient, and since overall values of lift/drag are typically about 6, it follows that the overall drag coefficients fall between 0.01 and 0.02. Thus even for the case of leading edge radii as large as the critical value, the drag arising from blunted leading edges amounts to only about 1% of the total drag for a wing loading of 50 lb/ft^2, and about 2% for a wing loading of 25 lb/ft^2.

However, the result of blunting the wing leading edges is also to reduce wing plan area, and hence overall lift, since a strip of constant width d has been lost from each lower wing surface (see Fig.D1). Assuming that the pressure coefficient on the remaining plane part of the lower surface is unaffected by the leading edge blunting, and ignoring any lift developed on the blunted leading edges themselves, then

$$\frac{(\text{Lift})_r}{(\text{Lift})_{r=0}} = \frac{(\text{Plan area})_r}{(\text{Plan area})_{r=0}} = \frac{(\text{Lower surface wetted area})_r}{(\text{Lower surface wetted area})_{r=0}}$$

$$= \left(1 - \frac{\ell' d}{S_L}\right)^2 \qquad \text{(D11)}$$

where S_L = lower-surface wetted area for wing with sharp leading edges (see equation (6) and Fig.2)

suffix r refers to wing with blunted edges of radius r

suffix r=0 refers to wing with sharp leading edges.

The distance d is related to the leading edge radius and the lower-surface incidence (in a plane normal to the leading edge, see Fig.D1) by

$$d \simeq \frac{2r}{\tan \alpha_{N_L}} = \frac{2r}{3\tau\,(s/\ell)^{\frac{1}{2}}} \frac{\tan \alpha_L}{\tan \alpha_{N_L}} \qquad \text{(D12)}$$

From equation (10) of Section 2.1 and equation (D3) above

$$\frac{\ell'}{\tan \alpha_{N_L}} = \frac{\ell^2}{s}\left[\frac{\tan^2 \zeta + s^2/\ell^2}{\tan \alpha_L} - \tan \zeta\right] \qquad (D13)$$

Hence from (D12)

$$\frac{\ell' d}{S_L} = 2\,\frac{r}{\ell}\,\frac{S}{S_L}\left(\frac{\ell}{s}\right)^2\left[\frac{\tan^2 \zeta + s^2/\ell^2}{\tan \alpha_L} - \tan \zeta\right] \qquad (D14)$$

This equation in conjunction with (D11) and Fig.2 for S/S_L gives the ratio of the lift with blunted edges to that with sharp edges, in terms of the wing and shock geometry. Equations (D1) and (D2) can be used to express $\tan \zeta$ and $\tan \alpha_L$ in terms of M_o and C_{p_L}.

Percentage lift losses have been calculated for wing loadings of 25 lb/ft^2, and 50 lb/ft^2, for the same values of critical leading edge radii as used previously for calculating drag increase, and the results are tabulated at the end of this Appendix. It can be seen that the lift loss arising from blunted edges varies between 2-5% for a wing loading of 25 lb/ft^2, and between 1-2% for a wing loading of 50 lb/ft^2.

This percentage decrease in lift is about twice the percentage increase in drag, and the total decrease in lift/drag is therefore 4-7% for a wing loading of 25 lb/ft^2 and 2-3% for a wing loading of 50 lb/ft^2. This is a significant loss in lift/drag, and emphasises the importance of designing for the smallest possible leading edge radii.

M_o	5	5	5	5	10	10	10	10
C_{p_L}	0.06	0.10	0.06	0.10	0.05	0.08	0.05	0.08
s/ℓ	0.2	0.2	0.3	0.3	0.2	0.2	0.3	0.3
$C_{D_{LE}}/(r/\ell)$	0.39	0.33	0.56	0.51	0.21	0.18	0.42	0.39
r_{crit} 25 lb/ft^2	0.05	0.10	0.05	0.10	0.065	0.125	0.085	0.15
10^4 $C_{D_{LE}}$ 25 lb/ft^2	2	3	3	5	1	2	4	6
r_{crit} 50 lb/ft^2	0.025	0.045	0.025	0.045	0.030	0.055	0.040	0.065
10^4 $C_{D_{LE}}$ 50 lb/ft^2	1	1	1	2	1	1	2	3
$-\Delta L\%$ 25 lb/ft^2	3.2	4.7	2.5	3.6	2.7	4.1	3.0	4.2
$-\Delta L\%$ 50 lb/ft^2	1.6	2.2	1.3	1.6	1.2	1.8	1.4	1.6

The above figures represent no more than an attempt to estimate very approximately the performance penalties of leading-edge blunting. Future work should be directed towards obtaining a more detailed understanding of the flow field in the region of the leading edge, so that a more accurate assessment can be made.

Appendix E

THE LIFT AND DRAG CHARACTERISTICS OF A TWO DIMENSIONAL WEDGE AT HYPERSONIC SPEEDS

(See Sections 2.6, 3.2 and 3.4.1)

E.1 Approximations for surface pressure ($\gamma = 1.4$)

For the lower surface, if $\alpha_L < 15^\circ$, $M_o > 2.2$, $M\alpha_L < 2.25$ radians, it is shown in Appendix B that the following expression predicts pressure coefficient to an accuracy of better than 1½%

$$M_o^2 C_{p_L} = 2 M\alpha_L + 1.2 (M\alpha_L)^2 + 0.28 (M\alpha_L)^3 \qquad (E1)$$

where

$$M\alpha_L = \frac{M_o^2}{\beta_o} \times \alpha_L \text{ radians}$$

For the upper surface, the above equation of course gives $M_o^2 C_{p_U}$ for α_U negative, with $-\alpha_U = +\alpha_L$. For α_U positive, equation (8) of Appendix B would be the appropriate expression for $-M_o^2 C_{p_U}$ comparable with equation (1) above. Up to $M\alpha_U = 0.6$ however, and for $M_o \geq 4$, equation (1) with $-\alpha_U = \alpha_L$ gives an accuracy of better than 2%. At $M\alpha_U = 0.85$, the error is increased to 4% but it is in the sense of predicting low values of $-C_{p_U}$, which may in fact be more realistic. Hence, for upper-surface pressure, it will be convenient to use equation (E1) with the appropriate sign changes, i.e.

$$-M_o^2 C_{p_U} = 2 M\alpha_U - 1.2 (M\alpha_U)^2 + 0.28 (M\alpha_U)^3 \qquad (E2)$$

E.2 Normal force coefficient

Using equations (E1) and (E2) above, it can readily be shown that the normal force coefficient C_N based on plan area for a wedge of semi angle ϑ radians and chord line incidence α radians is given by

$$\frac{\beta_o C_N}{\alpha} = 4\left[1 + 1.2 M\vartheta + 0.42 (M\vartheta)^2\right] + 0.56 (M\alpha)^2 \qquad (E3)$$

E.3 Axial force coefficient

If it is assumed that C_{DF}, the skin friction drag coefficient for both surfaces (based on plan area) and C_{DP}, the coefficient of base and extraneous drag items also based on plan area are both independent of incidence then with $\sin\vartheta = \vartheta$ the axial force coefficient C_A based on plan area is given by

$$M^2\beta_o C_A = M^2\beta_o C_{D_o} + (2.4 + 1.68\, M\vartheta)(M\vartheta)(M\alpha)^2 \qquad (E4)$$

i.e.
$$\beta_o \frac{(C_A - C_{D_o})}{\alpha^2} = (2.4 + 1.68\, M\vartheta)\, M\vartheta$$

where
$$M^2\beta_o (C_{D_o} - C_{DF} - C_{DP}) = 4\left[1 + 0.6\, M\vartheta + 0.14\, (M\vartheta)^2\right](M\vartheta)^2 \qquad (E5)$$

E.4 Lift and drag coefficients

$$C_L = C_N \cos\alpha - C_A \sin\alpha \simeq C_N (1 - \tfrac{1}{2}\alpha^2) - C_A\alpha$$

Hence from (E3) and (E4)

$$\beta_o \left(\frac{C_L}{\alpha} + C_{D_o}\right) = 4\left[1 + 1.2\, M\vartheta + 0.42\, (M\vartheta)^2\right] + \left[0.56 - \frac{2 + 4.8\, M\vartheta + 2.52\, (M\vartheta)^2}{M^2}\right](M\alpha)^2$$

... (E6)

Similarly,

$$C_D = C_N \sin\alpha + C_A \cos\alpha \simeq C_N\alpha + C_A (1 - \tfrac{1}{2}\alpha^2)$$

Hence, from (E3) and (E4)

$$\frac{\beta_o (C_D - C_{D_o})}{\alpha^2} = 4\left\{1 + 1.8\, (M\vartheta) + 0.84\, (M\vartheta)^2\right\} - 0.5\, \beta_o C_{D_o}$$

$$+ \left\{0.56 - \frac{1.2\, M\vartheta + 0.84\, (M\vartheta)^2}{M^2}\right\}(M\alpha)^2 \qquad (E7)$$

E.5 Lift/drag ratio

From the relation

$$\frac{1}{M}\frac{L}{D} = \frac{(M\alpha)\left\{\beta_o\left(\frac{C_L}{\alpha} + C_{D_o}\right) - \beta_o C_{D_o}\right\}}{\beta_o (C_D - C_{D_o}) \quad (M\alpha)^2 \frac{C_{D_o}}{\alpha^2} + M^2\beta_o C_{D_o}} \qquad \text{(E8)}$$

and equations (E6) and (E7), it is seen that L/MD depends mainly on the variables $M\vartheta$, $M\alpha$ and $M^2\beta_o C_{D_o}$, with Mach number itself a fourth, less important variable.

Approximate expressions can be derived from the foregoing equations for the maximum lift/drag ratio (as it varies with incidence) on a particular wedge at a given Mach number, and for the incidence at which this maximum is achieved, which will be denoted by α^*. For convenience, we rewrite equation (E6) in the form

$$\frac{\beta_o C_L}{\alpha} = 4\lambda_1 + \tfrac{1}{2}\lambda_2 (M\alpha)^2$$

where $\lambda_1 = 1 + 1.2\,(M\vartheta) + 0.42\,(M\vartheta)^2 - 0.25\,\beta_o C_{D_o}$

and $\lambda_2 = 1.12 - \dfrac{4 + 9.6\,(M\vartheta) + 5.04\,(M\vartheta)^2}{M^2}$

The magnitude of λ_1 will normally lie between one and three while that of of λ_2 will be approximately unity.

Similarly, equation (E7) may be written

$$\frac{\beta_o (C_D - C_{D_o})}{\alpha^2} = 4\lambda_3 + \tfrac{1}{2}\lambda_4 (M\alpha)^2$$

where $\lambda_3 = 1 + 1.8\,(M\vartheta) + 0.84\,(M\vartheta)^2 - 0.125\,\beta_o C_{D_o}$

and $\lambda_4 = 1.12 - \dfrac{2.4\,(M\vartheta) + 1.68\,(M\vartheta)^2}{M^2}$

the magnitudes of λ_3 and λ_4 being broadly similar to those of λ_1 and λ_2 respectively.

Now the value of $M\alpha$ for maximum lift/drag ratio of a given wedge at a fixed Mach number is denoted by $M\alpha^*$ and is given by the relevant solution of the following equation.

$$\lambda_1 M^2\beta_o C_{D_o} - \left\{4\lambda_1\lambda_3 - \tfrac{3}{8}\lambda_2 M^2\beta_o C_{D_o}\right\}(M\alpha^*)^2 - \left\{\tfrac{3}{2}\lambda_1\lambda_4 - \tfrac{1}{2}\lambda_2\lambda_3\right\}(M\alpha^*)^4 - \frac{\lambda_2\lambda_4}{16}(M\alpha^*)^6 = 0 \qquad \text{(E9)}$$

and the maximum lift/drag ratio is then

$$\left(\frac{L}{D}\right)_{max} = \frac{1}{2(\alpha^*)}\,\frac{\lambda_1}{\lambda_3}\left\{\frac{1 + \frac{3}{8}\frac{\lambda_2}{\lambda_1}(M\alpha^*)^2}{1 + \frac{1}{4}\frac{\lambda_4}{\lambda_3}(M\alpha^*)^2}\right\} \qquad \text{(E10)}$$

The factor in the large bracket in the above equation expresses the effect on maximum lift/drag of the variation with α of C_L/α and $(C_D - C_{D_o})/\alpha^2$.

The solution of equation (9) for $(M\alpha^*)$ can only be done by successive approximation. The first approximation is obtained by neglecting the "non-linear lift" terms λ_2 and λ_4, which gives, from equation (E9)

$$(M\alpha^*)^2 \simeq \frac{M^2\beta_o C_{D_o}}{4\lambda_3} \qquad \text{(E11a)}$$

i.e.

$$\alpha^* \simeq \left(\frac{\beta_o C_{D_o}}{4\lambda_3}\right)^{\frac{1}{2}} \qquad \text{(E11a)}$$

and from equation (10)

$$(M\alpha^*) \simeq \frac{M}{2(L/D)_{max}}\,\frac{\lambda_1}{\lambda_3} \qquad \text{(E11b)}$$

Thus, for most cases of interest, $(M\alpha^*)$, will be less than unity, except perhaps at Mach numbers in excess of 10.

Further refinement of the approximation for $(M\alpha^*)$ yields the following which is within 1% of exact solutions of equation (9) if $(M\alpha^*) < 1.1$.

$$(M\alpha^*) \simeq \left(\frac{M^2\beta_o C_{D_o}}{4\lambda_3}\right)^{\frac{1}{2}} \left\{1 + \frac{1}{16}\left(4\frac{\lambda_2}{\lambda_1} - 3\frac{\lambda_4}{\lambda_3}\right)\left(\frac{M^2\beta_o C_{D_o}}{4\lambda_3}\right) - \frac{7}{64}\frac{\lambda_2}{\lambda_1}\frac{\lambda_4}{\lambda_3}\left(\frac{M^2\beta_o C_{D_o}}{4\lambda_3}\right)^2\right\}$$

... (E12)

The effect of the "non-linear lift" factor in large brackets is to increase the optimum incidence by a maximum amount of only 2% at $M\alpha \simeq 0.65$; equation (E11a) is a very good approximation therefore.

Using equation (E12) for (α^*) and the first approximation given by equation (E11a) for $(M\alpha^*)^2$ in equation (E10), the following can be derived for maximum lift/drag

$$\left(\frac{L}{D}\right)_{max} \simeq \frac{\lambda_1}{(\lambda_3 \beta_o C_{D_o})^{\frac{1}{2}}}\left\{1 + \frac{1}{16}\left(2\frac{\lambda_2}{\lambda_1} - \frac{\lambda_4}{\lambda_3}\right)\left(\frac{M^2\beta_o C_{D_o}}{4\lambda_3}\right) + \frac{7}{64}\frac{\lambda_2}{\lambda_1}\frac{\lambda_4}{\lambda_3}\left(\frac{M^2\beta_o C_{D_o}}{4\lambda_3}\right)^2\right\}$$

... (E13)

This shows that the effect on maximum lift/drag of the non-linearity in the lift curve (which is expressed by the term in large brackets) is appreciable only if $(M\alpha^*)$ exceeds 0.5 or so. With $(M\alpha^*)$ equal to unity, the gain is about 10%.

The lift coefficient for maximum lift/drag is easily obtained; neglecting the small effect of non-linear lift on (α^*), this is

$$C_L^* = \left(\frac{4\lambda_1^2 C_{D_o}}{\beta_o \lambda_3}\right)^{\frac{1}{2}}\left\{1 + \frac{1}{8}\frac{\lambda_2}{\lambda_1}\left(\frac{M^2\beta_o C_{D_o}}{4\lambda_3}\right)\right\} \qquad \text{(E14)}$$

Similarly the drag due to incidence at $\alpha = (\alpha^*)$ is

$$C_D^* - C_{D_o} = C_{D_o}\left\{1 + \frac{1}{8}\frac{\lambda_4}{\lambda_3}\left(\frac{M^2\beta_o C_{D_o}}{4\lambda_3}\right)\right\} \qquad \text{(E15)}$$

Again, the terms outside the large brackets in equations (E14) and (E15) are those which would be obtained if C_L/α and $(C_D - C_{D_o})/\alpha^2$ were independent of α and equal to their values for $\alpha \to 0$, while the terms in large brackets express the effect of these quantities varying with α.

The incidence for maximum lift/drag as given by equation (E11a) is plotted on Fig.E1 as $(\alpha_U^*) = (\alpha^*) - \vartheta$ against semi angle ϑ for Mach numbers 5 and 10. Optimum upper-surface incidence is shown for three values of $(C_{DF} + C_{DP})$, viz. 0, 0.002 and 0.004, the first value corresponding to a wedge alone with zero extraneous or base drag in inviscid flow, the second to the case of a wedge alone, again with zero base drag but a typical surface friction coefficient C_{FS} of 0.001, and the third to $C_{FS} = 0.001$ and an extraneous and base drag coefficient C_{DP} of 0.002. Also shown on this figure by chain dotted lines are corresponding values calculated from the linear theory equations commonly used for lower supersonic Mach numbers, i.e.

$$C_L = \frac{4\alpha}{\beta_o}$$

$$C_{D_o} = 2C_{FS} + C_{DP} + \frac{4\vartheta^2}{\beta_o}$$

$$C_D = C_{D_o} + C_L \alpha$$

The significant features of the results presented on Fig.E1 are

(i) The non-linearities associated with hypersonic flow decrease the optimum upper-surface incidence for maximum lift/drag on a wedge by an amount which is roughly proportional to wedge angle.

(ii) Zero upper-surface incidence happens to correspond to the condition for maximum lift/drag, (when realistic friction and extraneous drag items are taken into account), if the wedge semi angle is 4°-5°.

Fig.E2 shows wedge lift/drag for the same range of wedge angle, Mach number and $(C_{DF} + C_{DP})$ as in Fig.E1. Two cases are presented, maximum lift/drag and lift/drag with upper-surface incidence zero (dashed lines). Taking a typical value for C_{DF} of 0.002 (which is presumed to be invariable with incidence) the difference between the two lift/drag ratios is not significant if ϑ lies between 3° and $5\frac{1}{2}^\circ$ for $C_{DP} = 0$, or between $3\frac{1}{2}^\circ$ and 6° for $C_{DP} = 0.002$.

SYMBOLS

C_A	axial force coefficient = axial force/$\frac{1}{2}\rho_o V_o^2 S$
C_D	drag coefficient = drag/$\frac{1}{2}\rho_o V_o^2 S$
C_{DF}	total friction drag coefficient for upper and lower surfaces
$C_{D_{LE}}$	increase in drag coefficient due to rounding a sharp leading edge
C_{D_o}	drag coefficient at zero lift (for a wedge)
C_{DP}	parasite drag coefficient (see Section 2.5)
C_f	local skin friction stress coefficient = friction stress/$\frac{1}{2}\rho V^2$
C_F	mean tangential force coefficient due to skin friction, based on a specified wetted area and $\frac{1}{2}\rho_o V_o^2$
$(C_{Fd})_{LAM}$	'datum' value of C_F for a laminar boundary layer on a constant chord wing surface
$(C_{Fd})_{TURB}$	'datum' value of C_F for a turbulent boundary layer on a wing surface of delta planform
C_{FS}	C_F for one complete surface of a wing
C_{FU}, C_{FL}	C_{FS} for the upper and lower surfaces respectively
C_L	lift coefficient = lift/$\frac{1}{2}\rho_o V_o^2 S$
C_N	normal force coefficient = normal force/$\frac{1}{2}\rho_o V_o^2 S$
C_p	pressure coefficient = $(p - p_o)/\frac{1}{2}\rho_o V_o^2$
C_{p_U}, C_{p_L}	C_p on the upper and lower surfaces, respectively
$C_{p_{stag}}$	C_p at the leading edge stagnation line
$\overline{C}_{p_{stag}}$	pitot pressure coefficient at specified Mach number
c	local wing chord
D	drag
d	width of plane lower wing surface, measured normal to leading edge, which is removed when sharp leading edge is rounded (see Fig.D1)
F	net thrust
g	acceleration due to gravity
i	local enthalpy at the edge of the boundary layer

SYMBOLS (Contd)

i_{int}	effective 'intermediate' enthalpy for a boundary layer
i_r	recovery enthalpy, the value corresponding to surface temperature with zero heat transfer
i_ω	enthalpy corresponding to actual surface temperature
k_{LAM}, k_{TURB}	coefficients on Fig.C5
L	lift
ℓ	overall length of wing, measured parallel to stream direction
ℓ'	length of one leading edge
M	local Mach number at the edge of the boundary layer
M_o	free stream Mach number
M_{N_o}	component of M_o normal to the leading edge
$\mathcal{M}$	M_o^2/β_o (in Appendix E)
n	$\frac{1}{g}\frac{dV_o}{dt}$
P	force/unit length of leading edge (in Appendix D)
p	local static pressure on the surface
p_o	free stream static pressure
R	range
R_A, R_C, R_G	ranges in acceleration, cruise and glide phases respectively
$\mathcal{R}$	radius of curvature of flight path, in a vertical plane
$\mathcal{R}_o$	radius of Earth
Re	Reynolds number, based on conditions at the edge of the boundary layer and a specified length x
Re_o	Reynolds number, based on free stream conditions and a specified length x
Re_t	Reynolds number, based on conditions at the edge of the boundary layer and distance from the leading edge to the midpoint of the transition zone
r	radius of leading edge rounding, measured in a plane normal to leading edge
r_{crit}	critical value of r, above which boundary layer transition begins at or near the stagnation line
S	reference area = plan area, projected onto a streamwise plane, at design incidence for a caret wing, zero incidence for a wedge

SYMBOLS (Contd)

S_S	wetted area of one surface of a wing of delta planform (in Appendix C)
S_U, S_L	S_S for the upper and lower surfaces respectively of a delta caret wing
S_{LAM}	area of laminar boundary layer on one surface
S_{TURB}	area of turbulent boundary layer on one surface
s	semispan
T	local static temperature at the edge of the boundary layer
T_o	free stream static temperature
T_r	recovery temperature = surface temperature with zero heat transfer
T_ω	actual surface temperature
t	time
V	total stream velocity over surface, at the edge of the boundary layer
V_C	aircraft velocity in cruise phase
V_o	free stream (aircraft) velocity
V_{N_o}	component of V_o normal to the leading edge
V_S	satellite velocity
W	weight of aircraft
x	distance along surface, in local stream direction
x_{LAM}	distance along surface, on wing centre-line, from leading edge to midpoint of transition zone (see Fig.C5)
x_{TURB}	overall length of a delta planform area covered by a turbulent boundary layer (see Fig.C5)
z	geometric altitude
α	angle of incidence of chord line (in Appendix E)
α_U, α_L	angle of incidence of upper and lower surfaces respectively, measured in the plane of symmetry, (see Fig.1)
α'_U	angle of incidence of upper surface, measured in a plane normal to the surface
α_N	angle of incidence of a surface measured in a plane normal to the leading edge
β_o	$\sqrt{M_o^2 - 1}$
γ	ratio of specific heat at constant pressure to that at constant volume

SYMBOLS (Contd)

γ	angle of climb (in Appendix A)
ε	variable in equation (B6)
ζ	angle between shock wave and stream direction, measured in the plane of symmetry (see Fig.1)
ζ_N	angle between shock wave and stream direction, measured in a plane normal to the leading edge
η	$\frac{\gamma+1}{4}\frac{M_o^2}{\beta_o}\sin\alpha$ (in Appendix B)
ϑ	semi angle of wedge (in Appendix E)
θ	angle in blunted leading edge geometry (in Appendix D, see Fig.D1)
Λ	effective sweepback of leading edge = $\cos^{-1}(M_{N_o}/M_o)$
$\lambda_1,\lambda_2,\lambda_3,\lambda_4$	functions of $M\vartheta$, (in Appendix E)
ρ	local density at the edge of the boundary layer
ρ_o	free stream density
σ	specific fuel consumption
$\bar{\sigma}_A$	average specific fuel consumption for the acceleration phase
σ_C	specific fuel consumption during the cruise phase
τ	volume coefficient = volume/$S^{3/2}$
ψ_U,ψ_L	anhedral angles of upper and lower-surfaces respectively, measured in a plane normal to the free stream direction

Suffices and index

$(\ )_L$	for lower wing surface
$(\ )_o$	free stream value
$(\ )_U$	for upper wing surface
$(\ )_Z$	with upper-surface streamwise
$(\ )_1$	initial conditions
$(\ )_2$	conditions prior to cruise
$(\ )_3$	conditions at end of cruise
$(\ )^*$	value giving maximum lift/drag

REFERENCES

No.	Author	Title, etc.
1	T.R.F. Nonweiler	Delta wings of shapes amenable to exact shock wave theory. A.R.C. 22644, March 1961 also J.R.Ae.S. 67, (625) January 1963
2	J.G. Jones	A method for designing lifting configurations for high supersonic speeds using the flow fields of non-lifting cones. A.R.C. 24846, March 1963
3	D.H. Peckham	On three-dimensional bodies of delta planform which can support plane attached shock waves. A.R.C. C.P. No. 640, 1963
4	L.H. Townend	On lifting bodies which contain two-dimensional supersonic flows. A.R.C. 25277, August 1963
5	J. Seddon	Aerodynamics of flight at Mach 4 to Mach 6. J. Roy. Aero Soc., (to be published)
6	J.W. Flower	Configurations for high supersonic speeds derived from simple shock-waves and expansions. J. Roy. Aero Soc., 67, 1963, pp 287-290
7	D. Küchemann	Hypersonic aircraft and their aerodynamic problems. Progress in Aeron Sci., 6, 271-353, Pergamon Press 1965
8	D. Küchemann	The aerodynamic development of slender wings for supersonic flight. Jahrbuch 1962, d. W.G.L.R., p 66-77, Frigor Vieweg & Sohn 1963
9	L.F. Nicholson	Engine airframe integration. J. Roy. Aero Soc., 61, pp 711-726, 1957
10	R.P. Probert D.H. Mallinson	Economics of ramjets as satellite launchers. J. Roy. Aero Soc., 66, p 3, 1962

REFERENCES (Contd)

No.	Author	Title, etc.,
11	R.J. Lane	Recoverable air-breathing boosters for space vehicles. J. Roy. Aero Soc., 66, pp 371-386, June 1962
12	Ames Research Staff	Equations, tables and charts for compressible flow. NACA Report 1135, 1953
13	D.A. Treadgold	Private communication
14	R. Michel	Examen des facteurs influencant la transition à la turbulence dans la couche limite. ONERA T.P. No. 143, 1964
15	J.L. Potter J.D. Whitfield	Effects of slight nose bluntness and roughness on boundary layer transition in supersonic flows. J. Fluid Mech. 12, 1962, 501
16	P.R. Owen D.J. Randall	Boundary layer transition on a sweptback wing. A.R.C. 15022 and addenda, A.R.C. 15741 and A.R.C. 16191, 1952-53
17	D.R. Topham	A correlation of leading edge transition and heat transfer on swept cylinders in supersonic flow. A.R.C. 26219, August 1964
18	J.R. Collingbourne Dr. L.F. Crabtree W.J. Bartlett	A semi-empirical prediction method for pressures on the windward surface of circular cones at incidence at high supersonic and hypersonic speeds (M → 3) A.R.C. C.P. 792
19	E.C. Capey	Private communication
20	Lester Lees	Hypersonic flow. Fifth International Aeronautical Conference, Los Angeles, pp 241-276
21	J.R. Collingbourne	An empirical prediction method for non-linear normal force on thin wings at supersonic speeds. A.R.C. C.P. No. 662, January 1962
22	E.R.G. Eckert	Survey on heat transfer at high speeds. W.A.D.C. Technical Report 54-70, April 1954
23	A. Naysmith	Unpublished M.O.A. Report.

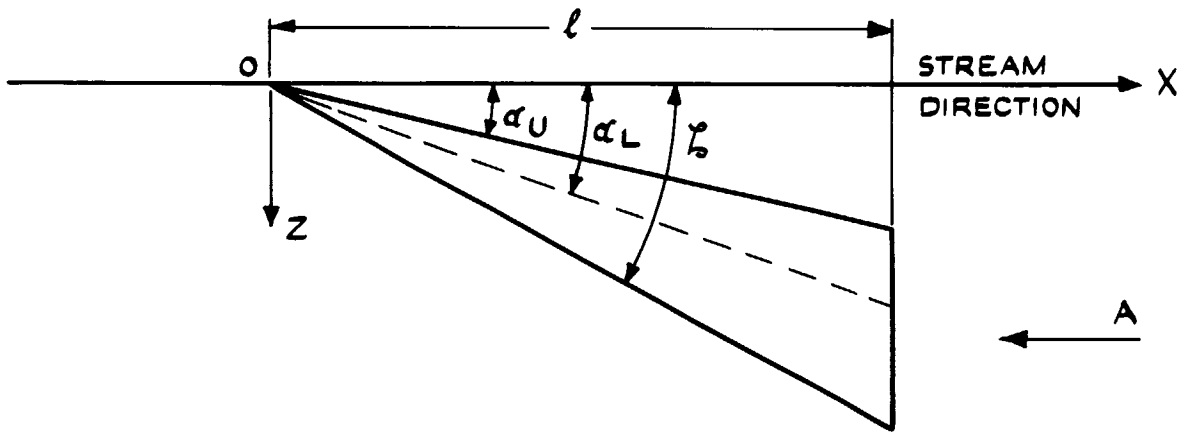

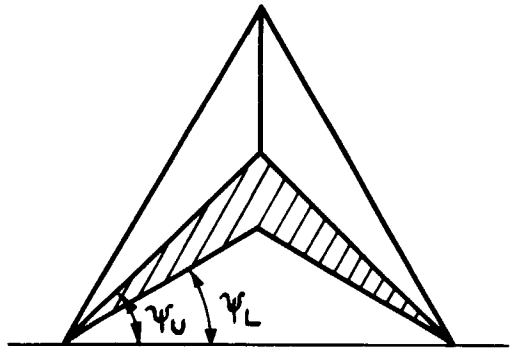

VIEW 'A'

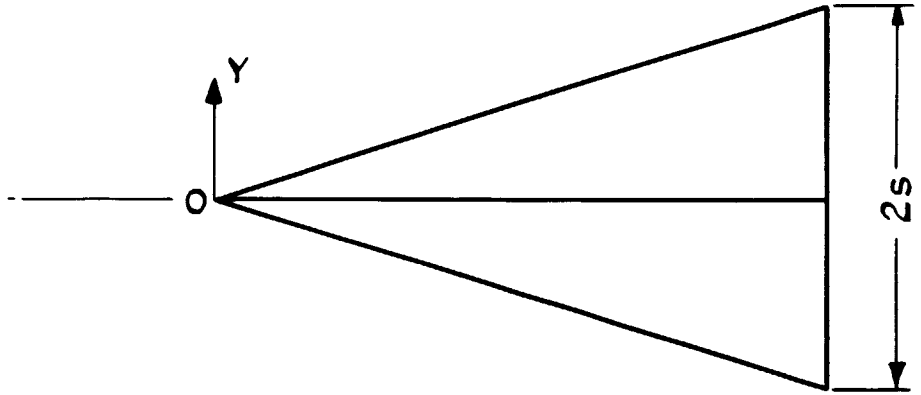

FIG. 1 CARET WING GEOMETRY

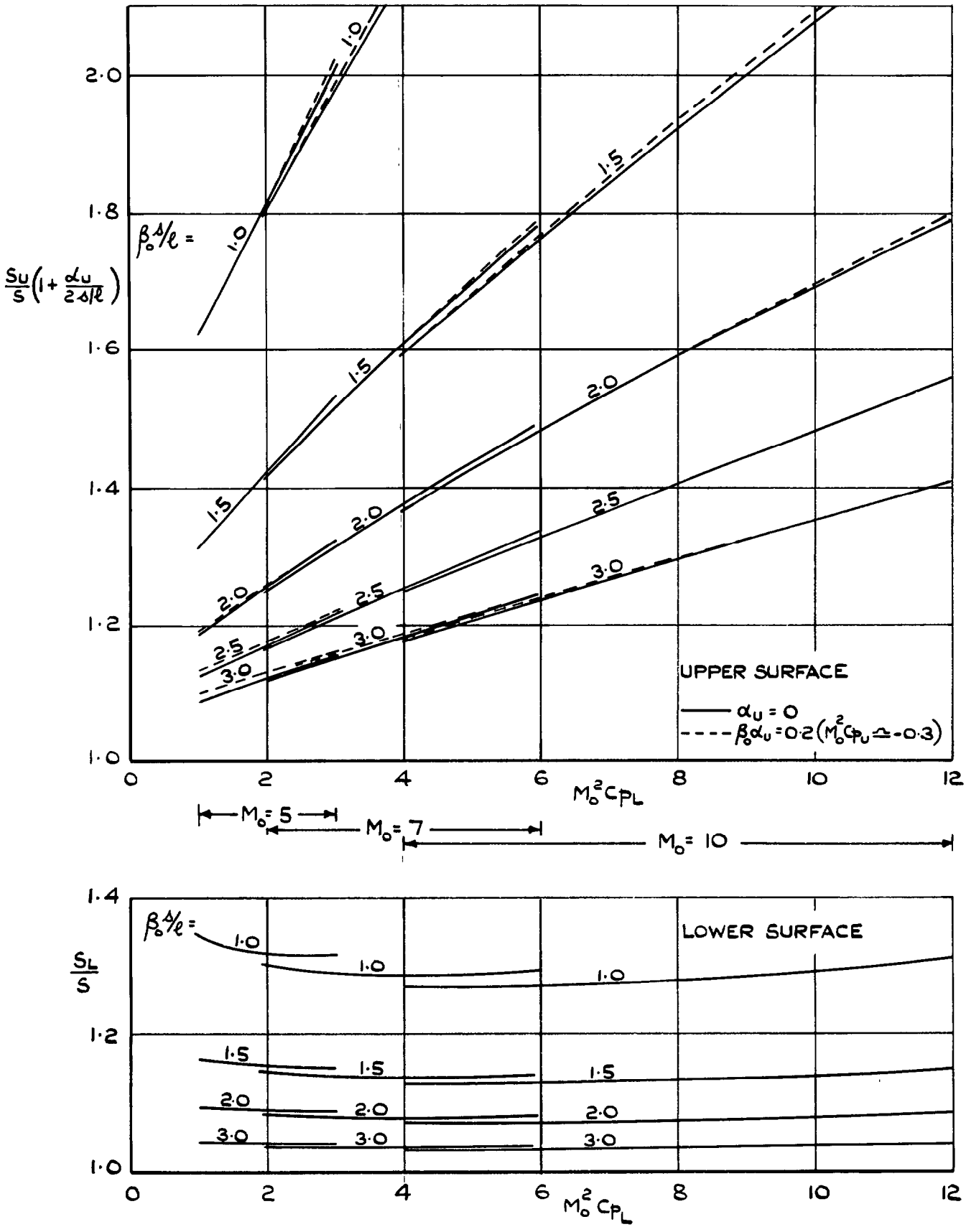

FIG. 2 RATIO OF WETTED AREA TO PLAN AREA

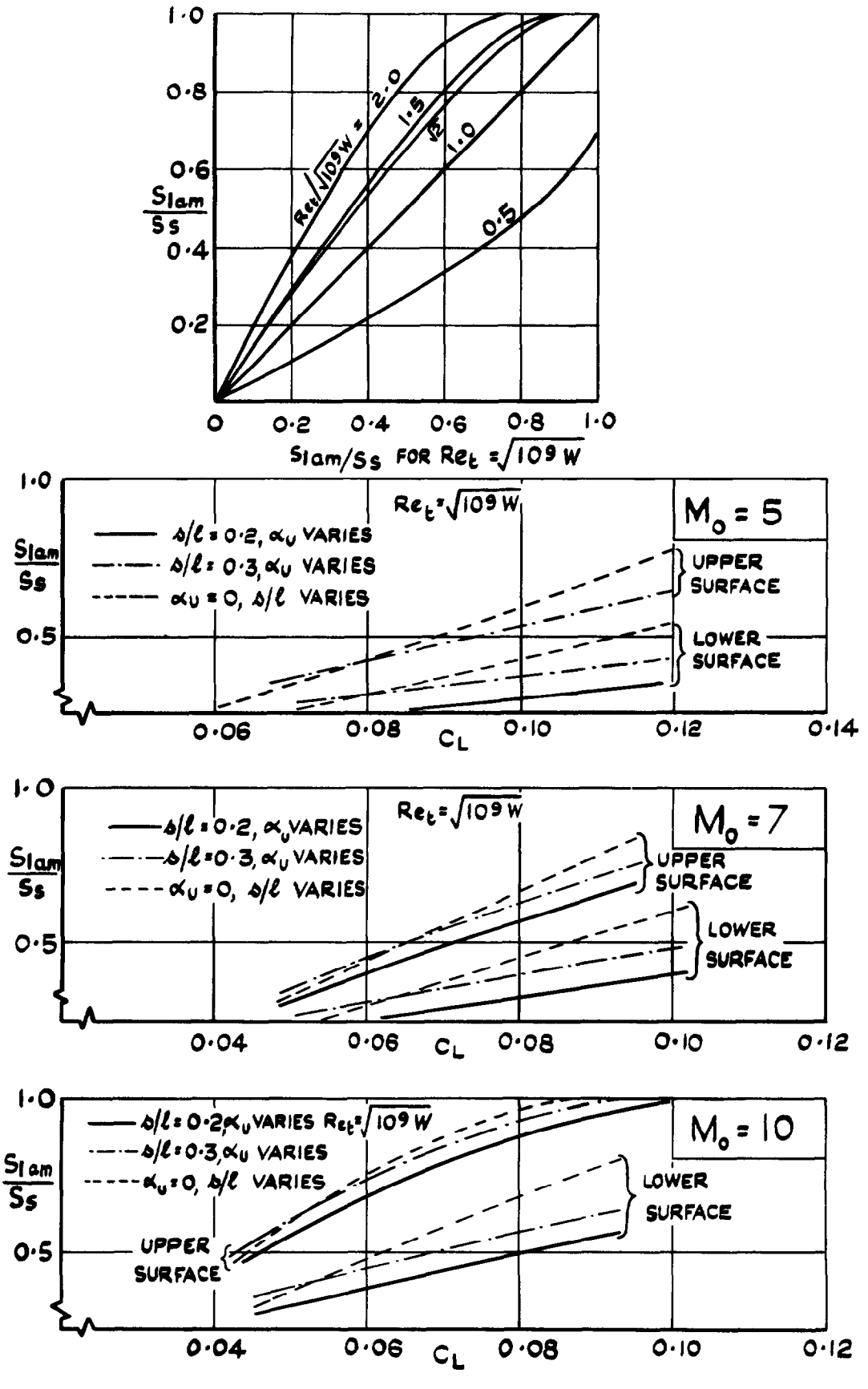

FIG. 3 PROPORTION OF WING SURFACE AREA WITH LAMINAR BOUNDARY LAYER, $\tau = 0{\cdot}08$, $W/S = 25\ lb/ft^2$.

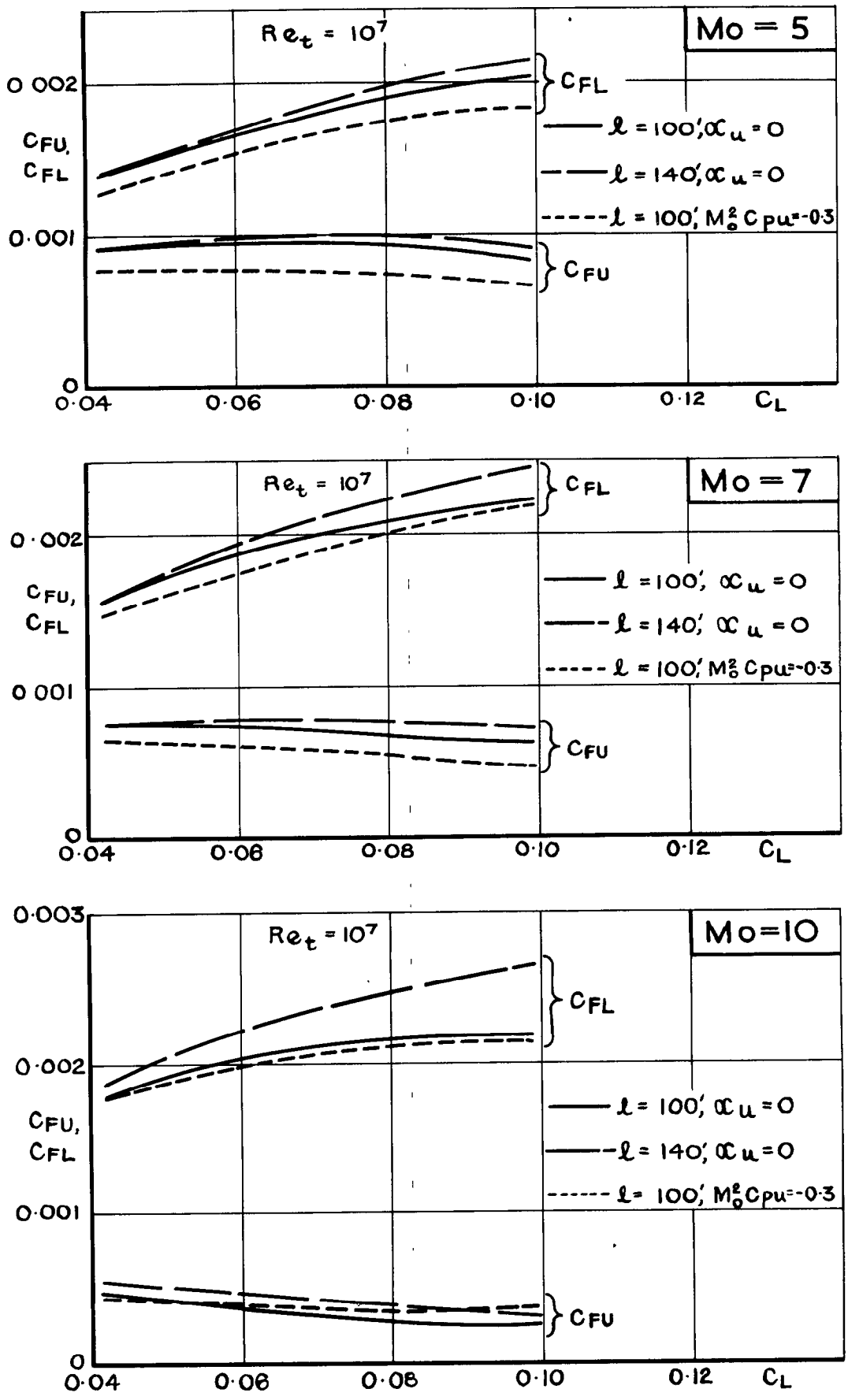

(a) W/S = 25 lb./ft.^{2}

FIG. 4 SKIN-FRICTION FORCE COEFFICIENT C_F VS C_L FOR $Re_t = 10^7$

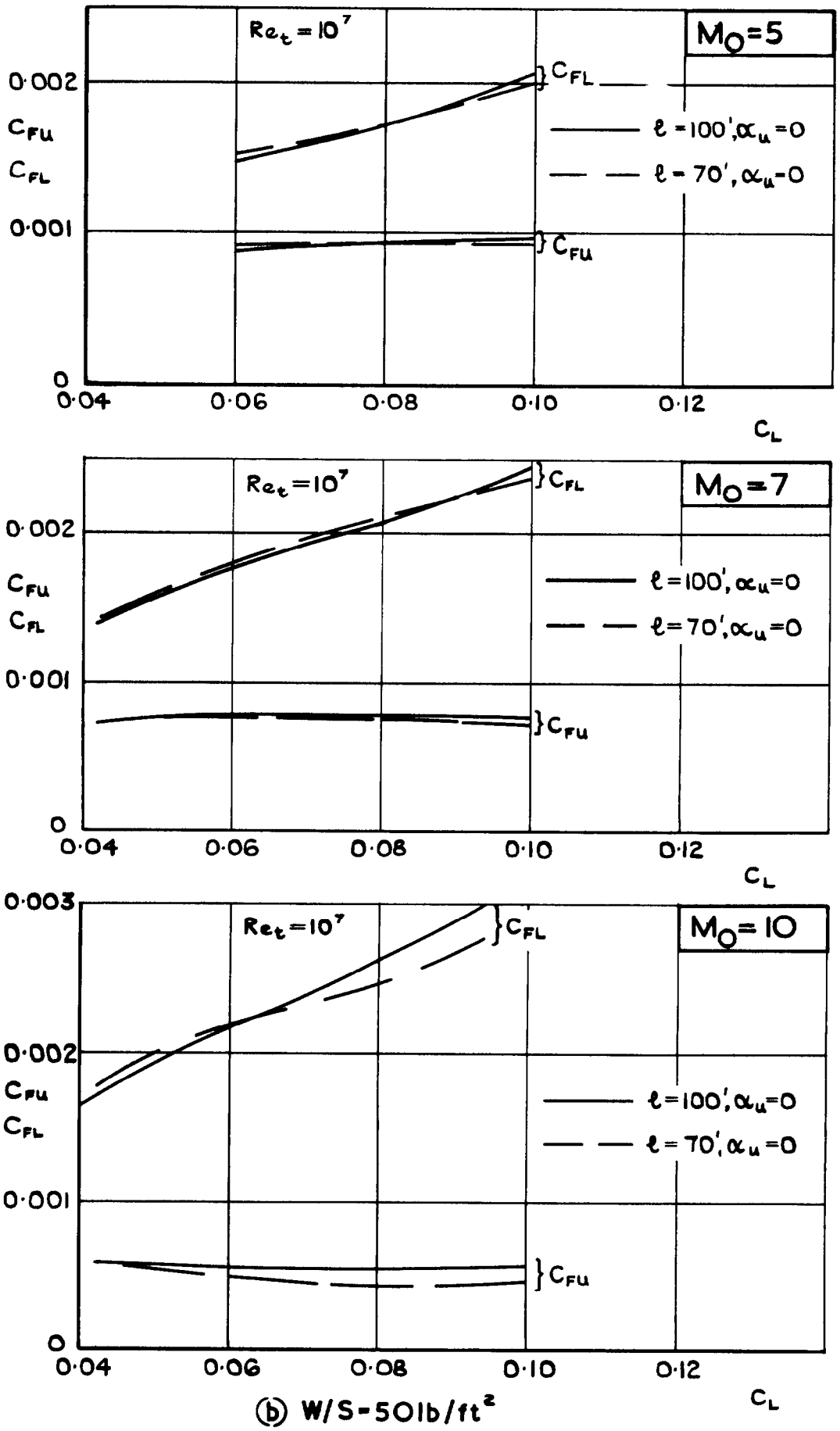

(b) W/S - 50 lb/ft²

FIG. 4 (CONTD) SKIN-FRICTION FORCE COEFFICIENT C_F = vs C_L FOR $Re_t = 10^7$

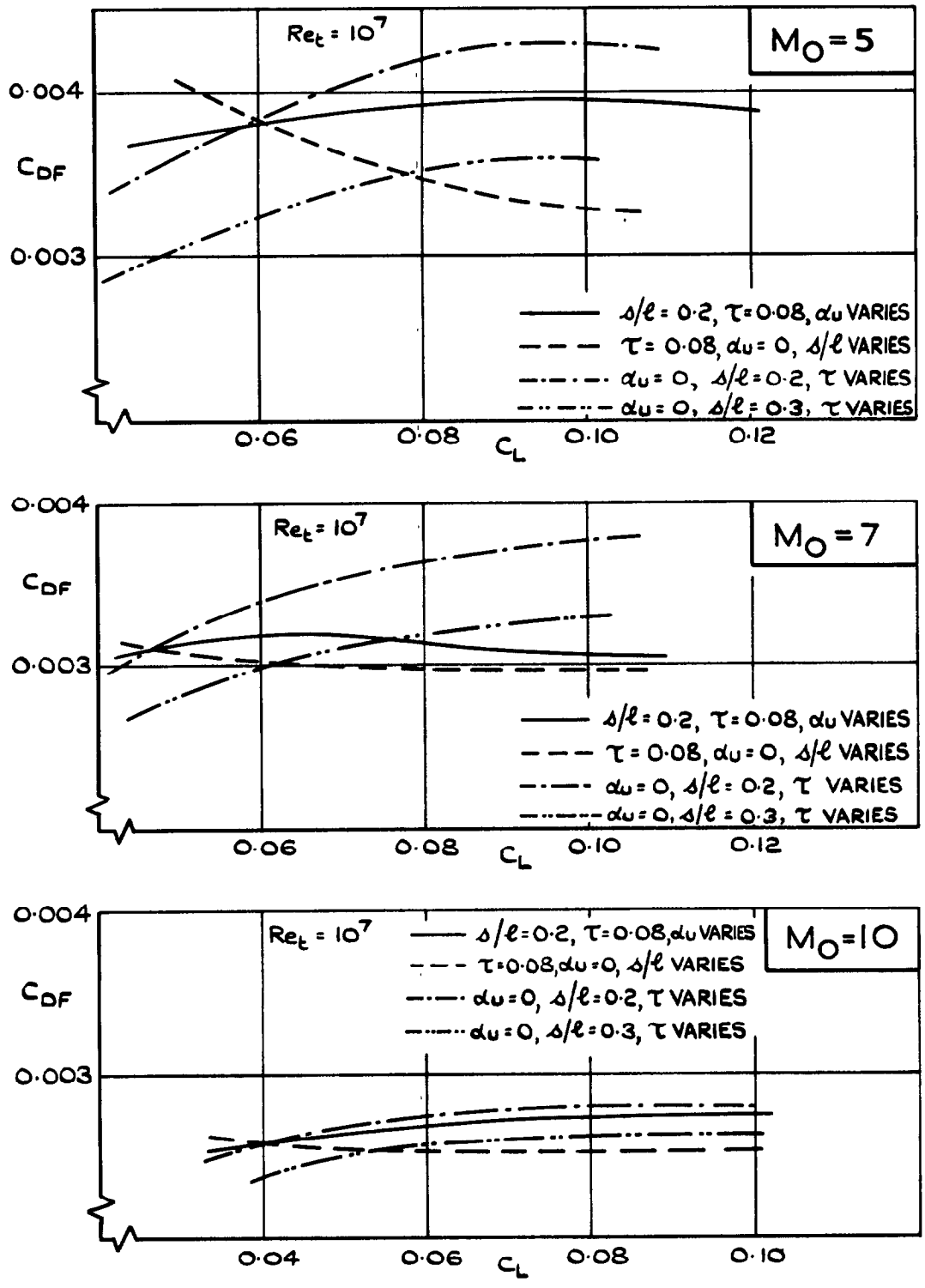

(a) W/S = 25 lb / ft^2

FIG. 5 SKIN-FRICTION DRAG COEFFICIENT C_{DF} VS C_L FOR $Re_t = 10^7$

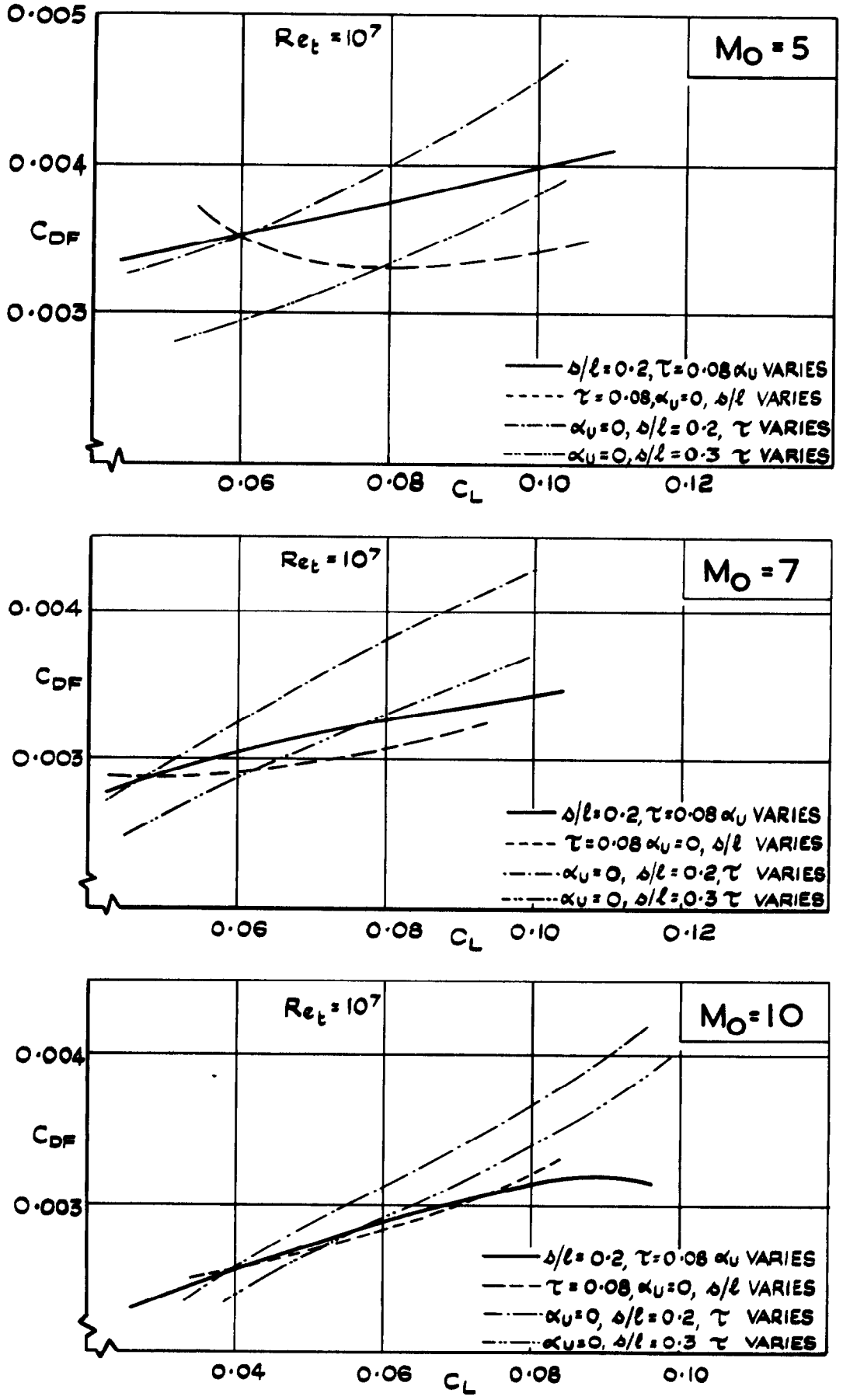

(b) $W/S = 50\ lb/ft^2$

FIG. 5 (CONTD) SKIN-FRICTION DRAG COEFFICIENT C_{DF} VS C_L FOR $Re_t = 10^7$

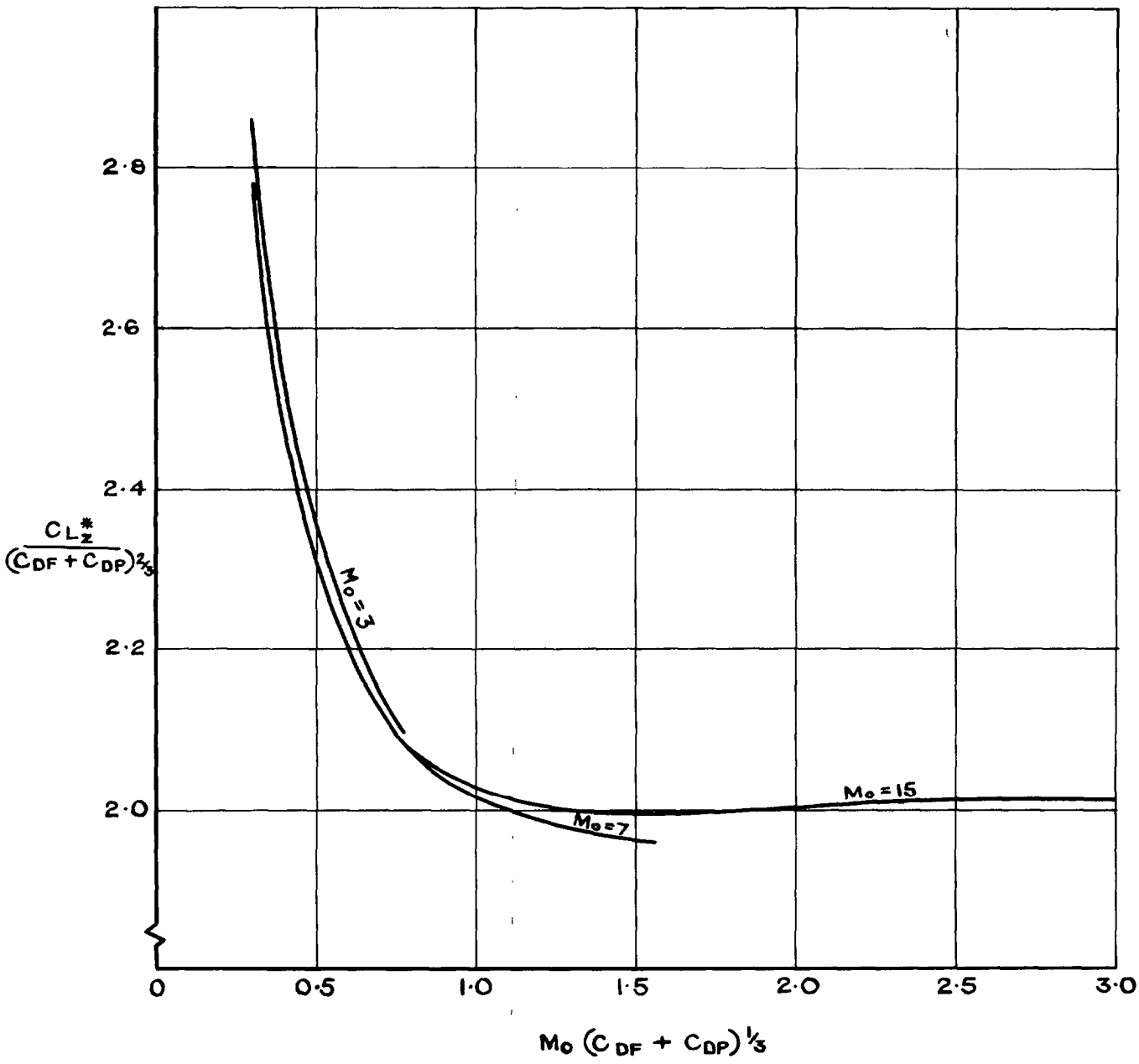

FIG. 6 LIFT COEFF. AT MAX. LIFT TO DRAG RATIO WITH STREAMWISE UPPER SURFACE AND CONSTANT $(C_{DF}+C_{DP})$

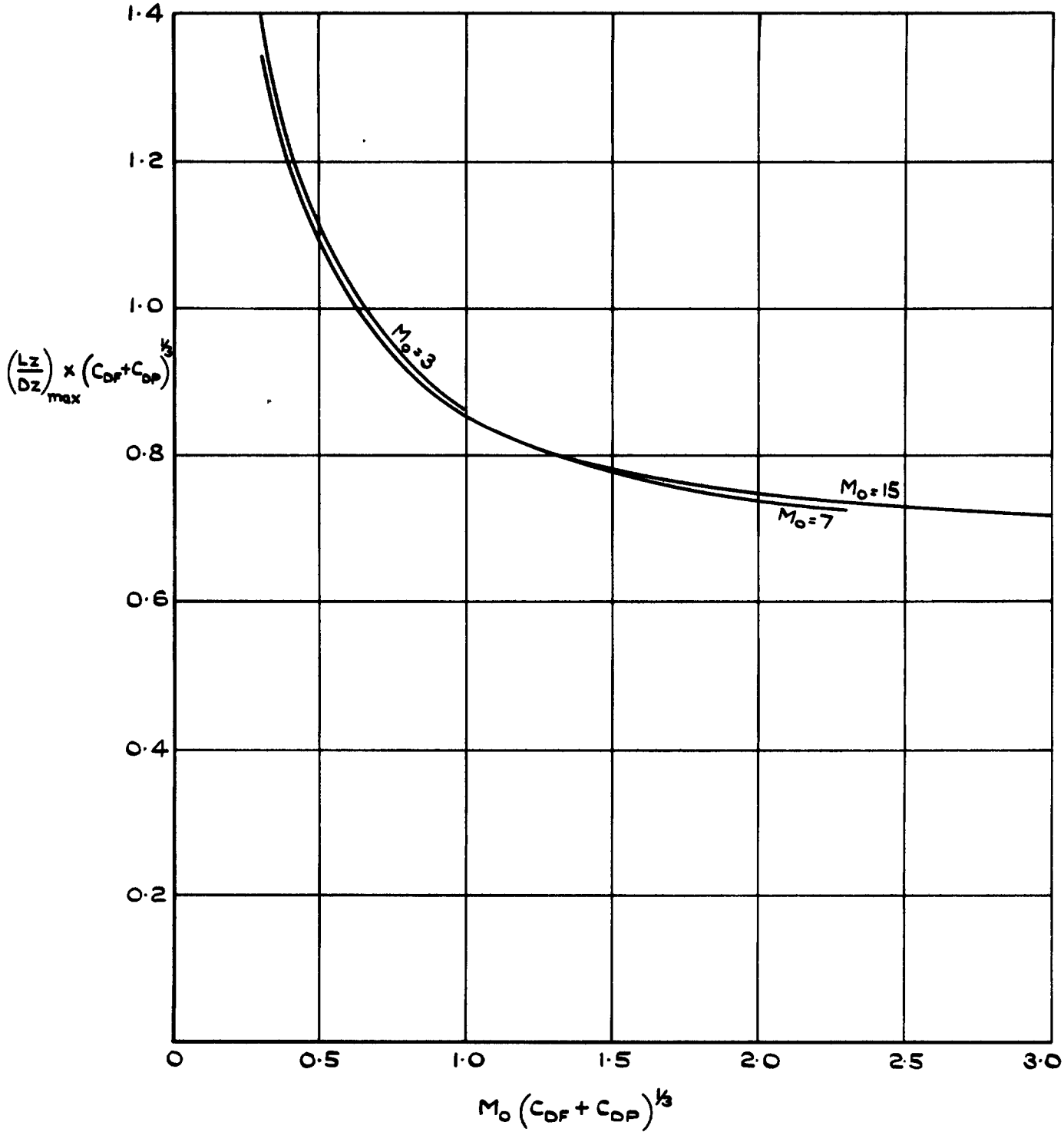

FIG.7 MAX LIFT TO DRAG RATIO WITH STREAMWISE UPPER SURFACE AND CONSTANT $(C_{DF}+C_{DP})$

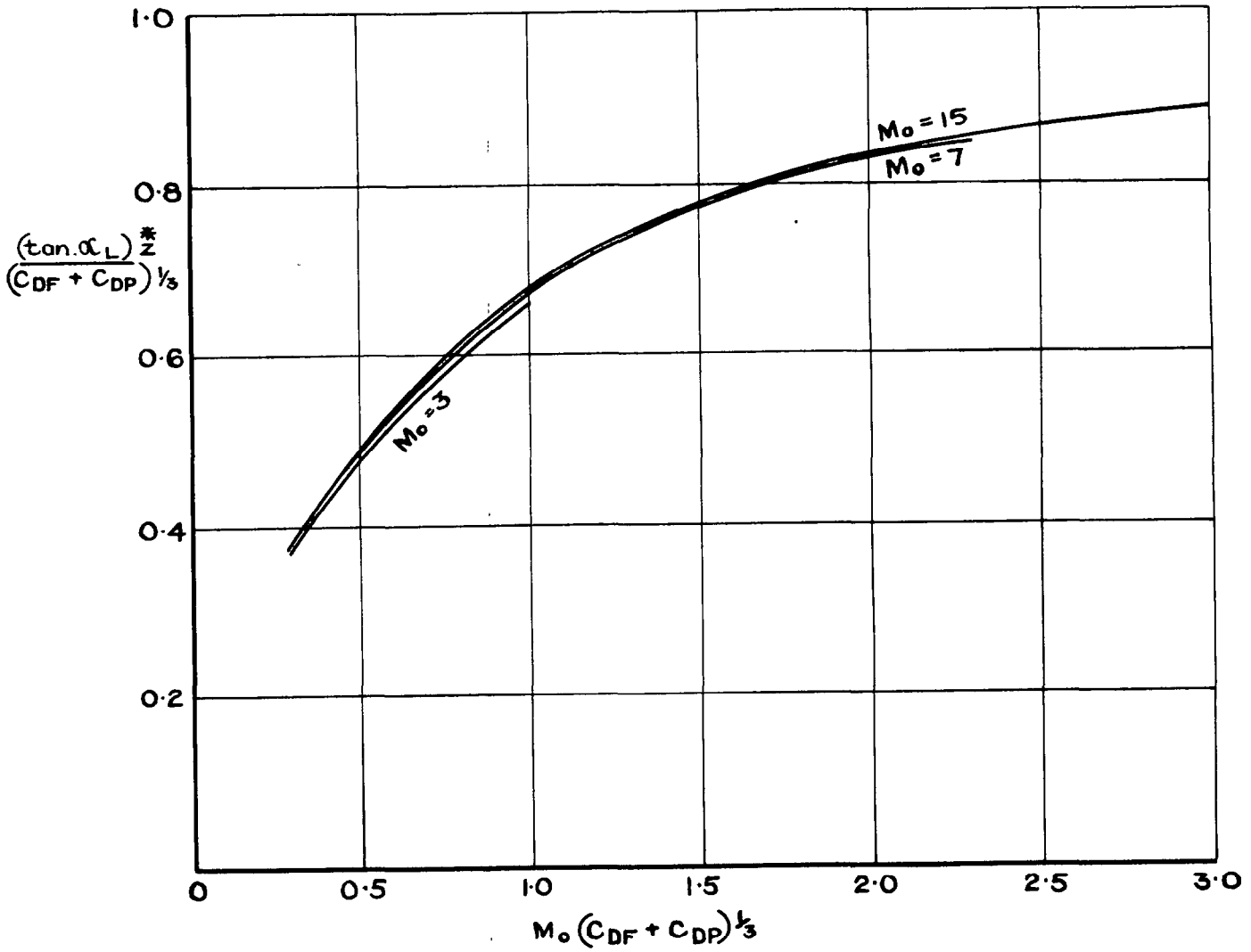

FIG. 8 INCIDENCE AT MAX. LIFT TO DRAG RATIO WITH STREAMWISE UPPER SURFACE AND CONSTANT $(C_{DF}+C_{DP})$

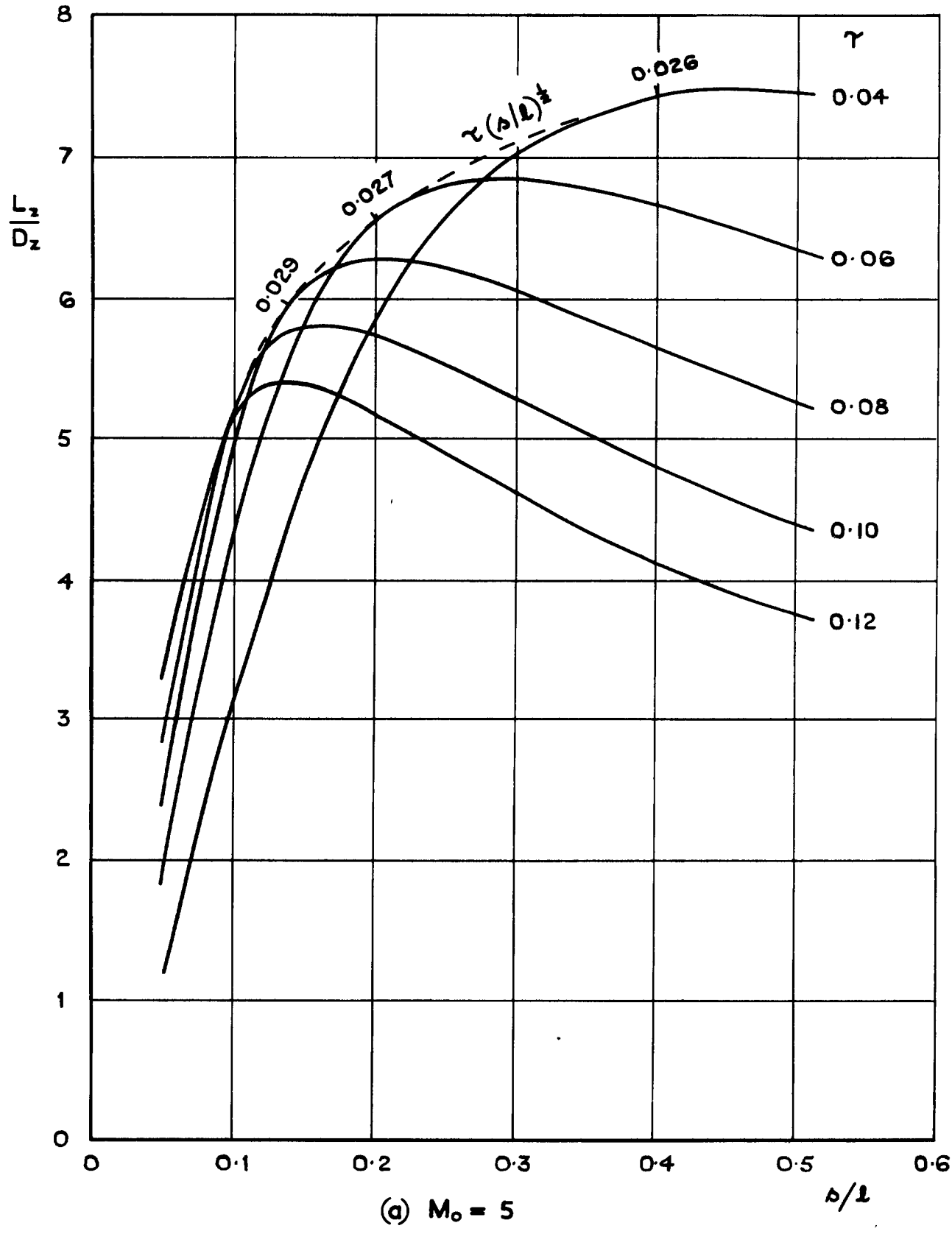

FIG.9 LIFT TO DRAG RATIO vs s/ℓ AT CONSTANT τ, WITH STREAMWISE UPPER SURFACE, $C_{FU}=C_{FL}=0{\cdot}001$, $C_{DP}=0$

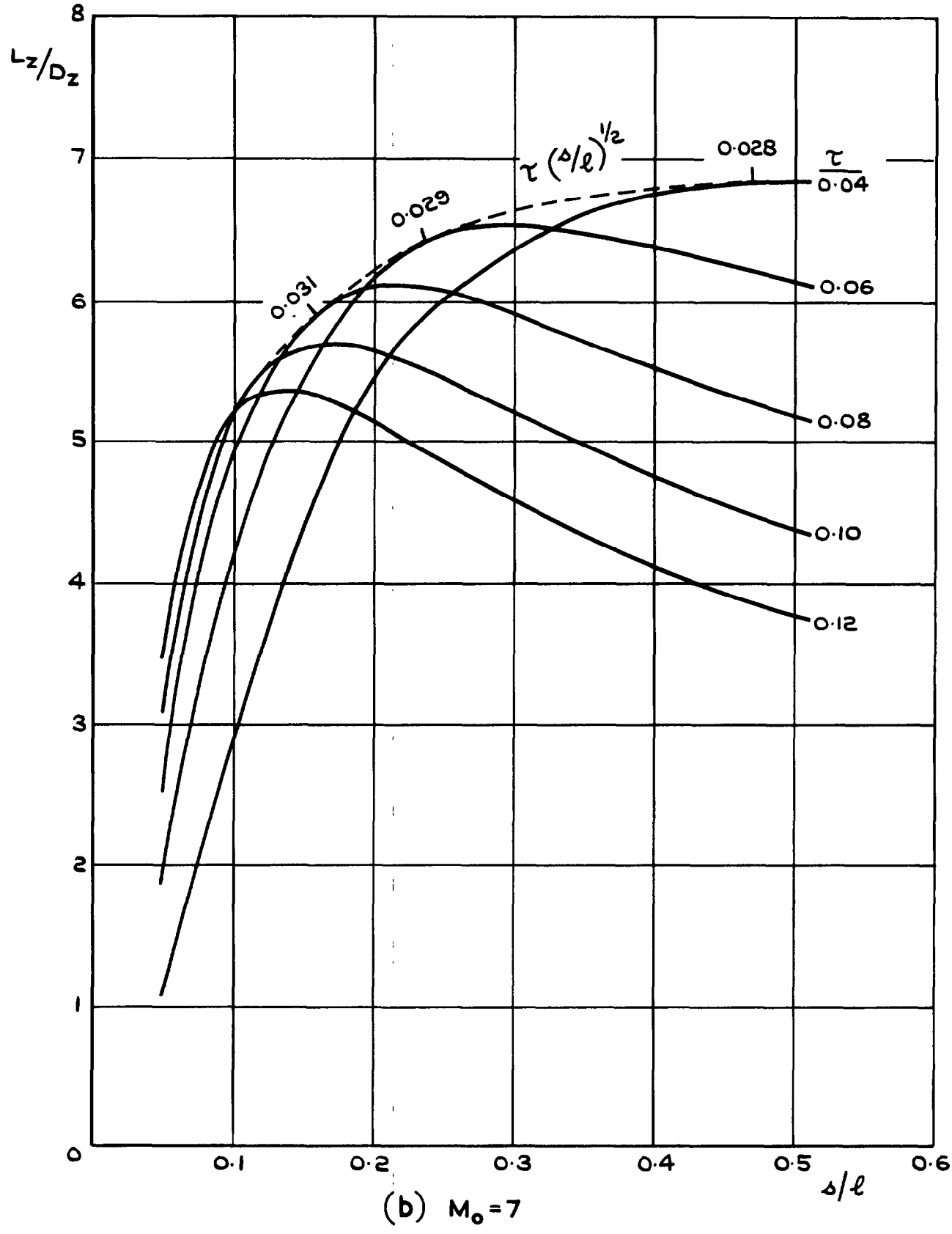

FIG.9 (CONTD) LIFT TO DRAG RATIO VS s/ℓ AT CONSTANT τ, STREAMWISE UPPER SURFACE, $C_{FU} = C_{FL} = 0·001$, $C_{DP} = 0$

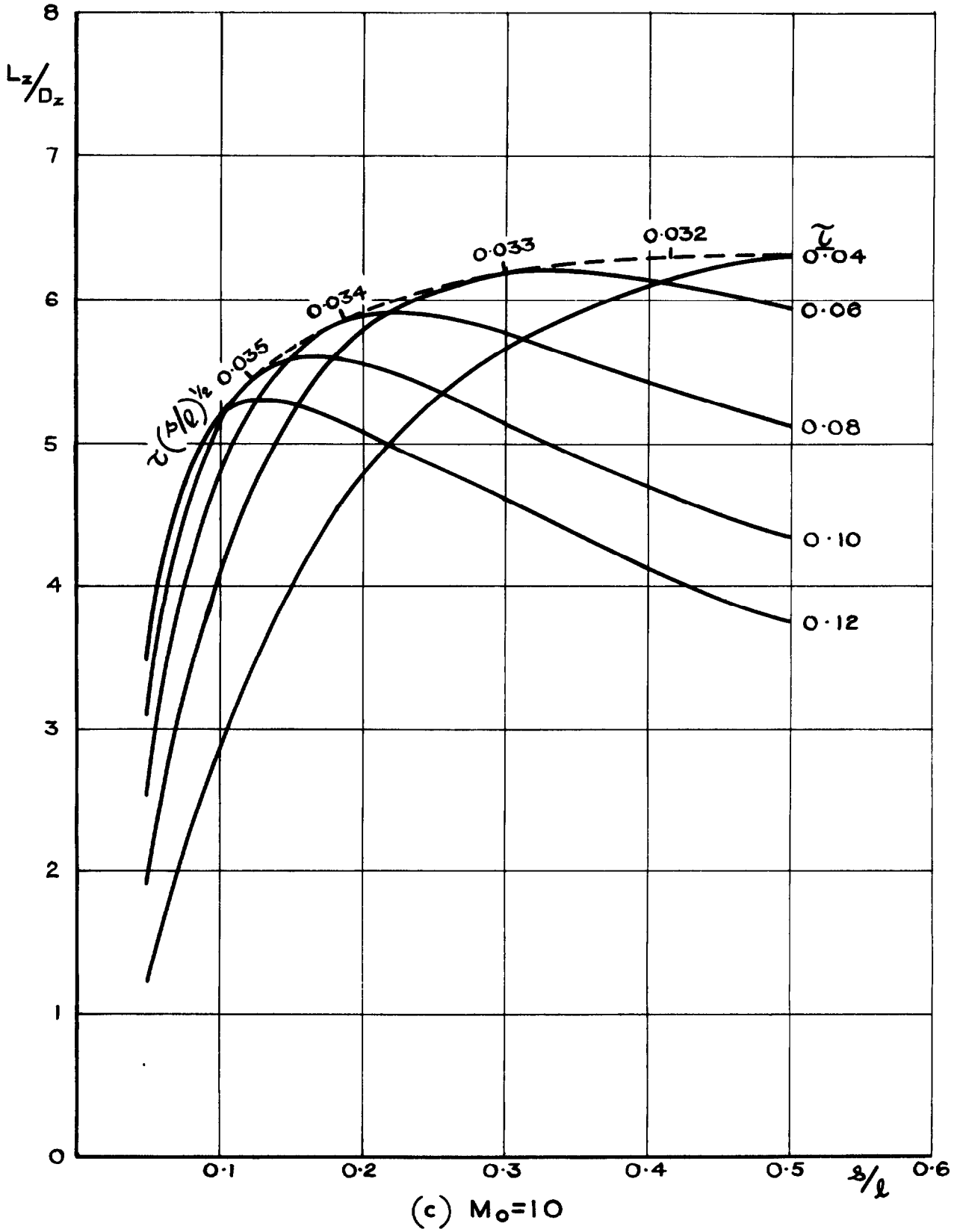

FIG. 9 (CONTD.) LIFT TO DRAG RATIO VS s/l AT CONSTANT τ WITH STREAMWISE UPPER SURFACE

$C_{FU} = C_{FL} = 0{\cdot}001$, $C_{DP} = 0$

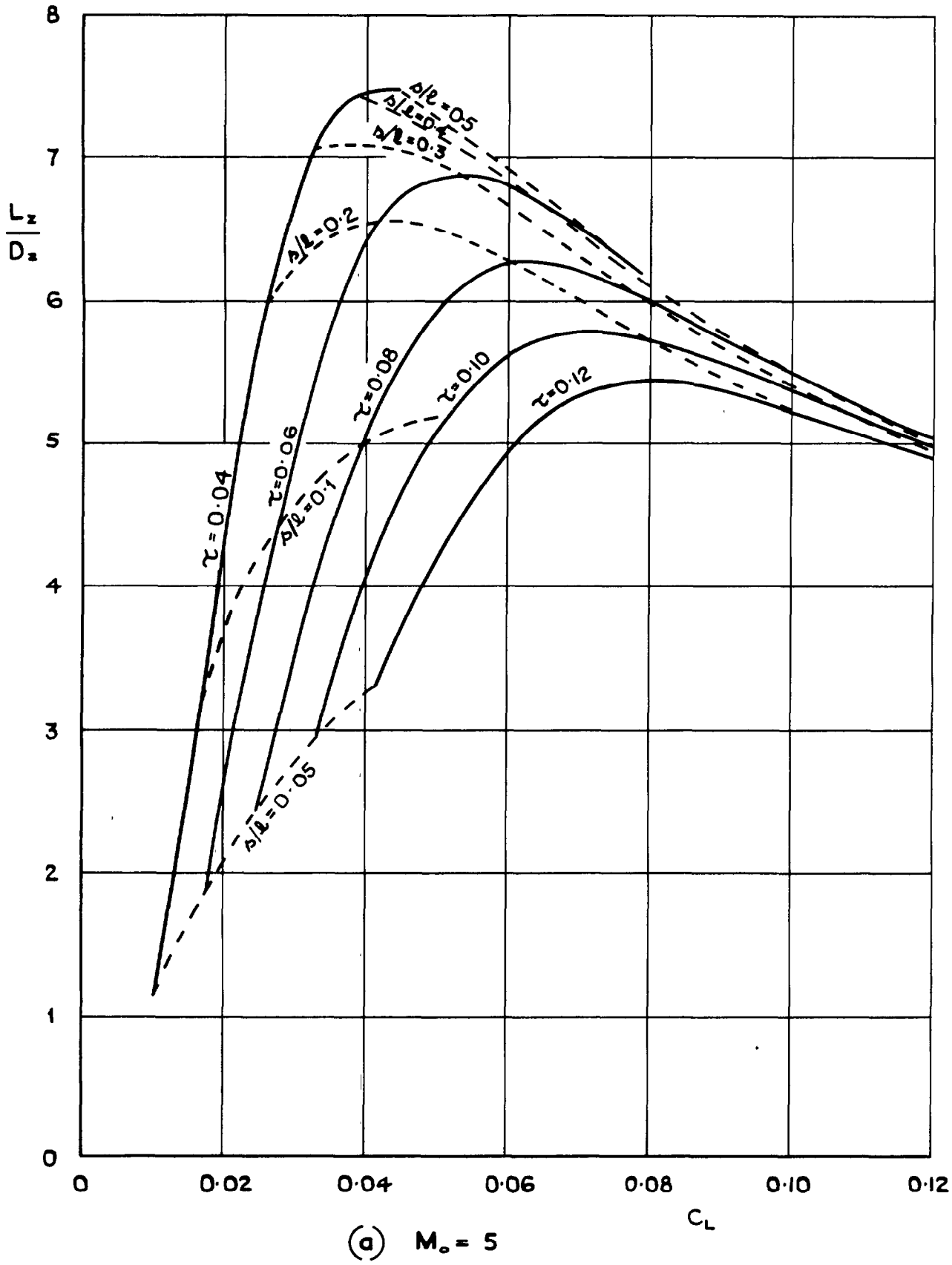

(a) $M_\infty = 5$

FIG. 10 LIFT TO DRAG RATIO vs C_L AT CONSTANT τ, WITH STREAMWISE UPPER SURFACE, $C_{FU} = C_{FL} = 0{\cdot}001$, $C_{DP} = 0$

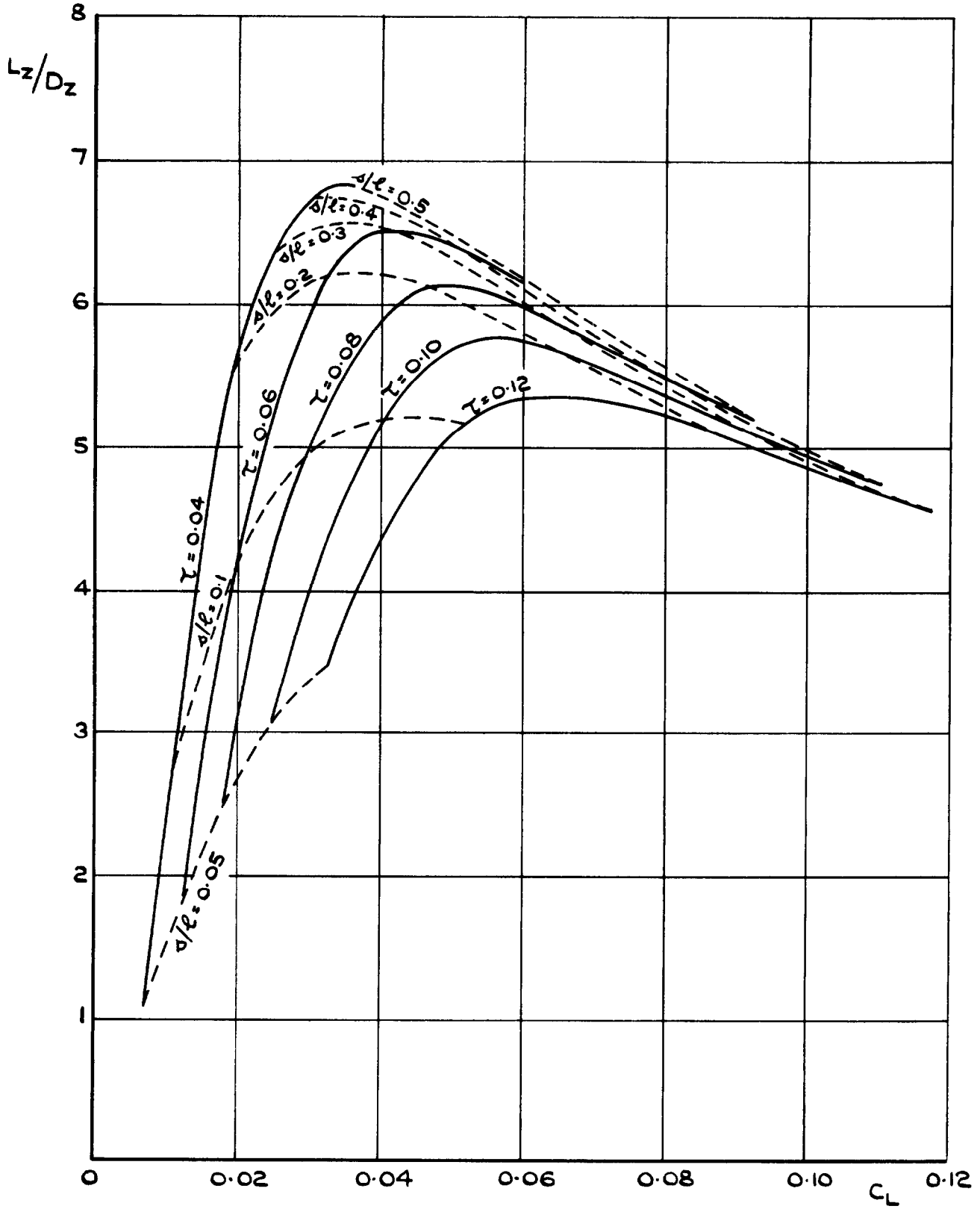

(b) $M_o = 7$

FIG. 10 (CONTD) LIFT TO DRAG RATIO VS C_L AT CONSTANT τ, WITH STREAMWISE UPPER SURFACE, $C_{FU} = C_{FL} = 0.001$, $C_{DP} = 0$

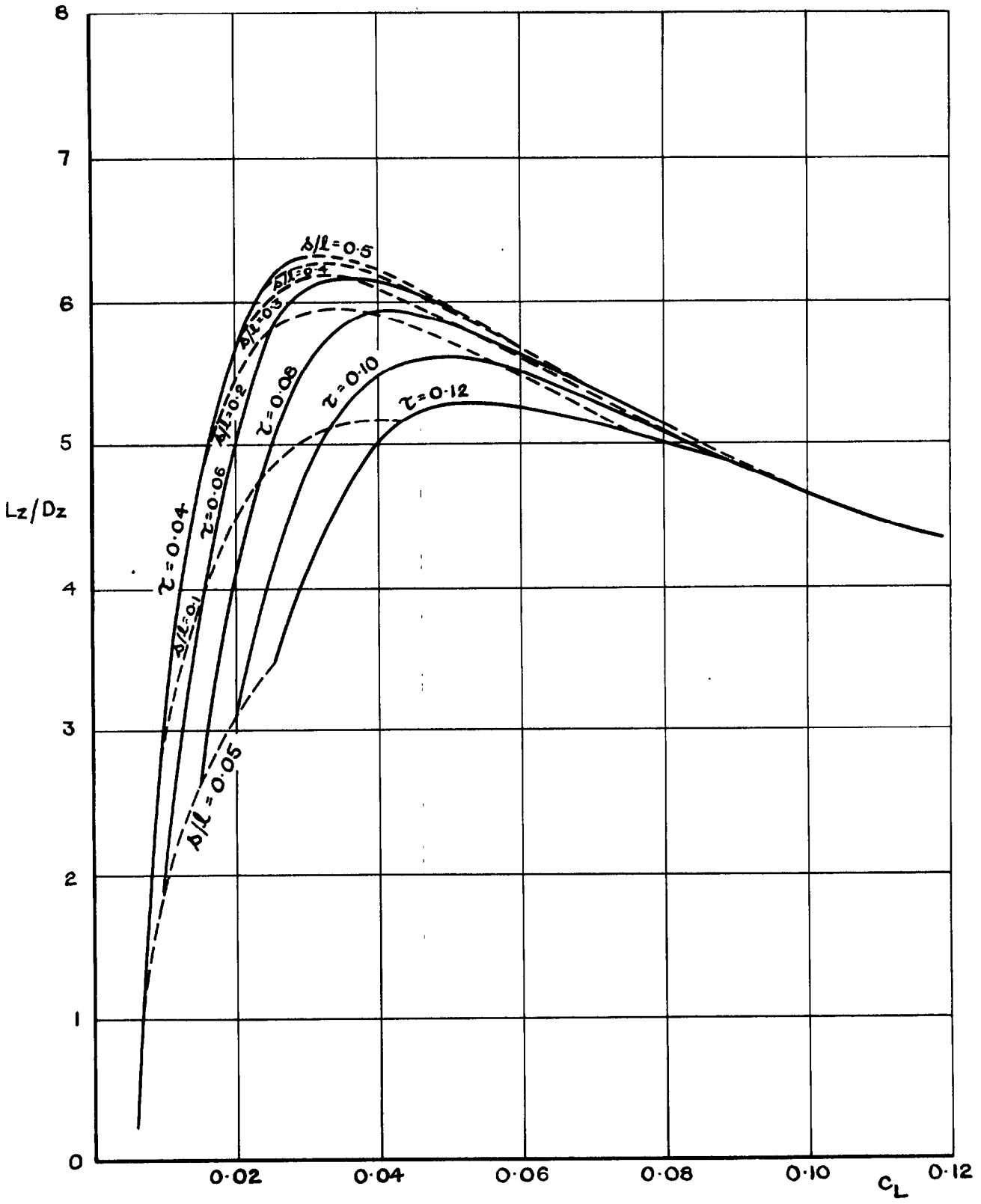

(c) $M_o = 10$

FIG.10(CONTD) LIFT TO DRAG RATIO VS C_L AT CONSTANT τ, WITH STREAMWISE UPPER SURFACE.

$C_{FU} = C_{FL} = 0{\cdot}001$, $C_{DP} = 0$

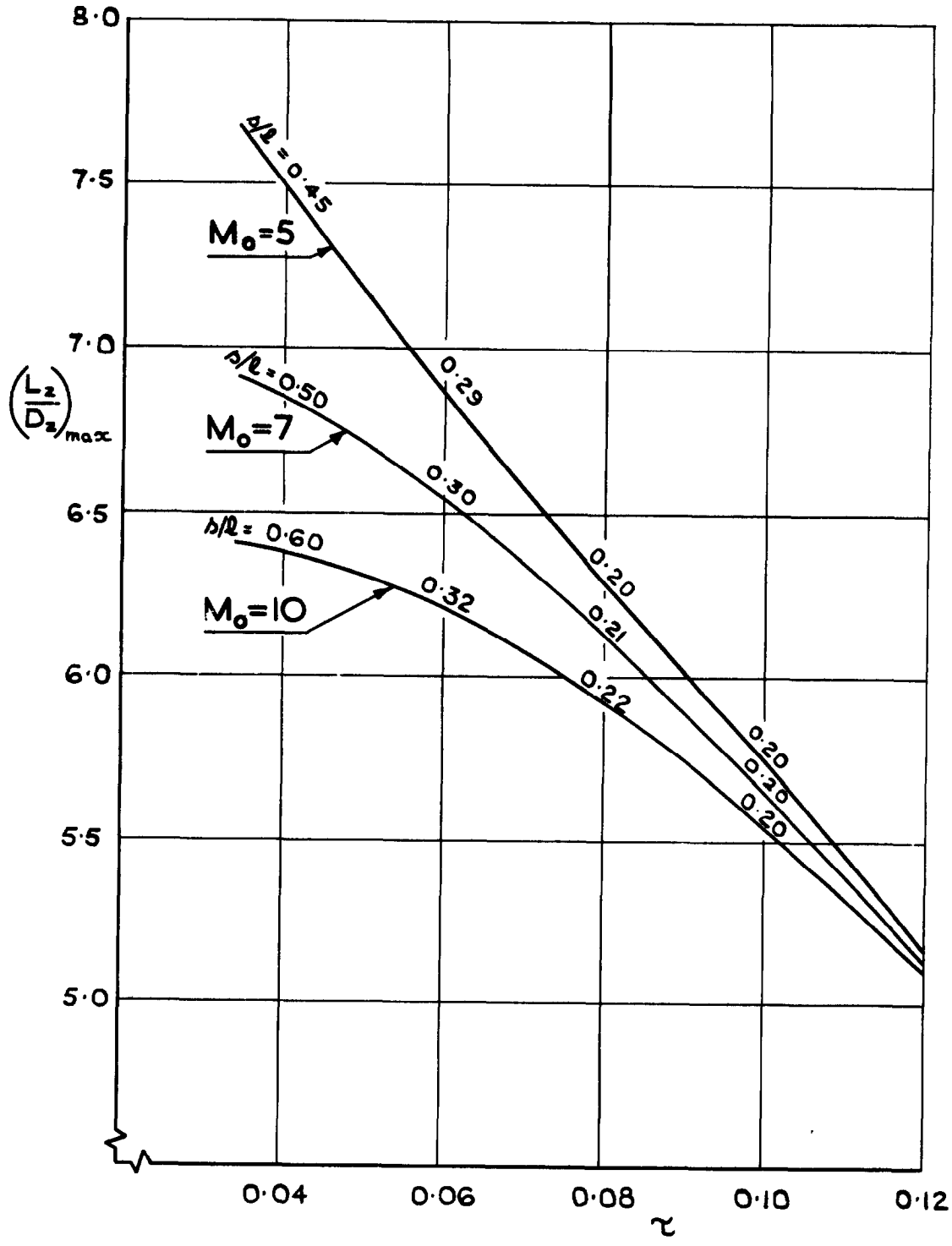

FIG. 11 MAX LIFT TO DRAG RATIO ($\delta/\ell \geq 0.2$) vs τ, WITH STREAMWISE UPPER SURFACE, $C_{FU} = C_{FL} = 0.001$, $C_{DP} = 0$

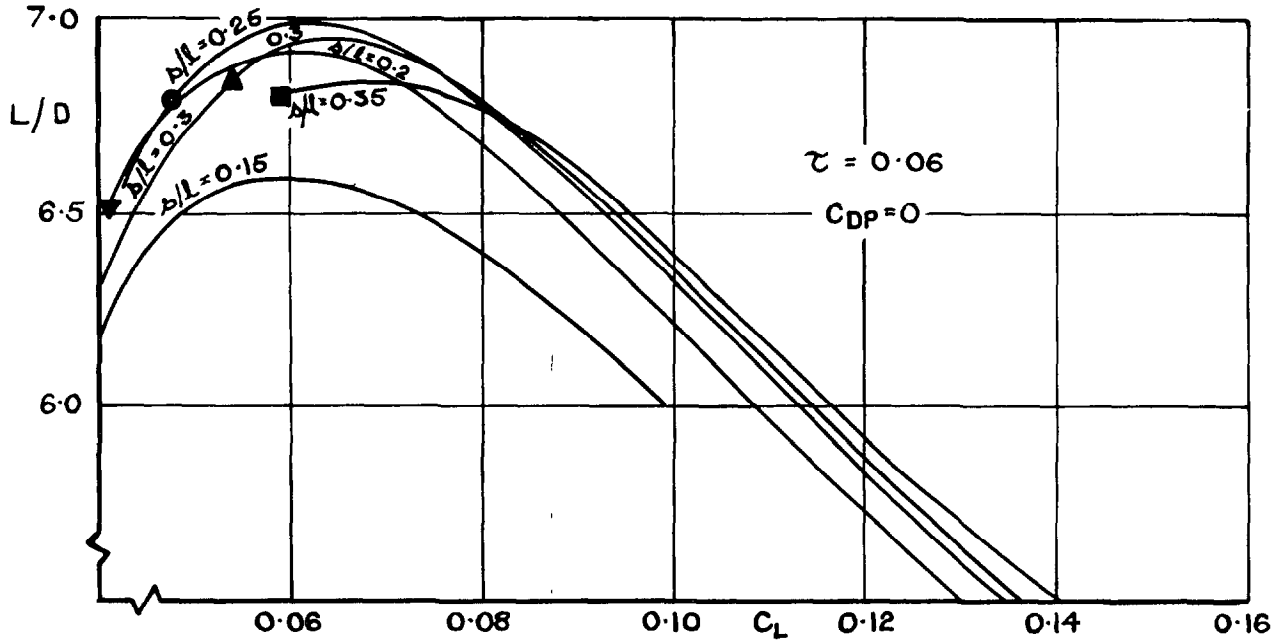

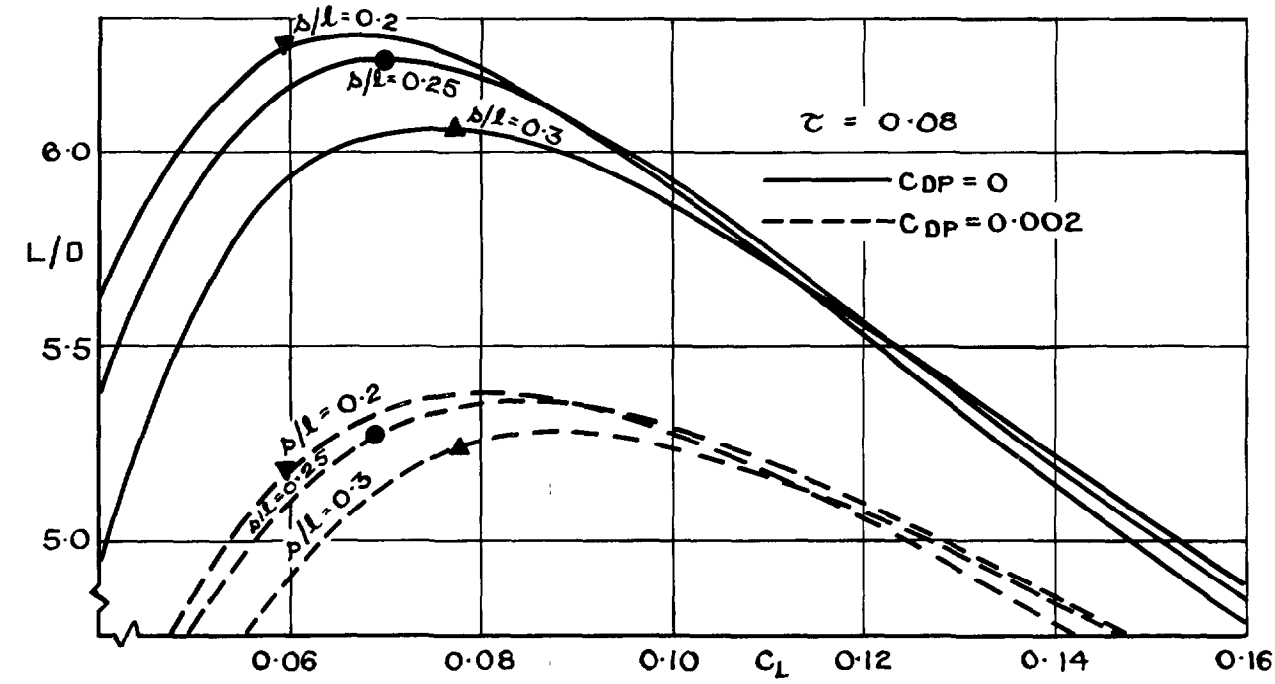

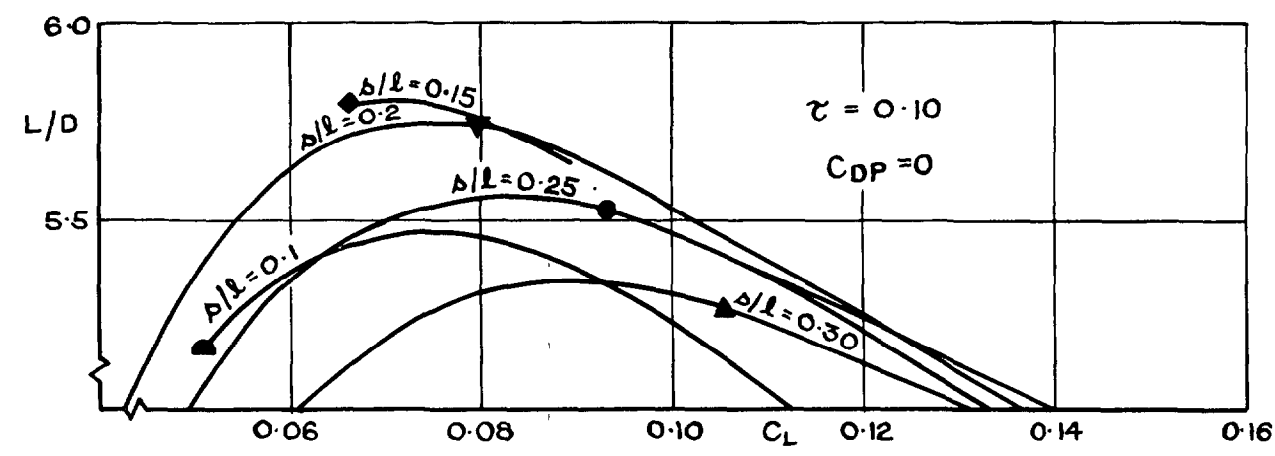

N.B. SYMBOL ON CURVE INDICATES $\alpha_U = 0$

(a) $M_0 = 5$

FIG. 12 LIFT TO DRAG RATIO VS C_L AT CONSTANT τ AND b/ℓ $C_{FU} = C_{FL} = 0{\cdot}001$

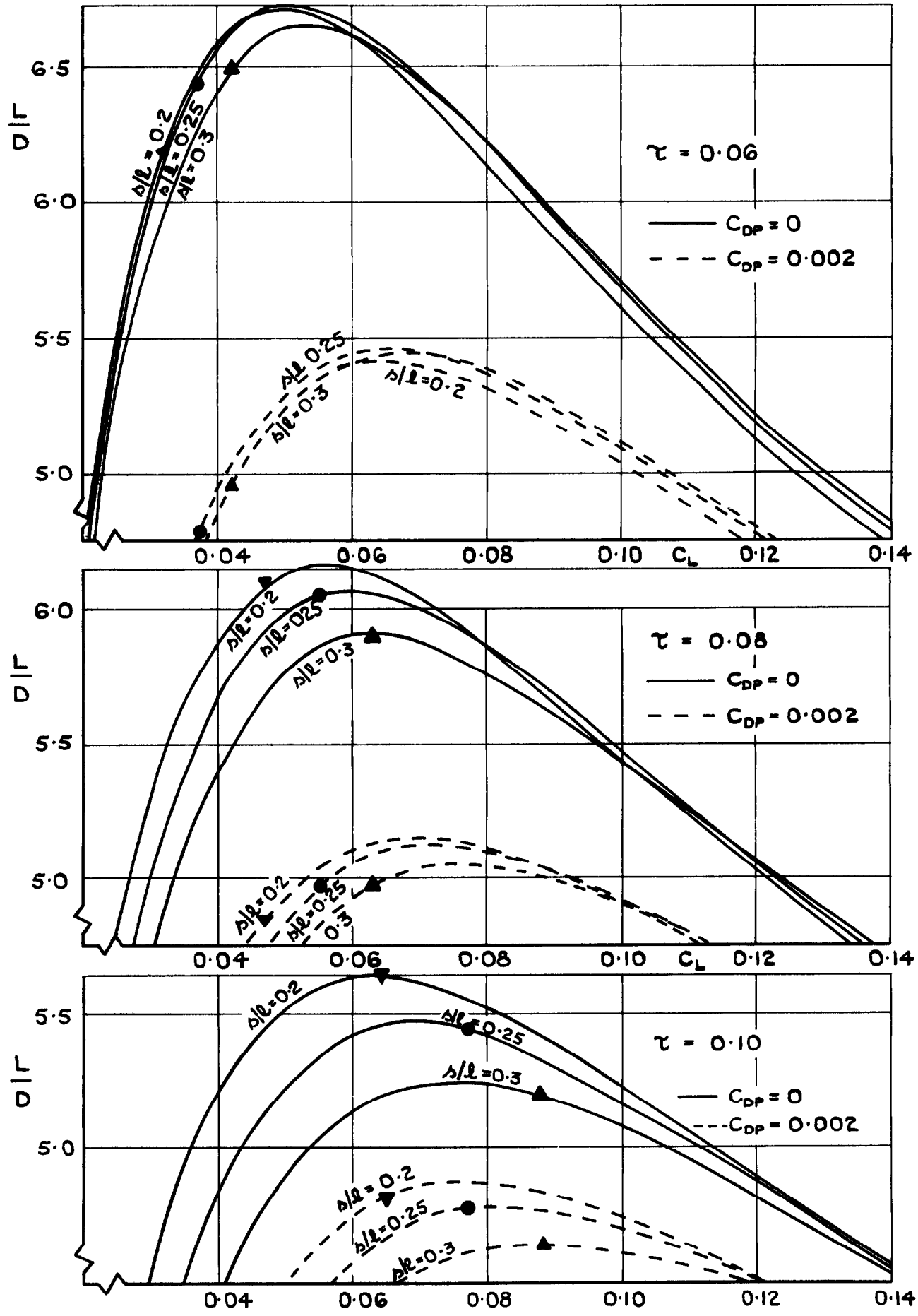

N.B. SYMBOL ON EACH CURVE INDICATES $\alpha_u = 0$

(b) $M_o = 7$

FIG.12 (CONTD) LIFT TO DRAG RATIO vs C_L AT CONSTANT τ AND s/ℓ $C_{FU} = C_{FL} = 0.001$

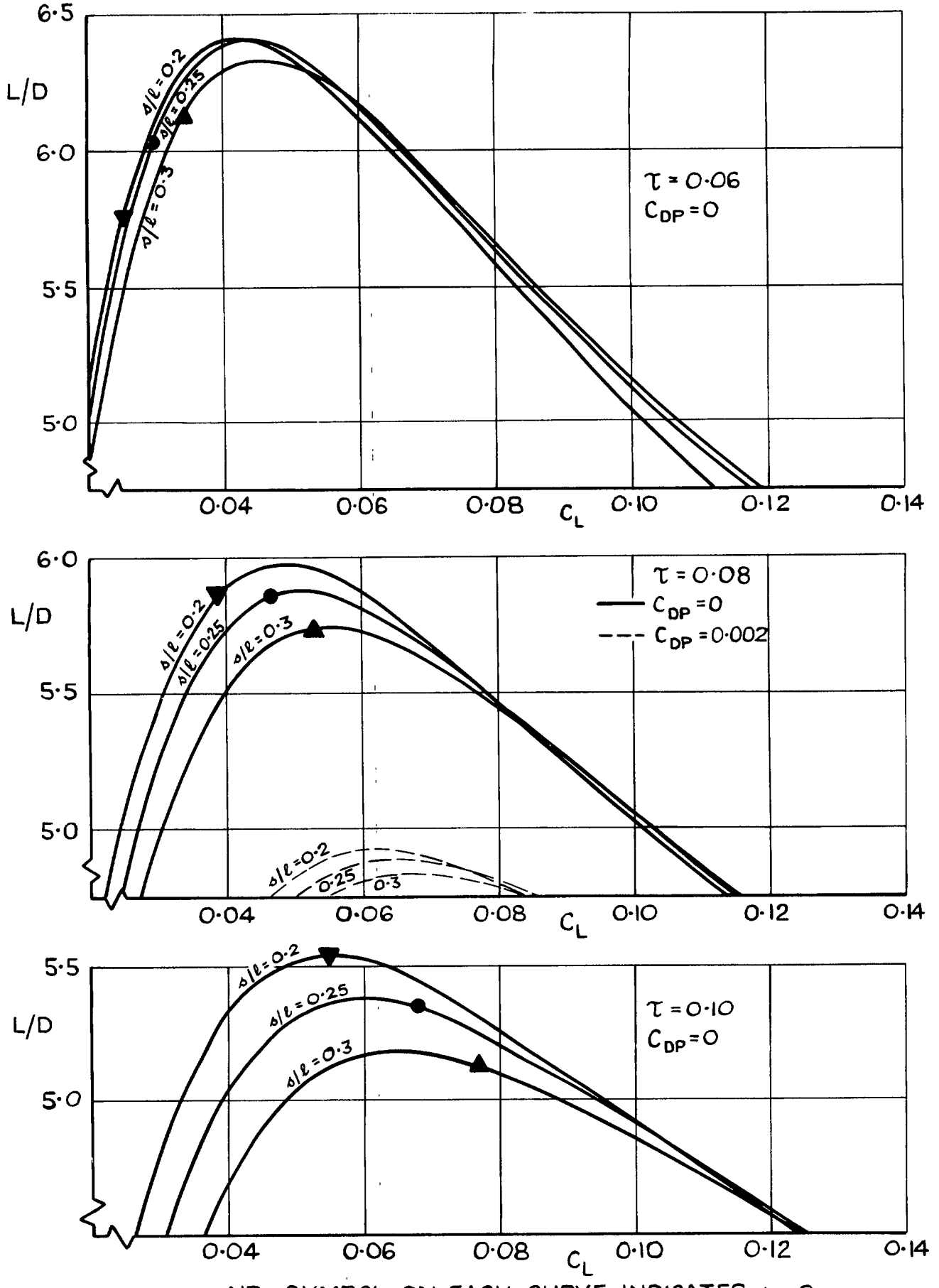

NB. SYMBOL ON EACH CURVE INDICATES $\alpha_u = 0$

(c) $M_0 = 10$

FIG. 12(contd) LIFT TO DRAG RATIO vs C_L AT CONSTANT τ AND δ/ℓ

$C_{FU} = C_{FL} = 0{\cdot}001$

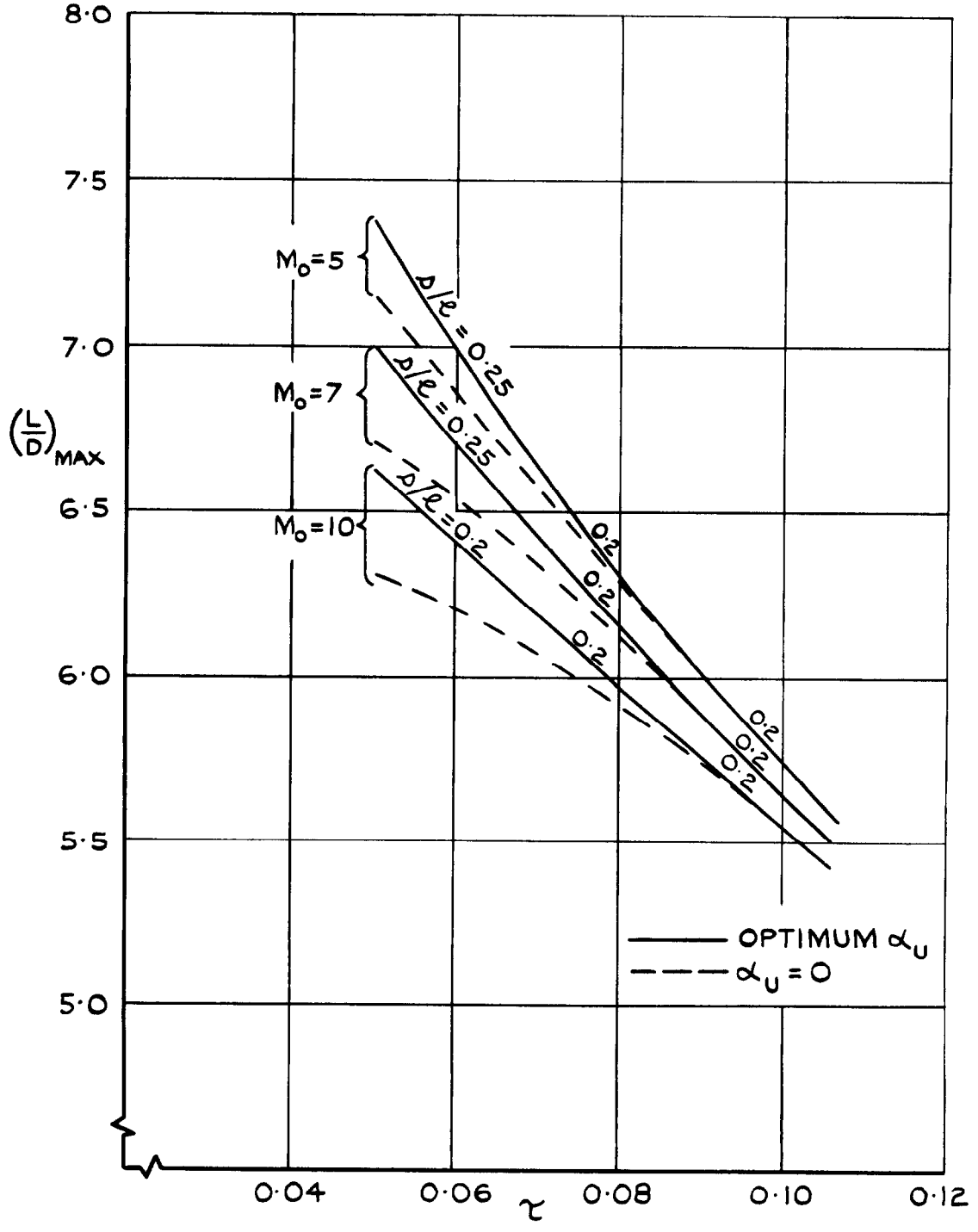

FIG.13 MAX. LIFT TO DRAG RATIO ($\delta/\ell = 0{\cdot}2$) vs τ
$C_{FU} = C_{FL} = 0{\cdot}001$, $C_{DP} = 0$

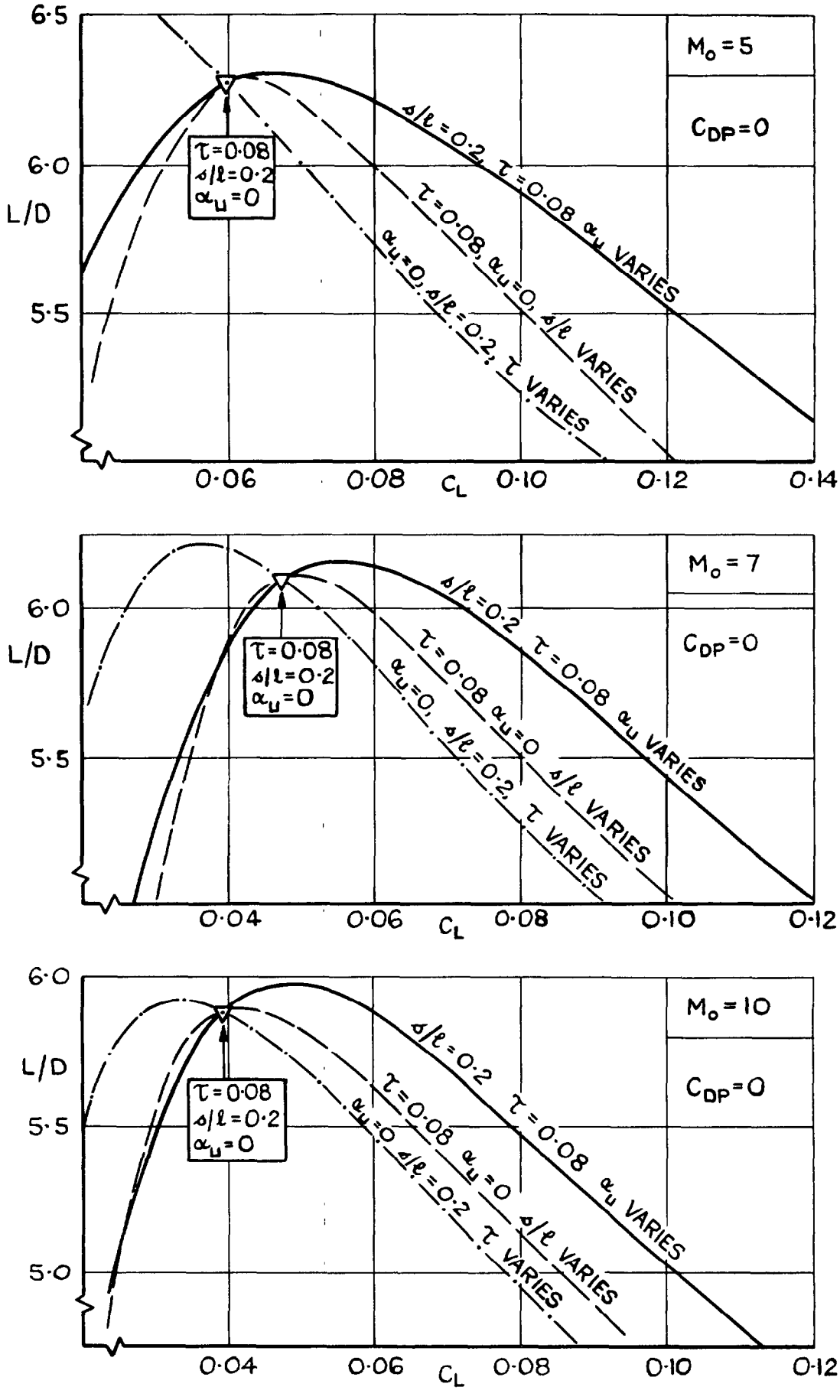

(a) DATUM CASE, $\tau = 0{\cdot}08$, $\delta/\ell = 0{\cdot}2$, $\alpha_u = 0$

FIG. 14 LIFT TO DRAG RATIO vs C_L, WITH $C_{FU} = C_{FL} = 0{\cdot}001$ -COMPARISON BETWEEN VARIATION OF α_u, δ/ℓ, τ

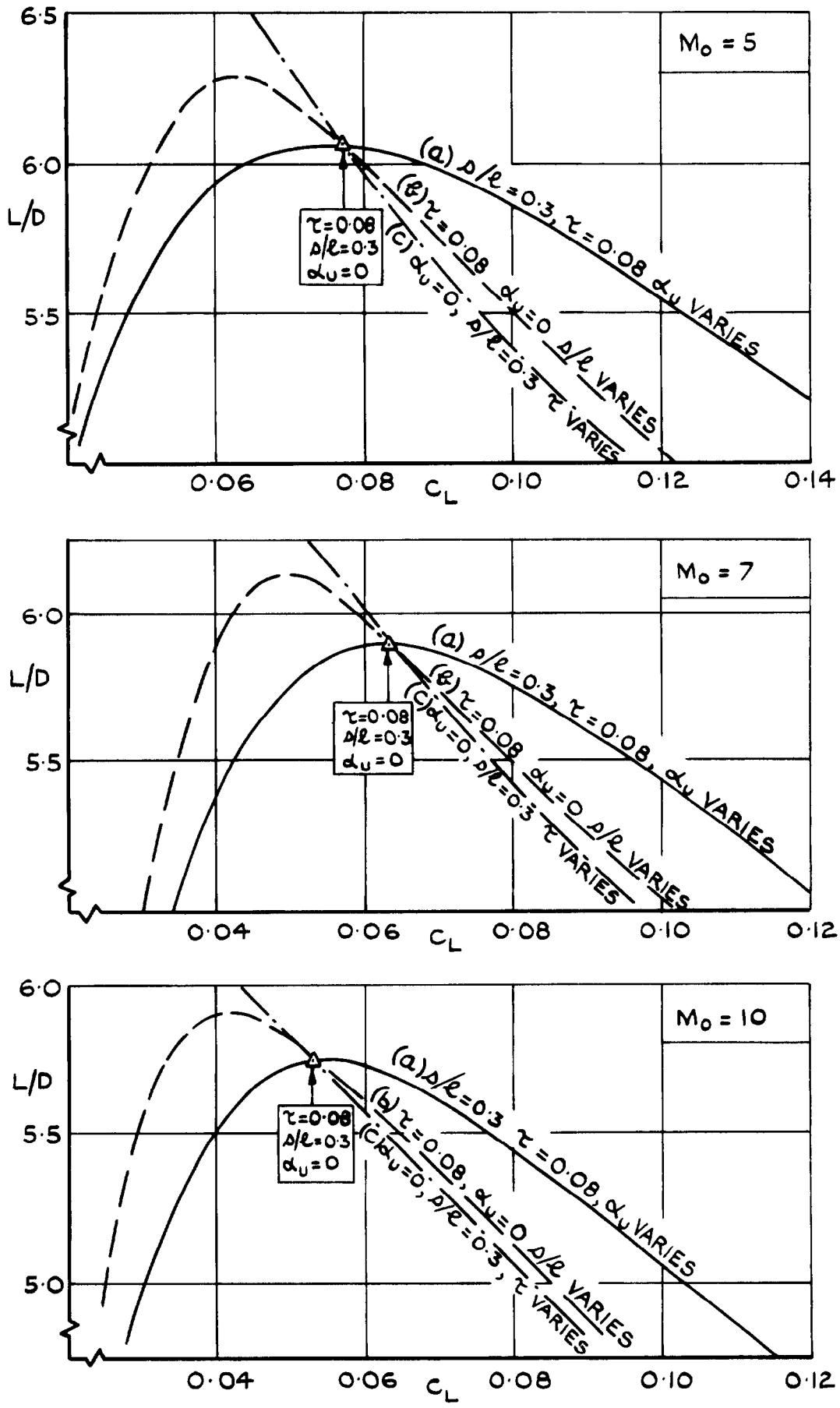

(b) DATUM CASE, $\tau = 0{\cdot}08$, $\delta/\ell = 0{\cdot}3$, $\alpha_U = 0$

FIG.14 (cont'd) LIFT TO DRAG RATIO vs C_L, WITH $C_{FU} = C_{FL} = 0{\cdot}001$
– COMPARISON BETWEEN VARIATION OF α_U, δ/ℓ, τ

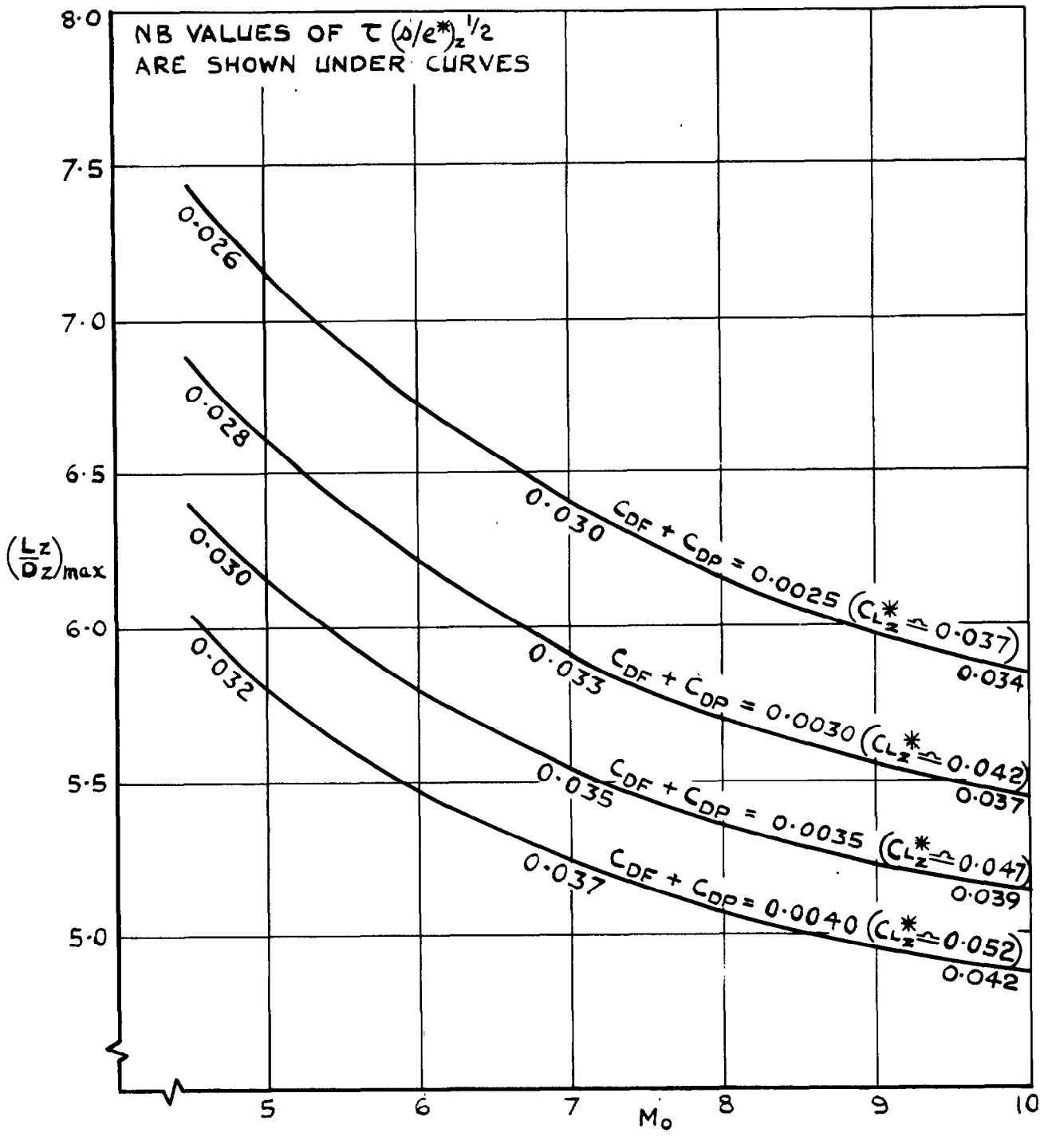

FIG. 15 MAX. LIFT TO DRAG RATIO vs M_o, WITH STREAMWISE UPPER SURFACE AND CONSTANT $(C_{DF}+C_{DP})$

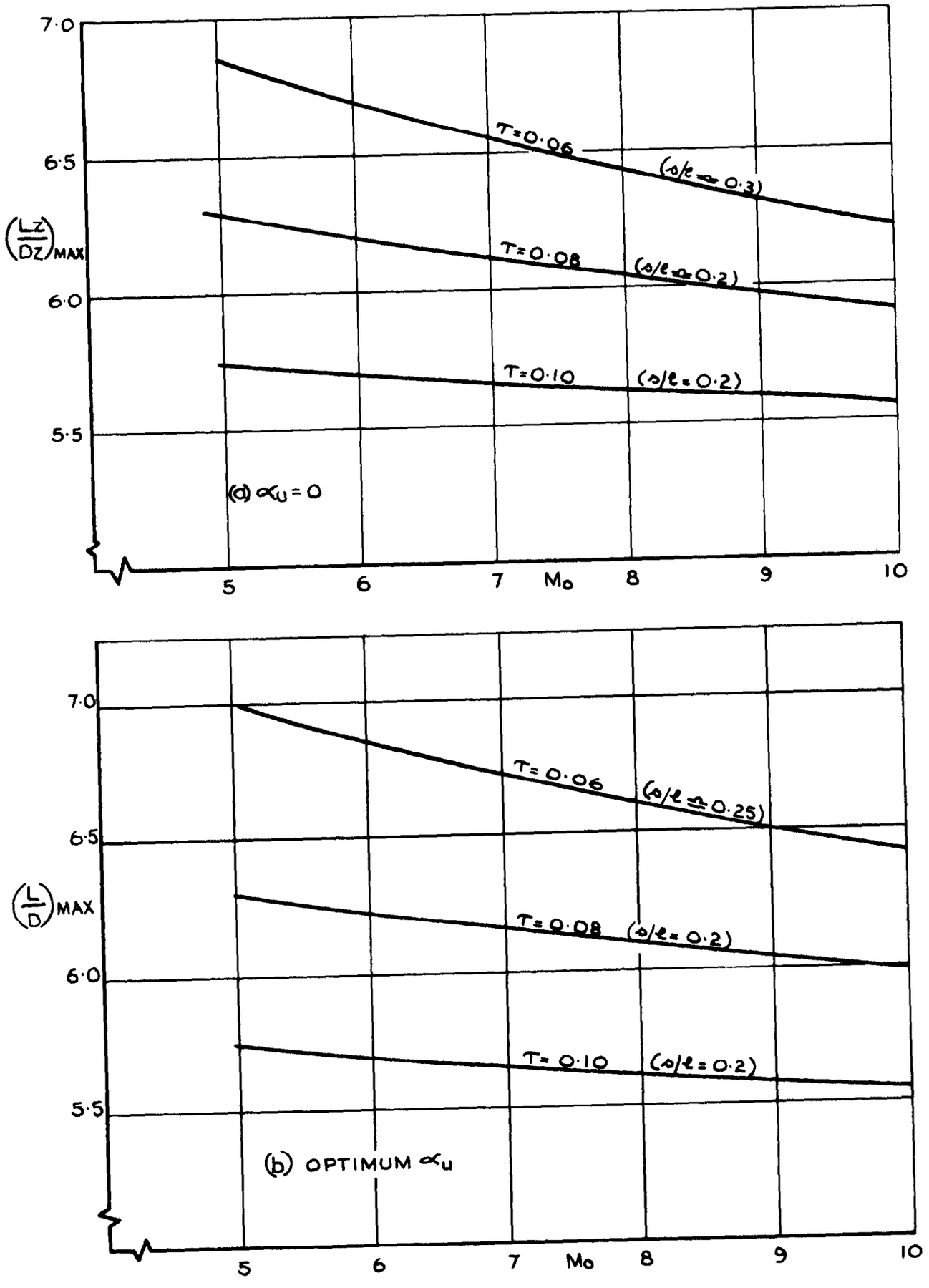

FIG. 16. MAX LIFT TO DRAG RATIO ($s/\ell \geq 0.2$) VS M_o AT CONSTANT τ, $C_{FU} = C_{FL} = 0.001$, $C_{DP} = 0$

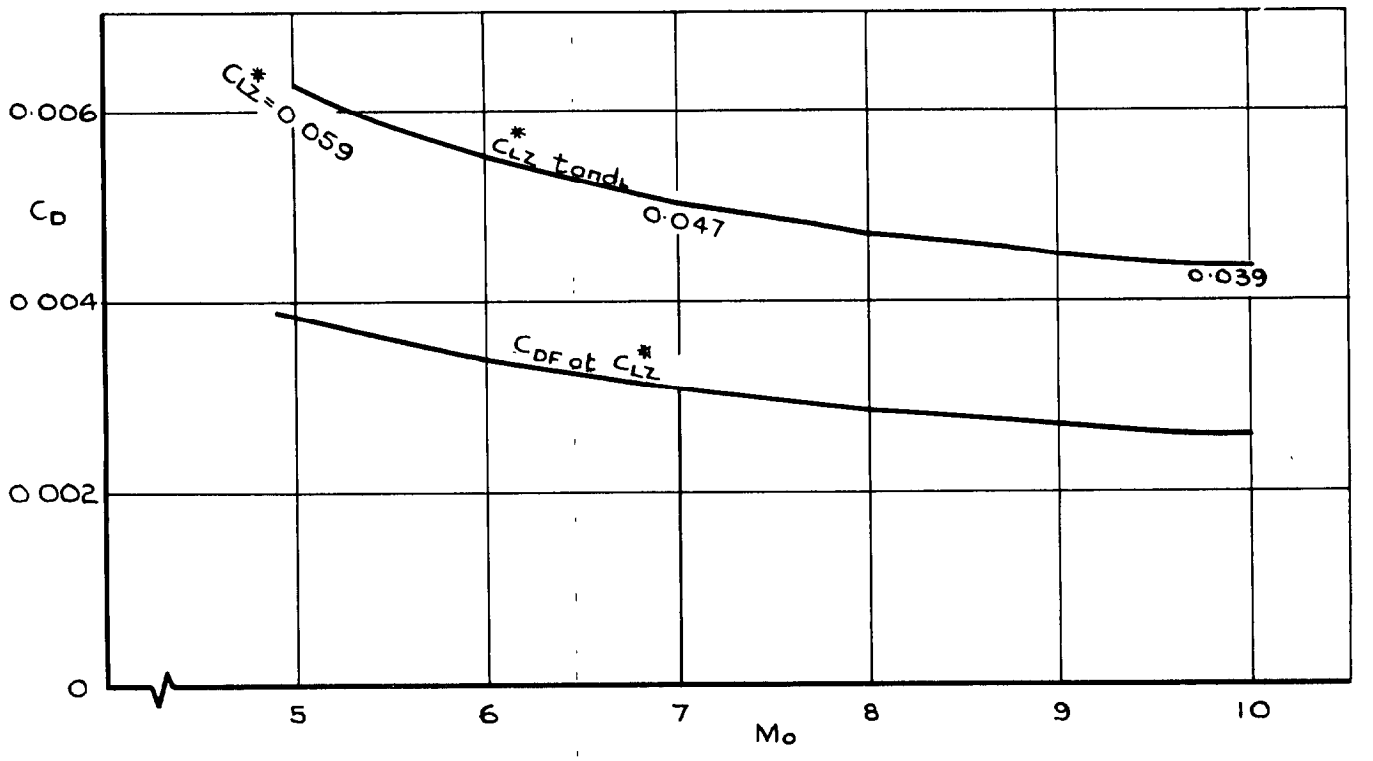

NB THESE RESULTS APPLY AT $Re_t = 10^7$, $W/S = 25$ lb/ft^2
OR $Re_t = 0$ $W/S = 50$ lb/ft^2

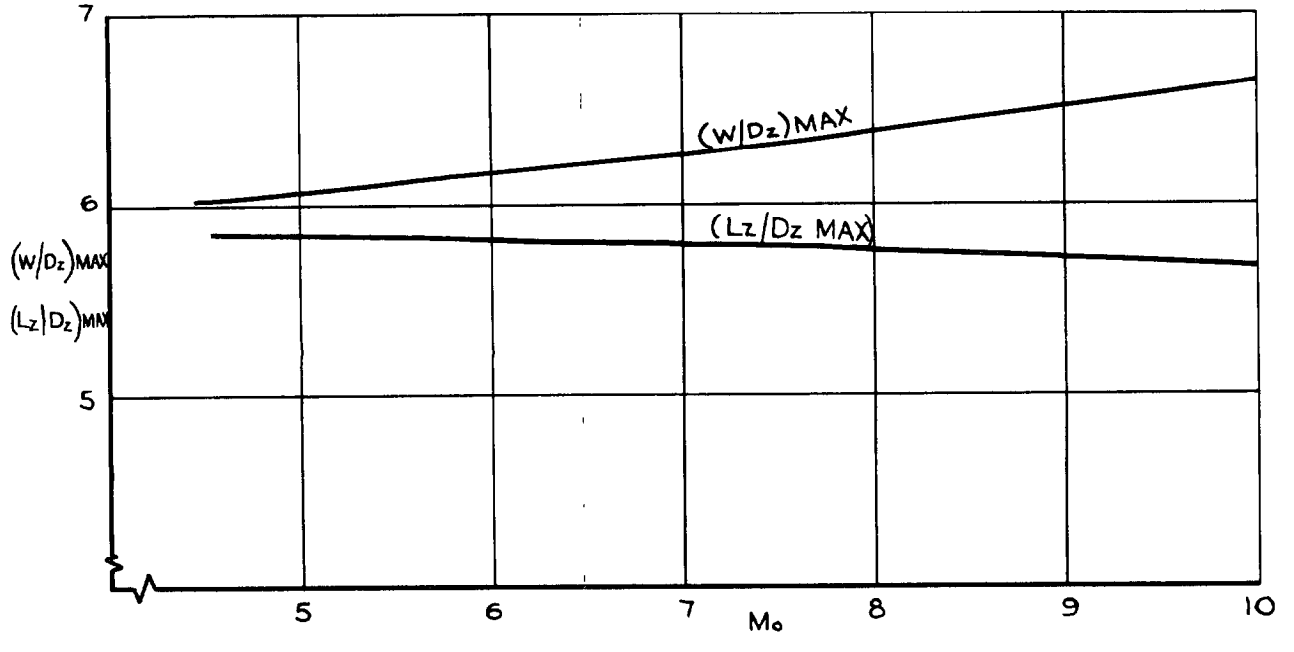

FIG.17. EXAMPLE OF EFFECT OF M_o ON MAX WEIGHT TO DRAG AND LIFT TO DRAG RATIO'S, WITH STREAMWISE UPPER SURFACE, τ=0·08 C_{DP}=0

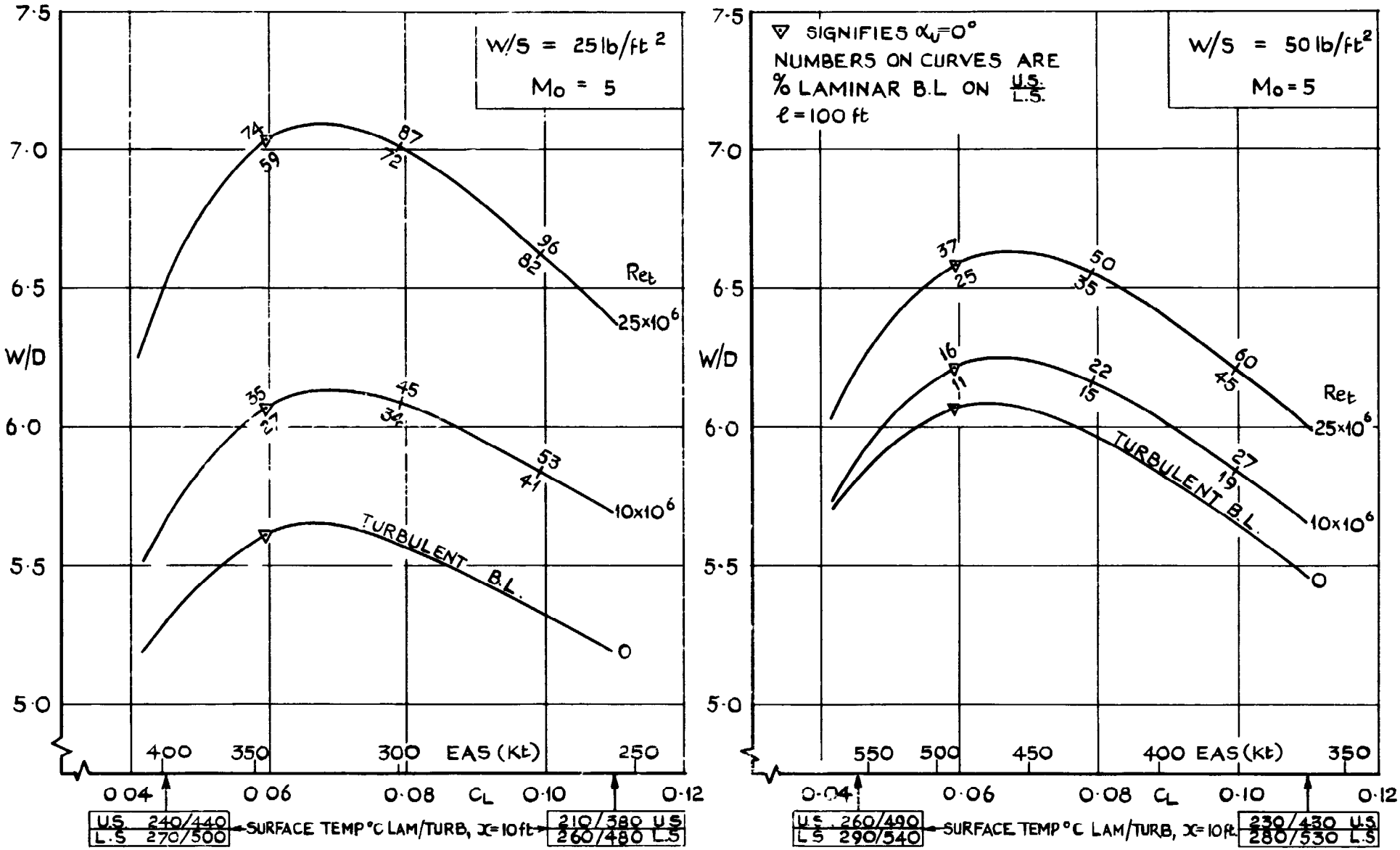

FIG.18 WT. TO DRAG RATIO vs C_L AT CONSTANT τ AND s/ℓ — CALCULATED FRICTION DRAG, $\tau = 0.08$, $s/\ell = 0.2$, $C_{DP} = 0$

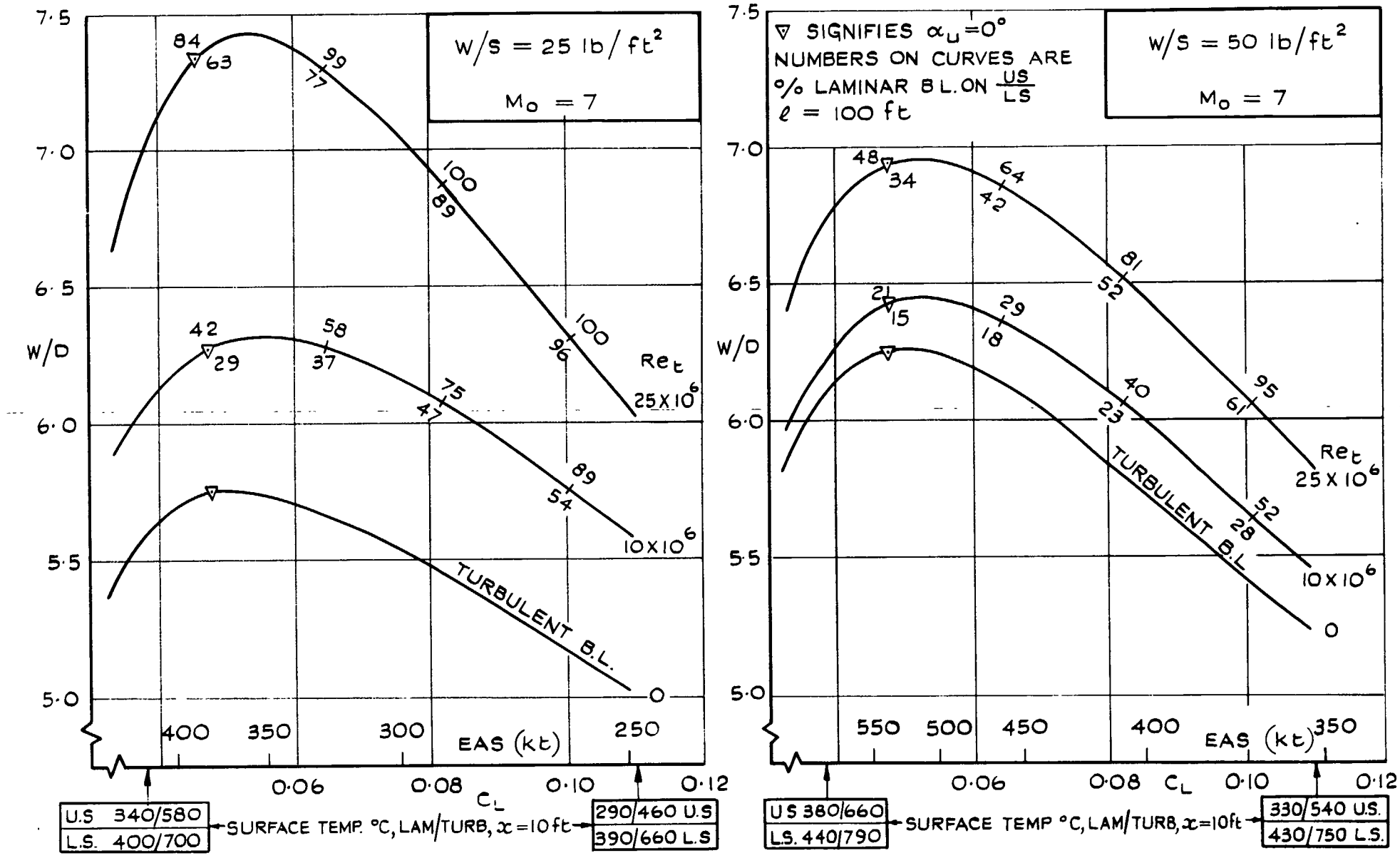

FIG.18(CONT'D) WT. TO DRAG RATIO vs C_L AT CONSTANT τ AND Δ/ℓ-CALCULATED FRICTION DRAG,
$\tau = 0.08, \Delta/\ell = 0.2, C_{DP} = 0$

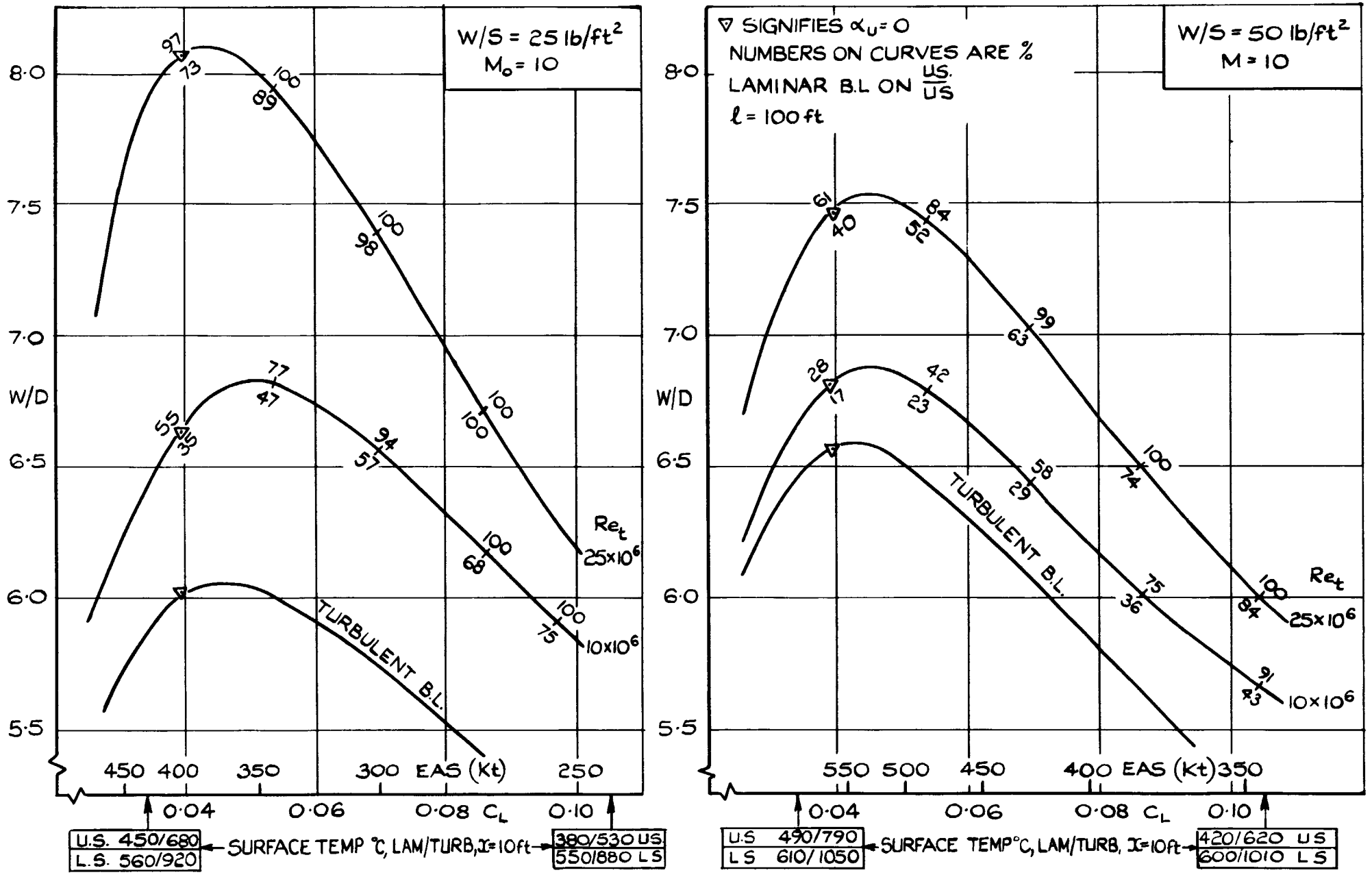

FIG.18(CONCL'D) WT. TO DRAG RATIO vs C_L AT CONSTANT τ AND s/ℓ – CALCULATED FRICTION DRAG,

$\tau = 0{\cdot}08$, $s/\ell = 0{\cdot}2$, $C_{DP} = 0$

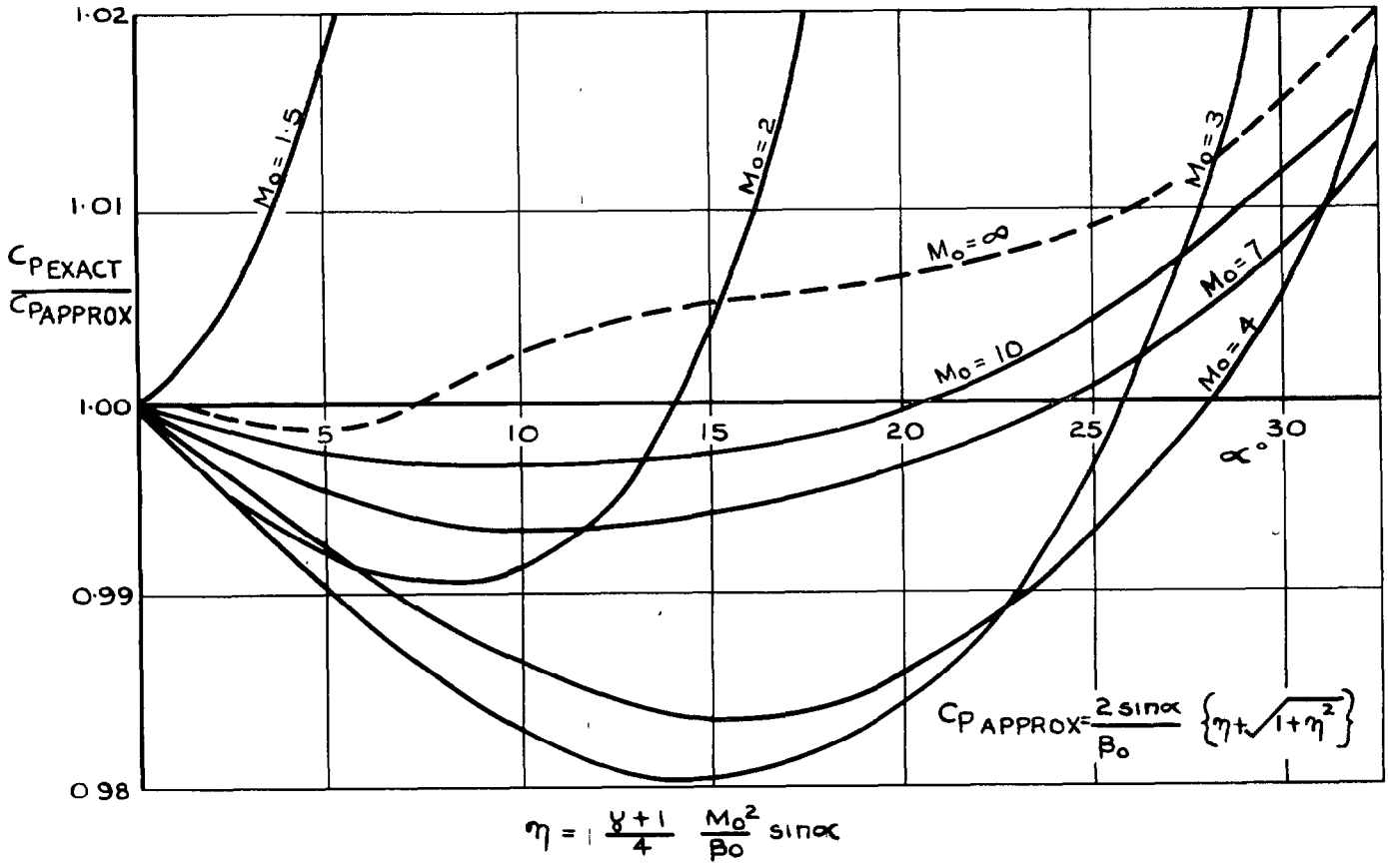

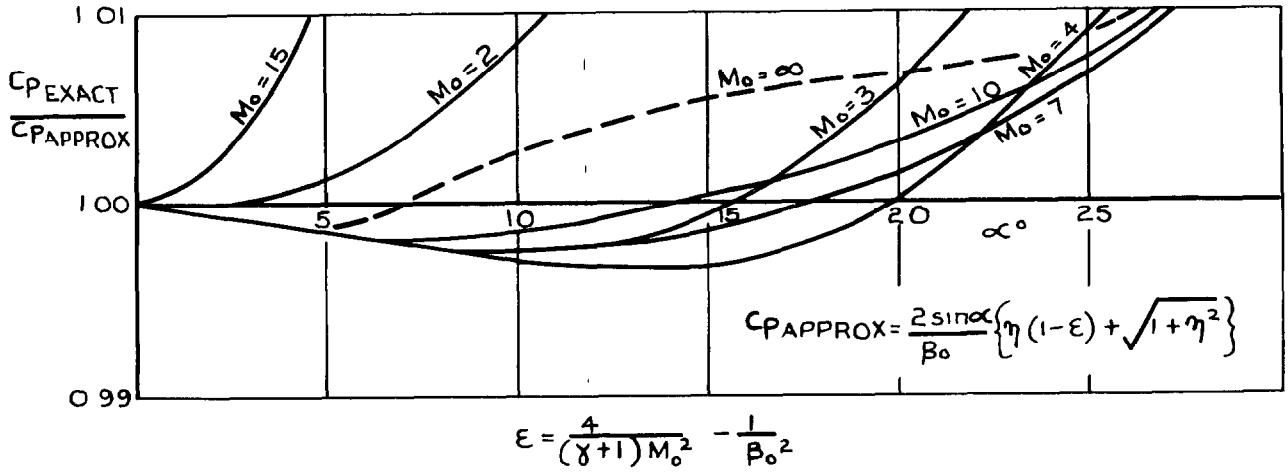

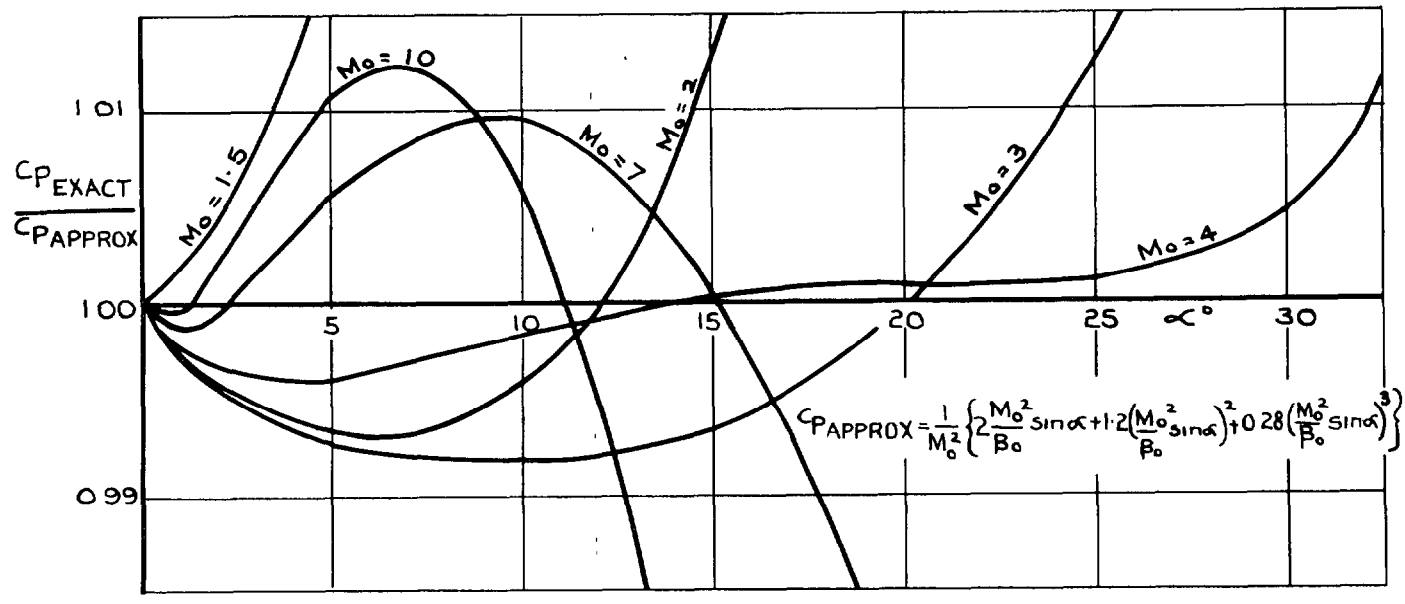

FIG. B1. ACCURACY OF APPROXIMATIONS FOR PRESSURE BEHIND AN OBLIQUE SHOCK, $\gamma = 1·4$

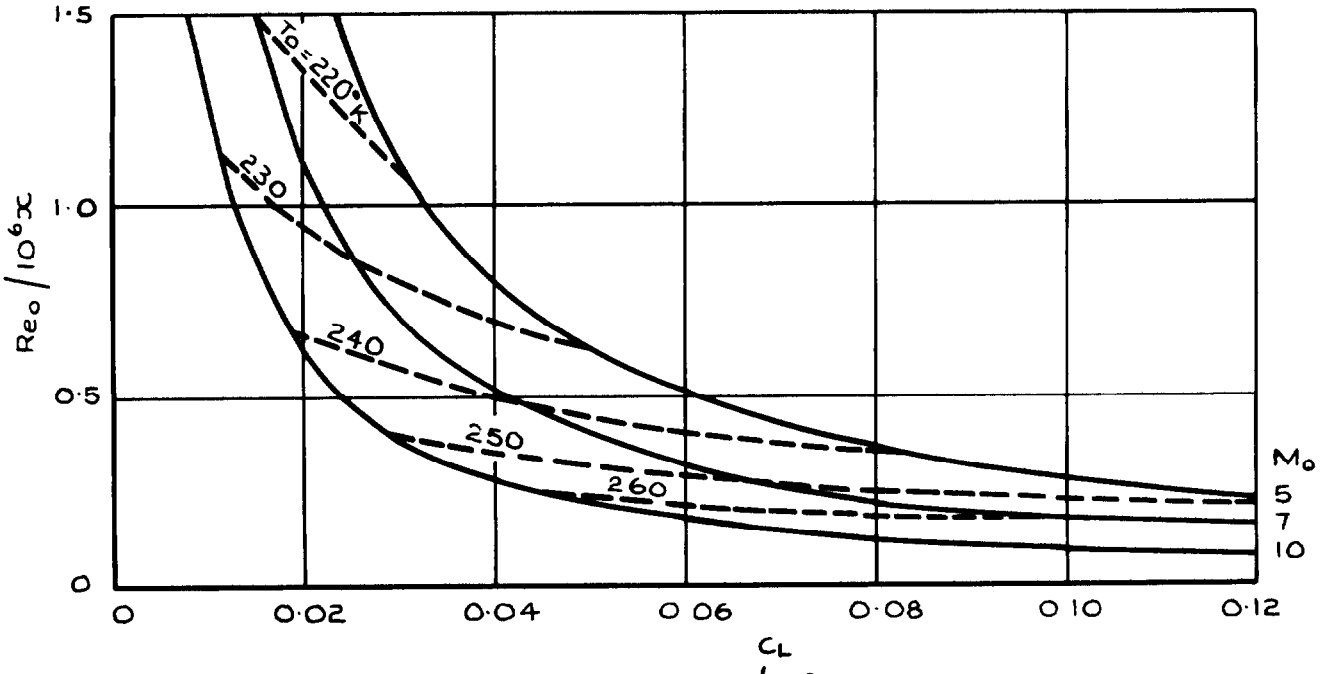

(a) W/S = 25 lb/ft²

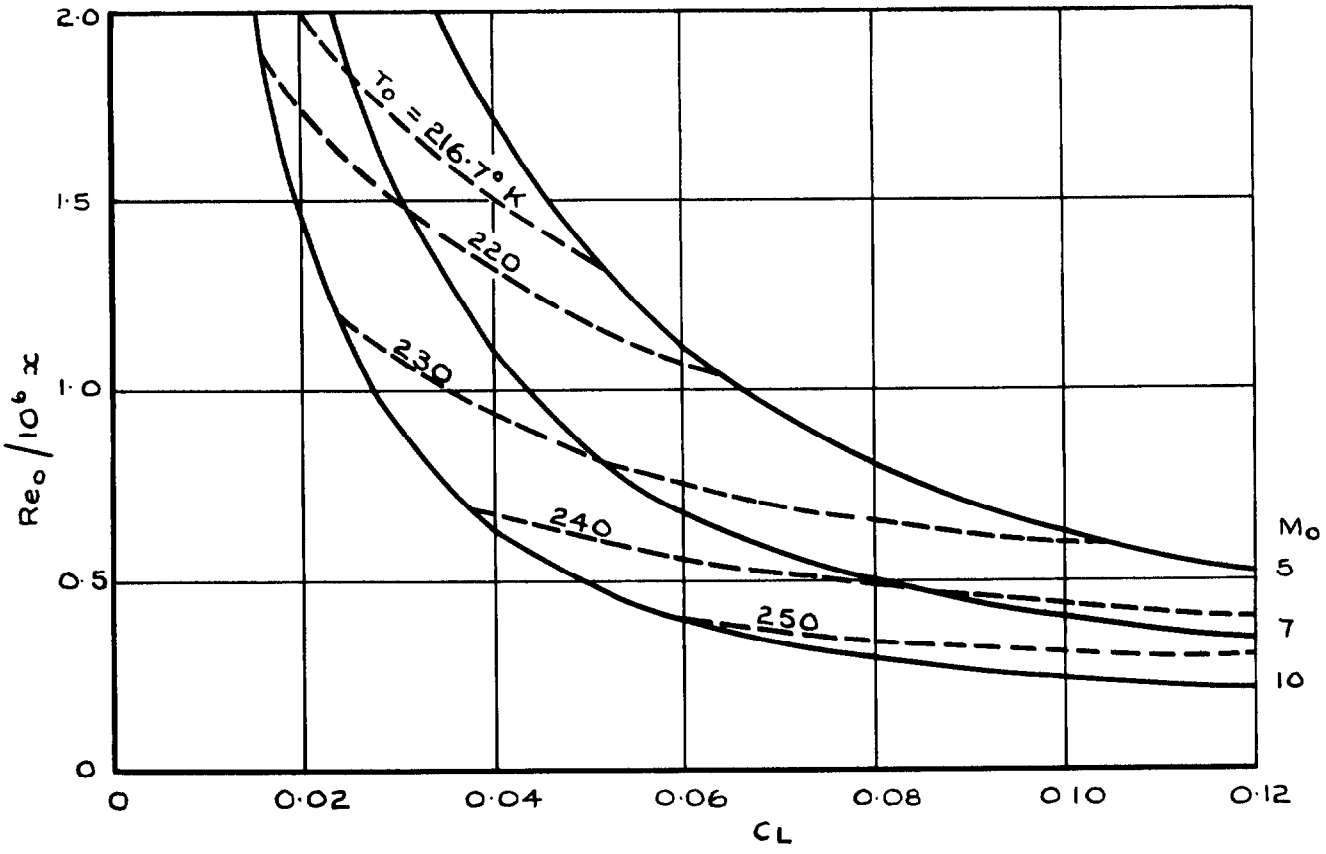

(b) W/S = 50 lb/ft²

FIG.C 1. (a) & (b) VARIATION OF FREE-STREAM REYNOLDS NUMBER PER FOOT IN CRUISING FLIGHT WITH MACH. NUMBER AND LIFT COEFFICIENT

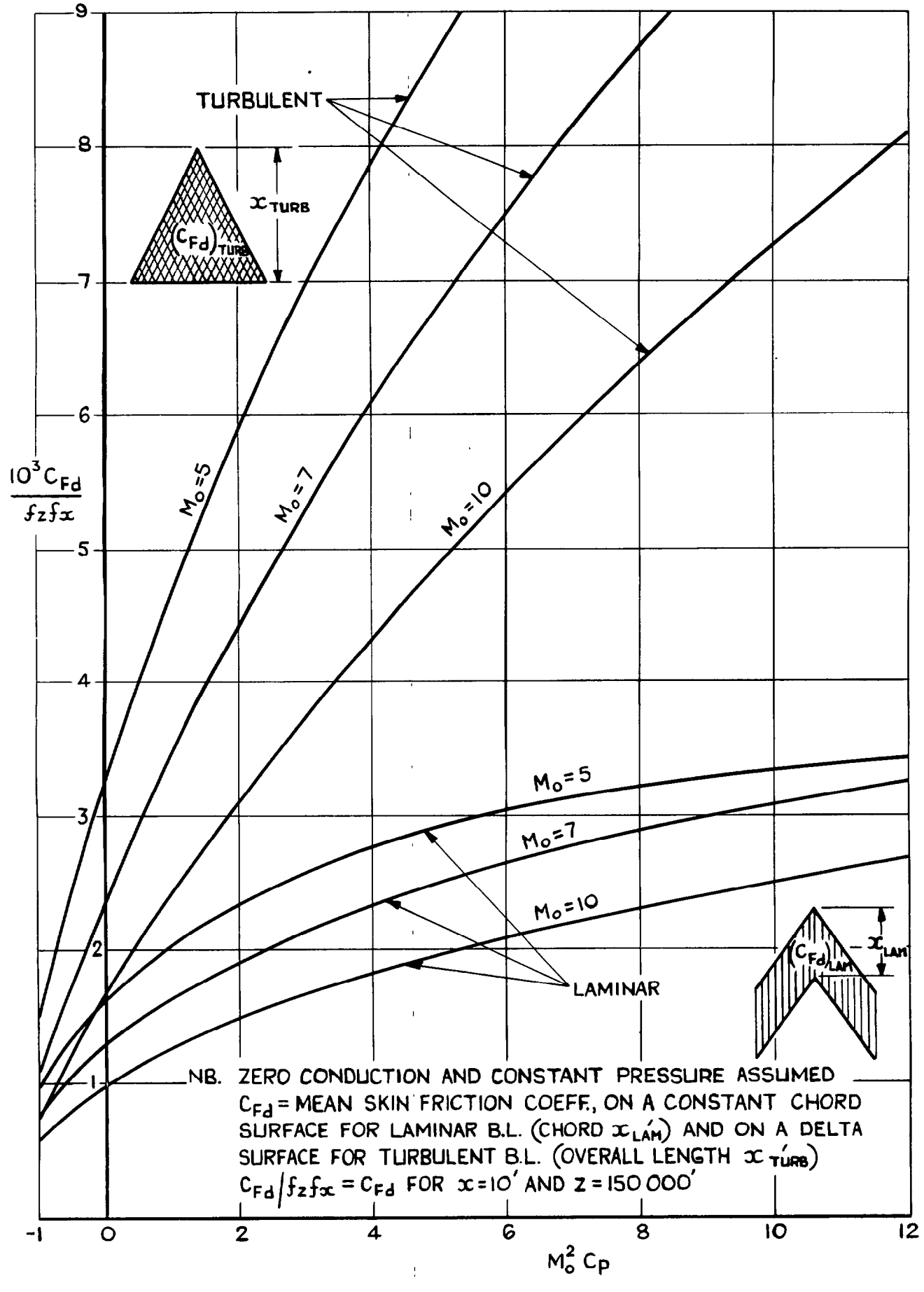

FIG. C2 DATUM MEAN SKIN FRICTION COEFFICIENT C_{Fd}

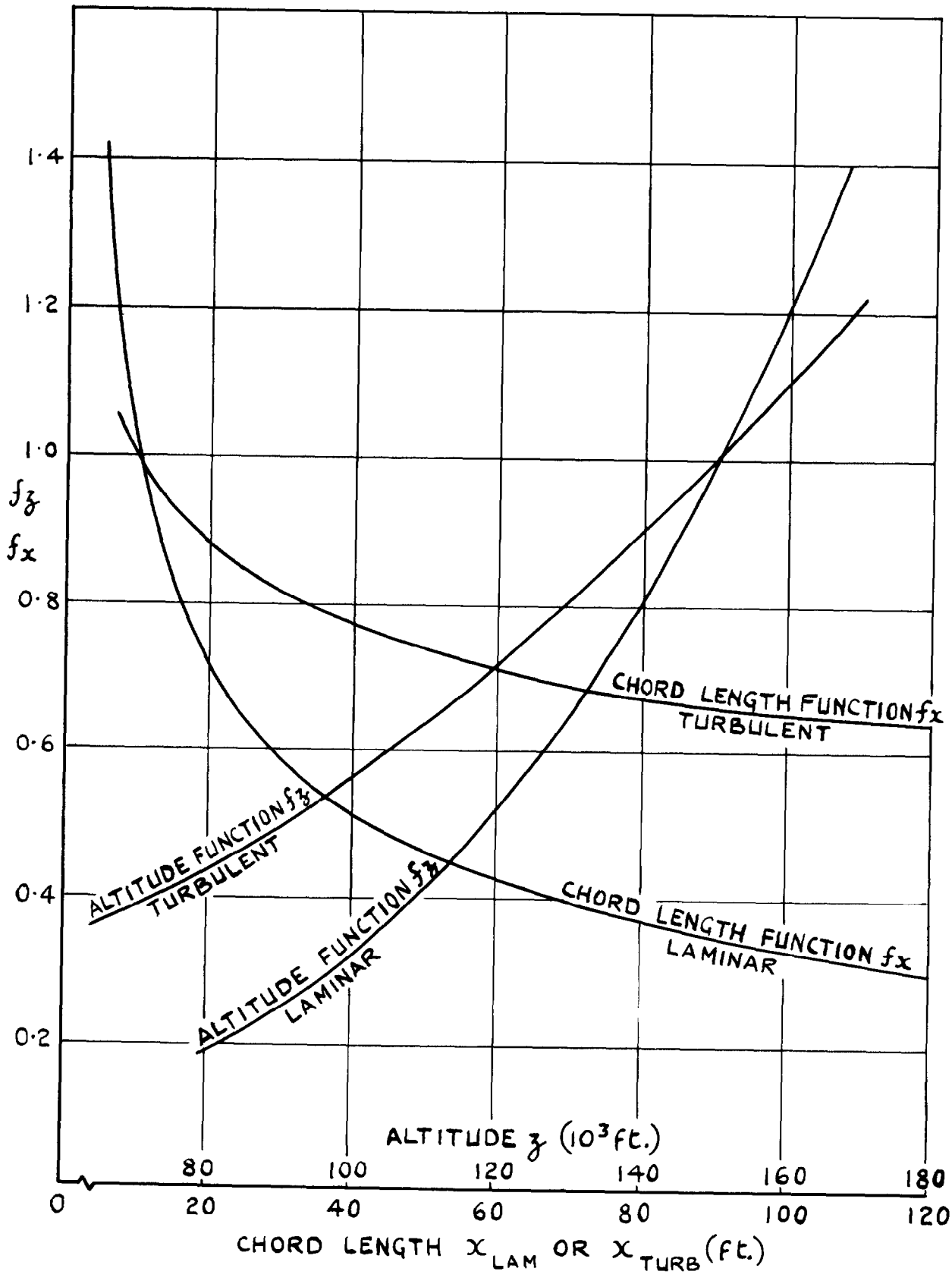

FIG. C3 CHORD LENGTH AND ALTITUDE FUNCTIONS FOR DATUM SKIN FRICTION

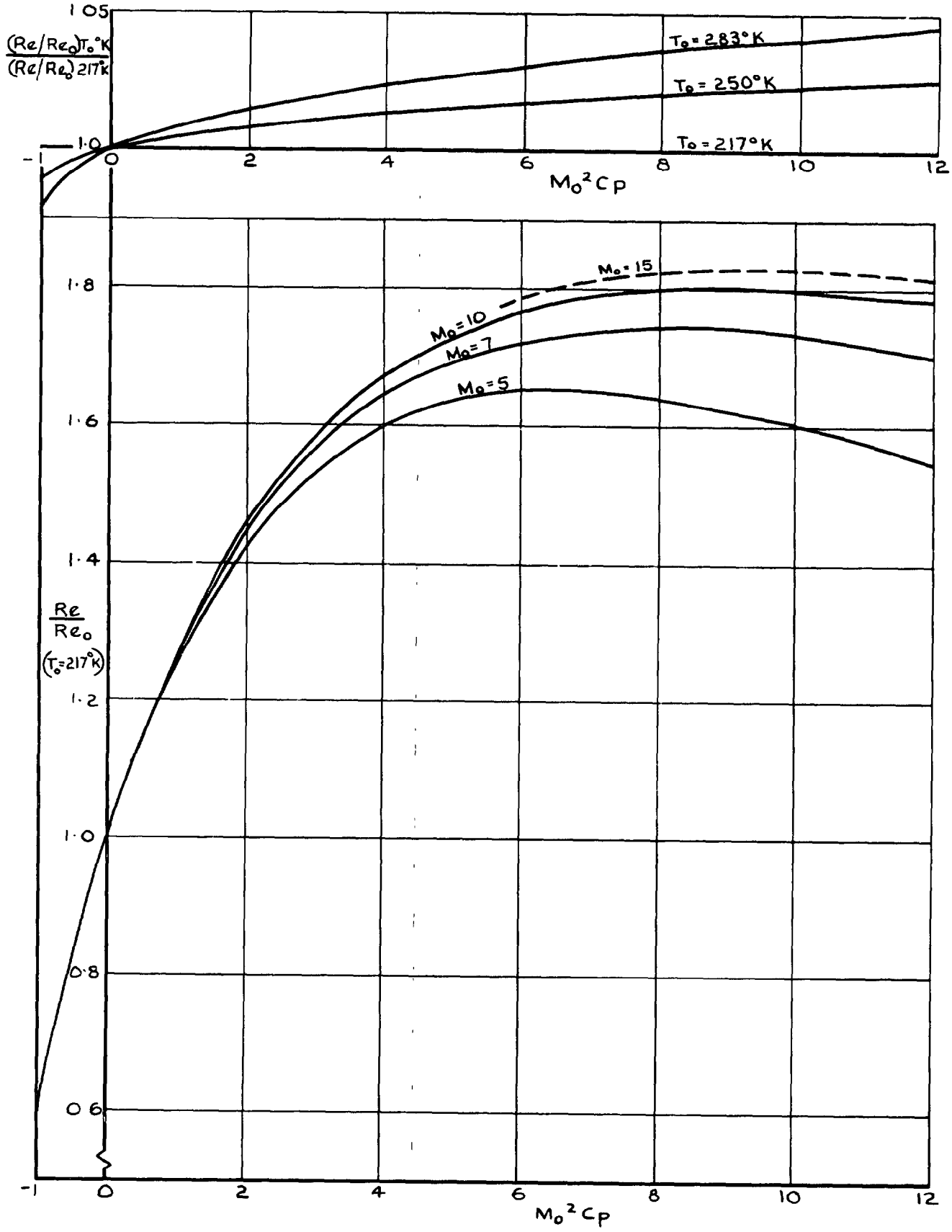

FIG.C 4 LOCAL REYNOLDS No/STREAM REYNOLDS No

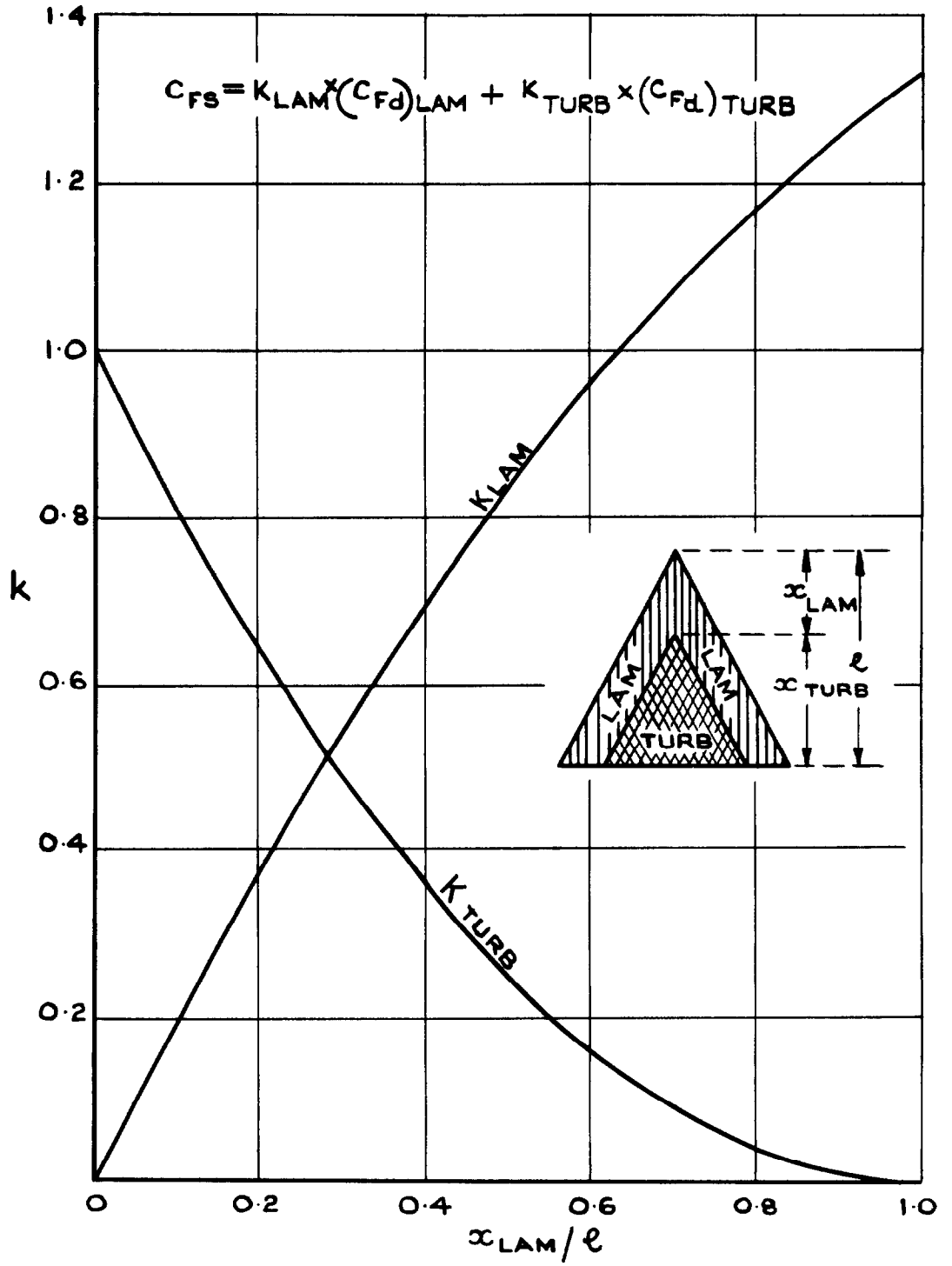

FIG. C 5. MEAN SKIN FRICTION COEFFICIENT FOR A DELTA SURFACE C_{FS}

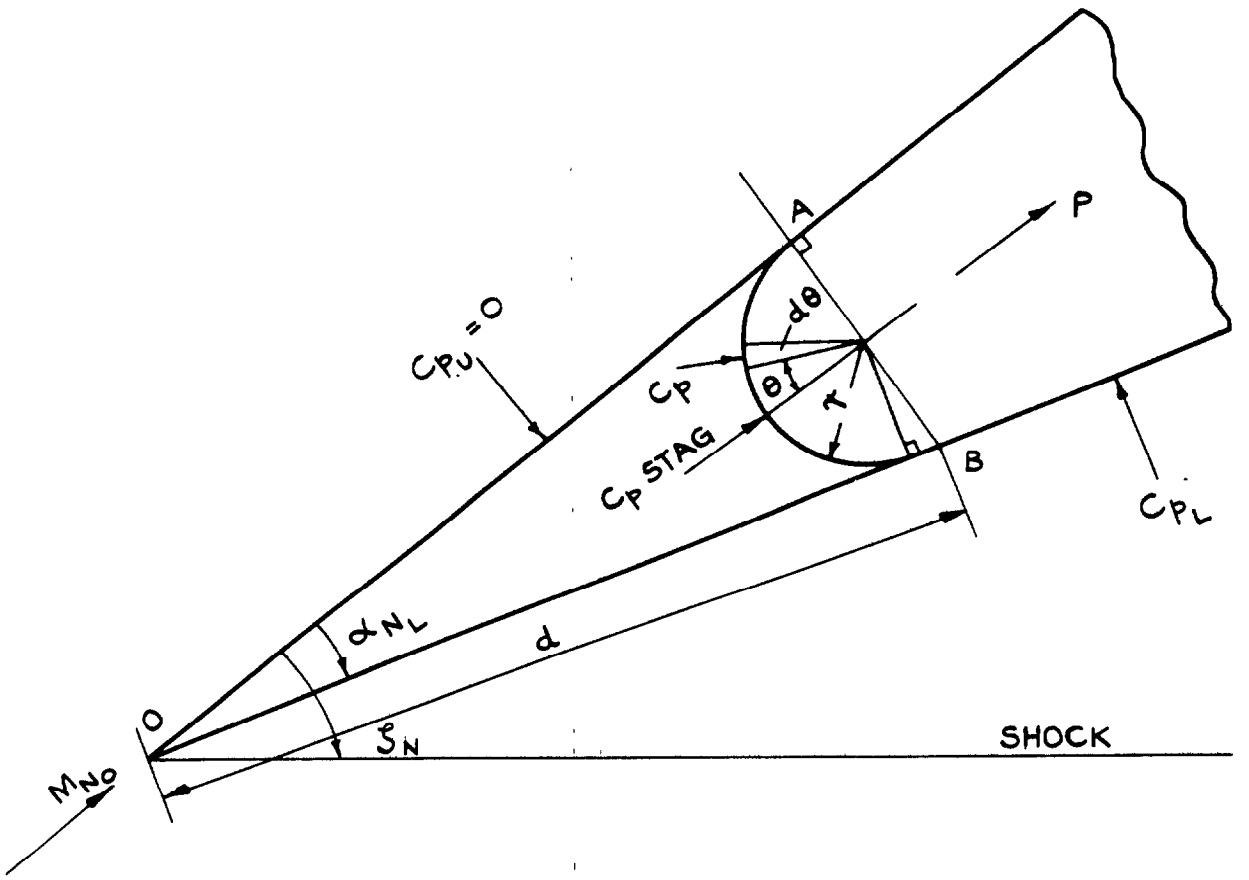

FIG. D1 GEOMETRY OF BLUNTED LEADING – EDGE IN PLANE NORMAL TO LEADING – EDGE

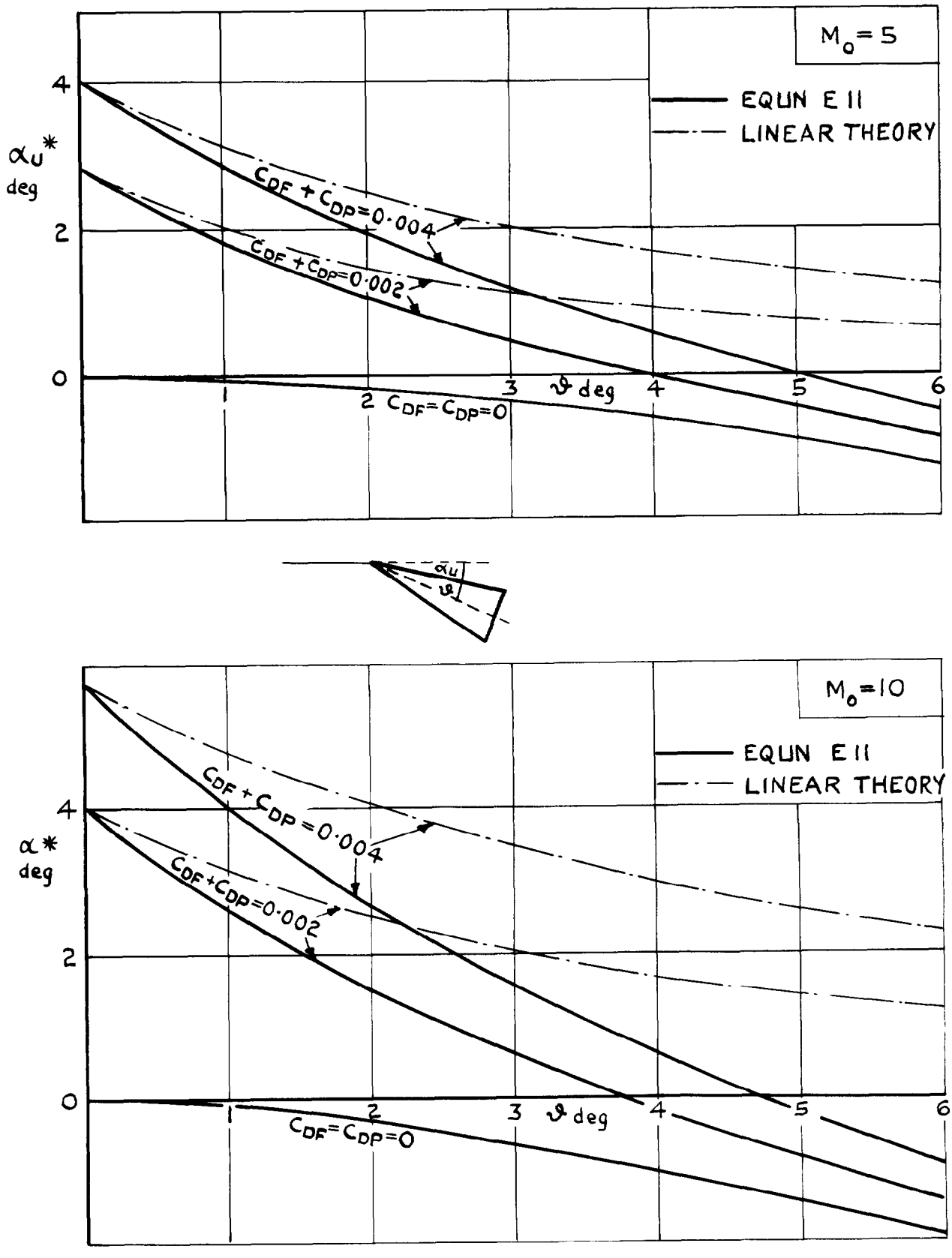

FIG.E1 UPPER SURFACE INCIDENCE AT MAXIMUM LIFT TO DRAG RATIO FOR A TWO-DIMENSIONAL WEDGE

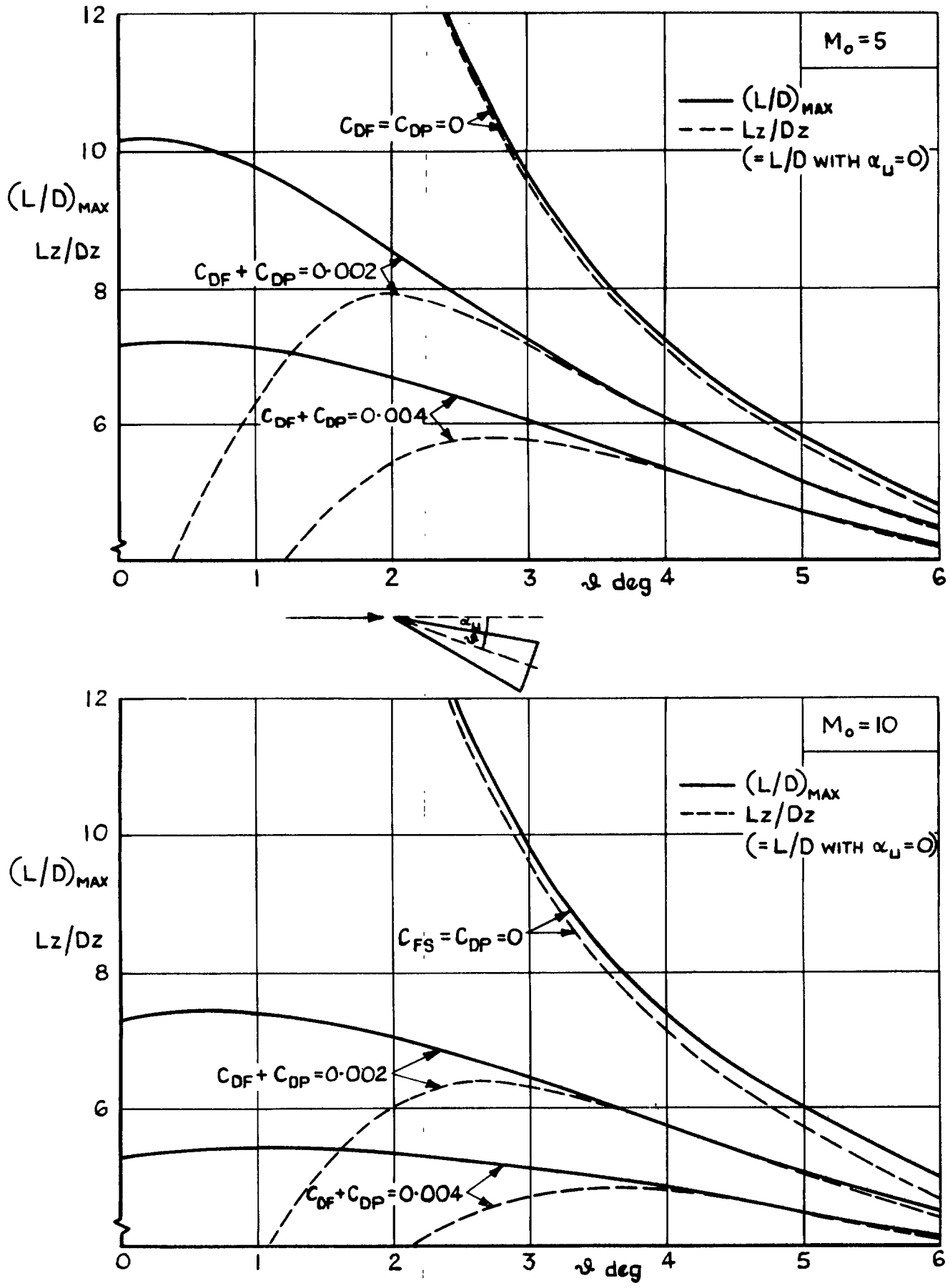

FIG. E2 LIFT TO DRAG RATIO FOR A TWO-DIMENSIONAL WEDGE

Printed in England for Her Majesty's Stationery Office by the Royal Aircraft Establishment, Farnborough. Dd.125875.K4.

A.R.C. C.P. No. 930
February 1966
Collingbourne, J.R. 533.693.3 :
Peckham, D.H. 533.6.013.13 :
533.6.013.12 :
THE LIFT AND DRAG CHARACTERISTICS OF CARET WINGS AT MACH NUMBERS BETWEEN 5 AND 10 533.6.011.55 :

The broad effects of certain variables on the aerodynamic efficiency of caret wings are investigated. The variables considered are slenderness ratio, volume coefficient and upper-surface incidence: skin friction, including the effects of wing loading, altitude and transition Reynolds number; and parasite drag. This study highlights the important areas for future investigation, and recommendations are made for experimental and theoretical work. Detailed conclusions are given at the end of the Report.

A.R.C. C.P. No. 930
February 1966
Collingbourne, J.R. 533.693.3 :
Peckham, D.H. 533.6.013.13 :
533.6.013.12 :
THE LIFT AND DRAG CHARACTERISTICS OF CARET WINGS AT MACH NUMBERS BETWEEN 5 AND 10 533.6.011.55

The broad effects of certain variables on the aerodynamic efficiency of caret wings are investigated. The variables considered are slenderness ratio, volume coefficient and upper-surface incidence: skin friction, including the effects of wing loading, altitude and transition Reynolds number; and parasite drag. This study highlights the important areas for future investigation, and recommendations are made for experimental and theoretical work. Detailed conclusions are given at the end of the Report.

A.R.C. C.P. No. 930
February 1966
Collingbourne, J.R. 533.693.3 :
Peckham, D.H. 533.6.013.13 :
533.6.013.12 :
THE LIFT AND DRAG CHARACTERISTICS OF CARET WINGS AT MACH NUMBERS BETWEEN 5 AND 10 533.6.011.55

The broad effects of certain variables on the aerodynamic efficiency of caret wings are investigated. The variables considered are slenderness ratio, volume coefficient and upper-surface incidence: skin friction, including the effects of wing loading, altitude and transition Reynolds number; and parasite drag. This study highlights the important areas for future investigations, and recommendations are made for experimental and theoretical work. Detailed conclusions are given at the end of the Report.

DETACHABLE ABSTRACT CARDS

Published by
HER MAJESTY'S STATIONERY OFFICE

To be purchased from
49 High Holborn, London W.C.1
423 Oxford Street, London W.1
13A Castle Street, Edinburgh 2
109 St Mary Street, Cardiff
Brazennose Street, Manchester 2
50 Fairfax Street, Bristol 1
35 Smallbrook, Ringway, Birmingham 5
7-11 Linenhall Street, Belfast 2
or through any bookseller

S.O. CODE No. 23-9017-30